CONDITION MONITORING TECHNIQUES FOR PERMANENT MAGNET SYNCHRONOUS MOTORS

by

Mohsen Zafarani

APPROVED BY SUPERVISORY COMMITTEE:

_____
Dr. Bilal Akin, Chair

_____
Dr. Babak Fahimi

_____
Dr. Mehrdad Nourani

_____
Dr. Murat Torlak

Copyright 2018
Mohsen Zafarani
All Rights Reserved

Dedicated to my family

CONDITION MONITORING TECHNIQUES OF PERMANENT MAGNET SYNCHRONOUS MOTORS

by

MOHSEN ZAFARANI, BS, MS

DISSERTATION

Presented to the Faculty of
The University of Texas at Dallas
in Partial Fulfillment
of the Requirements
for the Degree of

DOCTOR OF PHILOSOPHY IN

ELECTRICAL ENGINEERING

THE UNIVERSITY OF TEXAS AT DALLAS

August 2018

ACKNOWLEDGMENTS

I would like to express my sincere appreciation to my principal supervisor, Dr. Bilal Akin, for the continuous support of my Ph.D study and related research and projects. I have been always inspired with new ideas throughout many technical discussions I had with him, and his remarkable statements and comments revealed new aspects of the projects.

Besides my advisor, I would like to thank the rest of my dissertation committee Dr. Fahimi, Dr. Nourani, and Dr. Torlak for their insightful comments and encouragement which incented me to widen my research from various perspectives.

I would like to express my appreciation to Dr. Fedigan from Texas Instruments for the great support he had for me and the valuable statements and comments on my presentations.

I would also like to thank all the administrative assistants of the Department of Electrical Engineering, especially Suzanne Newsom and Rosarita Lubag, who were nice and helpful.

I am also thankful to my colleague Taner Goktas who always helped me and built my confidence. I am truly lucky that I experienced working with him during my PhD program.

This work was supported in part by the TXACE/SRC under Grant TASK 1836.149, and in part by Texas Instruments Inc.

June 2018

CONDITION MONITORING TECHNIQUES OF PERMANENT MAGNET SYNCHRONOUS MOTORS

Mohsen Zafarani, PhD
The University of Texas at Dallas, 2018

Supervising Professor: Dr. Bilal Akin

Due to the variety of electric motor applications in critical service systems, they need precise control and accurate health monitoring in order to operate reliably and safely. Fault diagnosis, as the earliest step of system health management, identifies impending faults through pre-specified indexes. This is a critical process as it provides early warnings for catastrophic failures well beforehand and enables preventive maintenance schedule updates. The most important advance in this field is the implementation of fault diagnosis system embedded to drive system. In this technology, the health monitoring system is programmed in the main CPU used for controlling purposes. Also, there is no need to install any additional sensor since the same measurement used for control is sent for monitoring. This technology is growing up and still is not mature enough to be used in industries widely.

In this study, rotor related faults such as magnet defect and eccentricity faults and their corresponding reflections on permanent magnet (PM) motor stator variables are investigated. An analytical approach based on a partitioned magnetic equivalent circuit is developed to determine the influence of rotor related faults on PM motor variables. Stator winding configuration, winding connection type and location of damaged rotor magnets are some of the physical

properties affecting the fault signature characteristics. Several cases with different numbers of pole and slot are investigated through the proposed method. In addition, different winding connections (including star and delta connection), different winding configurations (including single and double layer, fractional and full coil pitch), and different magnet defect numbers and locations are scrutinized. The proposed tool significantly reduces the computational burden and provides sufficient accuracy which significantly eases to simulate several magnet fault scenarios and examine detailed topology dependencies in shorter times.

At the last part of this research, a motor specific fault severity assessment method is proposed to calculate the amplitude of magnet defect fault signatures in the stator current and back-emf through machine and controller parameters of PMSM drive. A detailed mathematical analysis is developed based on the linear model of PMSM to predict the behavior of fault signatures in motor variables at various operating points. In order to understand and decouple the effects of motor controllers and operating points, the derivations are further extended to clarify the effects of current loop gains. Under the light of findings, the fault severity impact on the current and back-emf fault signatures is investigated exhaustively.

TABLE OF CONTENTS

ACKNOWLEDGMENTS.....v

ABSTRACT.....vi

LIST OF FIGURES.....xi

LIST OF TABLES.....xv

CHAPTER 1 INTRODUCTION.....1

1.1 Motivation.....1

1.2 Aims and Objectives.....3

1.3 Literature Review.....3

1.4 Outline of the Dissertation.....7

CHAPTER 2 MAGNET DEFECT FAULT ANALYSIS USING MAGNETIC EQUIVALENT CIRCUIT METHOD.....9

2.1 Stator Flux Linkage Calculation.....9

2.2 Mathematical Analysis of Magnet Defect Fault.....13

2.3 Different Number of Poles and Slots.....18

2.4 The Effect of Winding Connection.....19

2.5 Simulation Results.....20

2.5.1 Simulation Results for Back-emf.....21

2.5.2 Location and Number of Magnet Defects.....22

2.6 Experimental Results.....26

2.7 Conclusion.....29

CHAPTER 3 AN INVESTIGATION OF MOTOR TOPOLOGY IMPACTS ON MAGNET DEFECT FAULT SIGNATURES.....31

3.1 PM MOTOR WINDING LAYOUT.....31

3.2 Partitioned MEC Implementation.....34

3.2.1 Stator flux linkage calculation.....34

3.2.2 Back-Emf Calculation.....37

3.2.3 Magnet Defect Fault Modelling.....41

3.3 Analysis of Magnet Faults Signatures and Topology Dependencies....42
3.3.1 Winding Configuration, Number of Poles and Slots....43
3.3.2 Number and Location of Magnet Defects....48
3.3.3 Winding Configuration....50
3.4 Simulation and Experimental Results....51
3.5 Experimental Setup....57
3.6 Conclusion....58

CHAPTER 4 MODELING AND DYNAMIC BEHAVIOR ANALYSIS OF MAGNET DEFECT SIGNATURES IN PERMANENT MAGNET SYNCHRONOUS MOTORS....60
4.1 Modeling and Analysis of Magnet Defect Fault Signatures....60
4.1.1 Signatures in Back-emf....60
4.1.2 Current Signatures - Open Loop Operation....62
4.1.3 Current Signatures -Closed Loop Operation....66
4.2 Simulation Results....69
4.2.1 Fault Signatures in Back-emf....69
4.2.2 Current Fault Signatures-Open Loop Operation....73
4.2.3 Current Fault Signatures-Closed Loop Operation....75
4.2.4 Fault Severity....76
4.3 Experimental Result....79
4.3.1 Experimental Setup....79
4.3.2 Fault Signatures in Back-emf....81
4.3.3 Stator Current Fault Signatures- Open Loop Operation....81
4.3.4 Stator Current Fault Signature –Closed Loop Operation....83
4.4 Conclusion....85

CHAPTER 5 SUMMARY AND CONCLUSION....86

REFERENCES....89

BIOGRAPHICAL SKETCH....93

CURRICULUM VITAE

LIST OF FIGURES

Figure 1.1. a) A PMSM model in FEA b) MEC model of the PMSM 7

Figure 2.1. Side view of a) motor winding/magnet configuration b) corresponding magnetic equivalent circuit 10

Figure 2.2. Different type of crack a) Horizontal b) Vertical c) Zigzag 20

Figure 2.3. Air-gap flux density when the rotor is located at θ_r=42.5^o 22

Figure 2.4. Stator back-emf spectrum at rated speed, MEC results a) Healthy b) Faulty 22

Figure 2.5. Stator back-emf spectrum at rated speed, FE results a) Healthy b) Faulty 22

Figure 2.6. Phase "a" back emf spectrum when magnet number 1 and 3 are faulty a) MEC result b) FE result 23

Figure 2.7. Phase "a" back emf spectrum when magnet number 1 and 5 are faulty a) MEC result b) FE result 23

Figure 2.8. Stator current spectrum at rated speed and rated torque, FE results a) Healthy b) Faulty 24

Figure 2.9. Simulation results, the behavior of fault related harmonics in back-EMF at different speeds, a) Vertical crack b) Horizontal crack c) Zigzag crack 25

Figure 2.10. Simulation results, the behavior of 0.25th harmonic in phase current, a) Vertical crack b) Horizontal crack c) Zigzag crack 25

Figure 2.11. Simulation results, the behavior of 0.5th harmonic in phase current, a) Vertical crack b) Horizontal crack c) Zigzag crack 25

Figure 2.12. a) Healthy motor with rotor cover b) Vertically cut magnet 27

Figure 2.13. Experimental setup a) PMSM b) Dynamometer c) Motor drive d) Data acquisition e) Spectrum analyzer 27

Figure 2.14. Stator back-emf spectrum at rated speed, experimental results a) Healthy b) Faulty28

Figure 2.15. Stator current spectrum at rated speed and rated torque, experimental results a) Healthy b) Faulty 28

Figure 2.16. Experimental results, the behavior of fault harmonics in phase current under different speed and load conditions a) 0.25th b) 0.5th 29

Figure 2.17. Experimental results, the behavior of fault harmonics in back-EMF at different speeds....29

Figure 3.1. Coil magnetic field vectors of a double layer winding for a 9-slot and 8-pole PMSM, one of the test motors used in this study....32

Figure 3.2. Magnetic equivalent circuit of the test motor....33

Figure 3.3. Skew factor for different skew angle and harmonics....41

Figure 3.4. A three phase, 9-slot/6-pole double layer winding motor a) Magnetic field vector b) winding layout....45

Figure 3.5. A three phase, 36-slot/6-pole double layer winding motor a) Magnetic field vector b) winding layout....47

Figure 3.6. Stator back-emf spectrum at rated speed for the 9-slot/8-pole PMSM motor, MEC results a) Healthy b) One magnet defect....52

Figure 3.7. Stator back-emf spectrum at rated speed for the 9-slot/8-pole PMSM motor, FE results a) Healthy b) One magnet defect....52

Figure 3.8. Stator back-emf spectrum at rated speed for the 36-slot/6-pole IPM motor MEC results a) Healthy b) One magnet defect....53

Figure 3.9. Stator back-emf spectrum at rated speed for the 36-slot/6-pole IPM motor, FE results a) Healthy b) One magnet defect....53

Figure 3.10. Phase “a” back emf spectrum when magnet number 1 and 3 are defected a) MEC result b) FE result....54

Figure 3.11. Phase “a” back emf spectrum when magnet number 1 and 5 are defected a) MEC result b) FE result....54

Figure 3.12. Stator back-emf spectrum at rated speed for the 9-slot/8-pole PMSM motor, experimental results a) Healthy b) One magnet cracked....55

Figure 3.13. Stator back-emf spectrum at rated speed for the 36-slot/6-pole IPM, experimental results a) Healthy b) One magnet cracked....55

Figure 3.14. Stator current spectrum at rated speed and rated torque for 9-slot/8-pole PMSM motor, FE results a) Healthy b) One magnet defect....56

Figure 3.15. Stator current spectrum at rated speed and rated torque for a 9-slot/8-pole PMSM motor, experimental results a) Healthy b) One magnet defect....56

Figure 3.16. Experimental setup a) PMSM b) Dynamometer c) Motor drive d)Data acquisition card e) Spectrum analyzer 57

Figure 4.1. Linear model of PMSM.....63

Figure 4.2. Characteristic of 0.25^{th} component versus speed 65

Figure 4.3. Finite element model of test motor a) Healthy b) Faulty motor.....70

Figure 4.4. Stator back-emf spectrum at rated speed for the 9slot/8pole PMSM, FE results a) Healthy b) Faulty 70

Figure 4.5. FE simulation results for back-emf harmonics behavior vs speed a) 0.25^{th} b) 0.5^{th} c) 0.75^{th} d) 1.25^{th} e) 1.5^{th} f) 3^{rd} g) 3.25^{th} h) 3.5^{th}.....71

Figure 4.6. Stator current fault signature behavior versus speed and load of healthy and faulty conditions, FEA results a) 0.25^{th} b) 0.5^{th} c) 1.25^{th} d) 2.75^{th} e) 3.25^{th} f) 3.5^{th}.....74

Figure 4.7. Stator back-emf fault signature behavior versus fault severity at 600 rpm a) 0.25^{th} b) 0.5^{th} c) 0.75^{th} d) 1.25^{th} e) 3^{rd} 77

Figure 4.8. Stator back-emf fault signature behavior versus fault severity at 3000 rpm a) 0.25^{th} b) 0.5^{th} c) 0.75^{th} d) 1.25^{th} e) 3^{rd} 78

Figure 4.9. Stator current fault signature behavior versus fault severity for different rotor speed and torque a) 0.25^{th} harmonic b) 0.5^{th} harmonic 79

Figure 4.10. Experimental setup a) PMSM b) Dynamometer c) Motor drive d) Data acquisition card e) Spectrum analyzer f) Oscilloscope 79

Figure 4.11. Experimental results for back-emf harmonic behavior vs speed a) 0.25^{th} b) 0.5^{th} c) 0.75^{th} d) 1.25^{th} e) 1.5^{th} e) 3^{rd} g) 3.25^{th} h) 3.5^{th} 80

Figure 4.12. Stator current fault signature behavior versus speed and load for healthy and faulty conditions, open loop experimental results a) 0.25^{th} b) 0.5^{th} c) 1.25^{th} d) 3.25^{th} e) 3.5^{th} ...82

Figure 4.13. Stator current fault signature behavior versus speed and load for healthy and faulty conditions, closed loop experimental results a) 0.25^{th} b) 0.5^{th} c) 1.25^{th} d) 3.25^{th} e) 3.5^{th}.84

LIST OF TABLES

Table 2.1. Electrical and mechanical parameters of PMSM....10

Table 2.2. Phase shift of harmonics in back-emf for 9-slot/8-pole motor....17

Table 2.3. Normalized product of coil factor and magnet coefficient for different number of poles and slots....18

Table 3.1. Specifications of the test motors....35

Table 3.2. Phase shift of harmonics in back-emf for 9-slot/8-pole motor....44

Table 3.3. Normalized construction filter magnitude for different number of poles and slots (Double layer winding)....45

Table 3.4. Normalized construction filter magnitude for different number of poles and slots (Single layer winding)....46

Table 3.5. Missing fault signatures due to magnet defect location....49

Table 3.6. Phase different between two stator phase back-emf for different harmonics (double layer winding)....51

Table 4.1. Electrical and mechanical parameters of PMSM....72

Table 4.2. The amplitude of 0.25^{th} component versus speed for different k_p and k_i coefficients .75

CHAPTER 1

INTRODUCTION

1.1 Motivation

Motors and generators are vital electric energy conversion devices that have been increasingly applied to renewable energy conversions or electric drive systems in modern industry (wind turbine, tide power generation, hybrid electric vehicle/train/ship). Condition monitoring and health management of these devices is very important in industry since it predicts and prevents any huge damages to them and can save a lot of money and time. Ignoring the importance of science in designing a system reduces the reliability and increase the risk of failure. As an example, the generator bearings installed in one of the wind farm's turbines in Oregon first failed in May 2006, 11 months after the turbine was brought online [1]. A failed 1.5 MW generator can account for over $48,000 of lost revenue if down for a month and repair costs can add up to as much as $50,000.

As emerging and not being a mature enough technology which is applied to critical service system in daily life, electric motors need precise control and accurate health monitoring for safe and reliable operation. Fault diagnosis, as the earliest step of system health management, identifies impending faults through pre-specified indexes. This is a critical process as it provides early warnings for catastrophic failures well beforehand and enables preventive maintenance schedule updates. The most important advance in this field is the implementation of fault diagnosis system embedded to drive system. In this technology, the health monitoring system is programmed in the main CPU used for controlling purposes. Also, there is no need to install any additional sensor since the same measurement used for control is sent for monitoring. This

technology is growing up and still is not mature enough to be used in industries widely. The main problem about them is the lack of memory to be used for the online sampled data. There are several solutions to overcome this problem. The main one is to find new fault diagnosis methods which need less memory and is feasible by improving the fault modeling approaches and using advanced signal processing techniques. Another solution is to use new CPUs which are faster and have more storage capacity.

The goal of health monitoring systems is to ensure the proper operating of the system and to protect the system at the instant of failure. This goal is achieved by providing information that indicates system anomalies. Having informative data from the operating system keep operators informed about the system status and assist them to take proper remedial actions in advance of any catastrophic failure.

Depending on the available information from the system, the features of the information which are used for evaluation, the fault modeling technique and the evaluation techniques the success level of a fault diagnosis system is defined.

The main motivations behind this research are summarized below to fill a major gap in electric motor health monitoring systems:

- Continuous monitoring of electric motors improves safety and prevents costly shutdowns.
- A proper health monitoring and fault diagnosis system cut unplanned maintenance, extends the meantime between failures, improve the overall equipment effectiveness and helps the productions to meet their schedule.

- The condition of electric motors without on-line health monitoring system has to be observed through external devices and additional sensors. Integrating the fault diagnosis system with motor controller reduces the size and cost of the whole system and improve the overall reliability.

1.2 Aims and Objectives

Objective 1: In order to diagnose any type of fault in electric motors, it has to be analyzed and investigated. The main objective of this research is to model and analyze different types of fault occurred in permanent magnet synchronous motors (PMSM). This analysis can help to understand the effect of different faults on the motor variables and parameters.

Objective 2: Every PMSM has different specifications such as different number of slot and pole or winding configurations, the proposed model should be adjustable to verify the effect of these parameters of the fault related indexes.

Objective 3: The amplitude of any fault indexes in motor variables such as frequency signatures in stator current are affected by the control parameters. To scrutinize the effects of controller on any fault related signatures in the stator current of PMSM, both motor and controller together has to be modeled. This modeling should describe the behavior of fault indexes in the stator current with respect to controller's parameter variation.

1.3 Literature Review

Thanks to increasing the demand on higher efficiency and power density, permanent magnet (PM) motors have been in the limelight in many industrial applications such as wind turbines,

pumps and electrical tractions, etc. [1]. As a natural consequence of this trend, PM motor condition monitoring has been becoming an emerging technology that improves the overall reliability of drive systems [2-3]. Various faults are possible to occur in the permanent magnet (PM) motors where some of which are more common and critical, and naturally are of interest in the recent diagnosis studies. Eccentricity faults, demagnetization, unbalanced magnetic pull, winding fault, and inverter faults are some of common faults in PM motors [4]. Various methods are proposed in the literature to detect faults in electric motors including vibration monitoring [5], [6], search coils [7], stator current sequence components [8], motor current signature analysis, [9, 10], residual stator current based on the difference between the actual and estimated current [11], instantaneous power [12], time delay embedding and stator inductances [13]. Additionally, there are some observer based methods such as model reference adaptive system observer proposed in [14] to detect the open phase fault of a permanent magnet motor. These methods enable successful fault signature monitoring but mostly focus on particular case studies and operating points. There is a huge research gap to generalize all the findings in the literature. Rotor fault including static and dynamic eccentricity and broken magnet are studied in [15] and motor current signature analysis (MCSA) is used to detect the fault in a low power PM motor. A very simple and low cost model reference adaptive system (MRAS) based is proposed in [16]. This model is used to detect the open phase fault in a BLDC motor which is driven through six-step control. In most of these discussions specific motors are tested for certain faults under specific operating points, hence not easy to generalize the findings for various PM motors. In [17], the effect of winding configuration on the harmonic content of stator current and zero voltage sequence component due to demagnetization fault is discussed and simulated. Accurate,

simple and efficient magnetic-field solution requirements have been driving the research on numerical and analytical methods [18].

Among all rotor faults, magnet related faults are one of the most widely encountered fault types in permanent magnet motors which are classified as partial [19] and uniform or full demagnetizations [20] depending on the defect distribution. Magnet defects are caused by mechanical, electrical and thermal stresses; and results in reduced performance, torque ripples, high q-axis current, acoustic noise to name a few.

In order to identify magnet related issues, the indexes in current [21], voltage [22], magnet flux [23] and torque [24] have been investigated in detail. Among the alternatives, stator current analysis has been one of the most popular one since it is relatively easier to analyze and readily available in most applications for control purposes. However, there are some certain cases where the magnet defect signatures may significantly change the current spectrum [25] which led some studies introduce various signatures and patterns. The zero sequence voltage components (ZSVC) is an example which is introduced in [22] to detect the demagnetization fault. This voltage is the difference potential between motor and source neutral voltage. It is shown that the third and fifth harmonics in this voltage spectrum are proper indexes to detect the magnet defect fault. Moreover, the stator winding configuration effect on the appeared harmonic orders in the stator current and ZSVC is investigated in [26, 27]. But theoretically no mathematical equation is presented to relate the harmonic amplitudes to the motor parameters [28].

In addition to fault diagnosis and classification, the fault severity assessment is the next essential step in the health management process. Depending on the motor, certain responses to impending faults and corresponding signature amplitudes should be classified to obtain fault severity index.

Unlike diagnosis techniques, the fault severity assessment has not been studied in detail for PM motors, and there is a huge room for research to set a meaningful motor specific threshold and minimize false alarms. Though the expected signatures introduced by magnet faults are well-known, it is still a very challenging task to report the severity of the fault based on the signature amplitude. In particular, developing a plug-in algorithm for motor drives that can be used for a random motor is quite complicated since each motor responds differently and generates signatures with different amplitudes. One approach is to create a rich database and propose a statistical approach based on the collected data. This approach is not very practical due to challenges in collecting experimental data from several artificially modified PM motors. Considering the structural and design variations in PM motors, correlating the signature amplitude to fault severity is another aspect of this challenge. In addition, the signature amplitudes are dynamic in adjustable speed motor drives and highly depend on operating point which makes the problem more complicated. Another aspect of this challenge is the impact of controllers in control loops. Though partially investigated for asynchronous motors, the effects of controllers on magnet defect fault signatures in PM motors haven't been investigated, which can significantly change the fault response and result in false alarms.

As well known, magnetic equivalent circuit (MEC) is used to analyze electromagnetic systems and electric machines such as transverse flux machines [29], switch reluctance motors [30] to name a few. This technique is also applicable for practical design of more complicated multi-phase motors Figure 1.1 [31], [32]. Several numerical approaches are used in analyses such as finite difference method, finite element method, boundary element method, point mirroring method. Among those magnetic equivalent circuit technique is one of the most popular

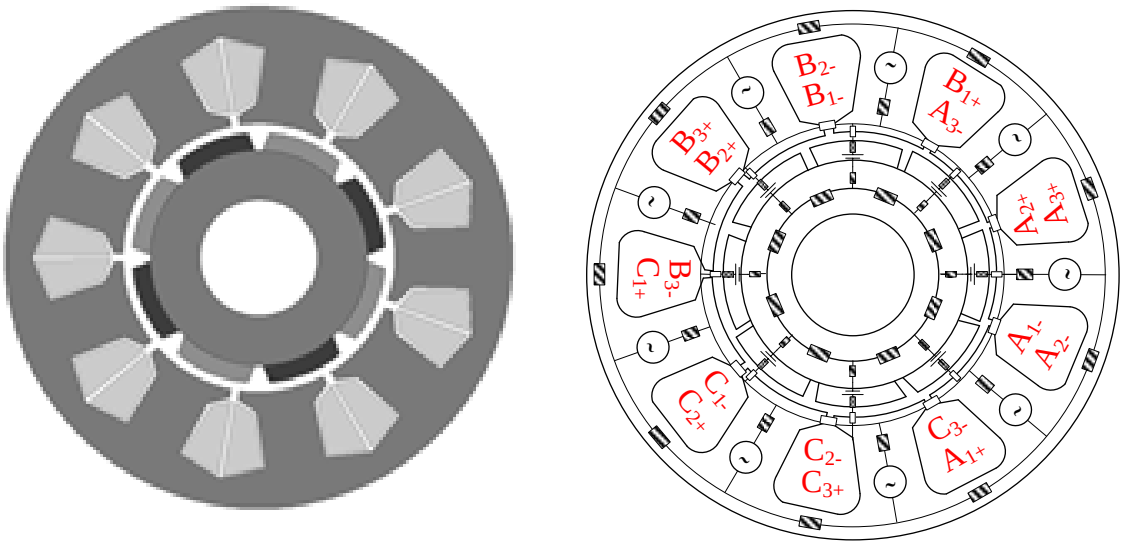

(*a*) (*b*)

Figure 1.1. a) A PMSM model in FEA b) MEC model of the PMSM

alternatives which is able to reduce computational burden [33] and has sufficient accuracy for design, electromechanical analysis and fault diagnosis.

1.4 Outline of the Dissertation

In Chapter 2, an analytical approach based on the partitioned magnetic equivalent circuit is presented to analyze magnet defects in the PM motors and observe the corresponding effects on the stator back-emf waveforms. In particular, it is employed to analyze magnet defect faults and describe the behavior of faulty motor by separating the individual effect of coils and magnets. The proposed method helps to explain the differences in the current spectrum of PM motors with various winding configurations as well. In addition to the amplitude of the fault signatures, the phase angles of fault related harmonics can be calculated which helps to clarify the minor discrepancies between current spectrum and back-emf spectrum of faulty PM motors and missing current spectrum components. Furthermore, the fault signatures generated by different

number and location of damaged magnets on the rotor can be identified. Finally, different crack types are examined to investigate the effect of crack shape and direction.

In Chapter 3, it is justified that the proposed approach can provide details regarding topology dependencies and yield consistent results with finite element tools and experiments. Topology dependent analysis is presented including different number of pole and slot, various numbers of defected magnets and different winding connections. 2-D finite element method is used to compare the findings and analyze the effect of fault. An experimental setup has been prepared to validate the analysis and simulation results.

The effect of Field Oriented Control (FOC) coefficients and motor parameters on fault related tones is scrutinized in Chapter 4. In this chapter, a motor specific fault severity assessment method is proposed which calculates the amplitude of magnet defect fault signatures in the stator current and back-emf through given machine parameters of PM motor. The operating point and current loop controller gain dependency are also investigated to achieve a complete and practical assessment, and hence determine the corresponding threshold for monitored fault levels. In order to verify the results, a three phase PMSM is modeled using finite element analysis (FEA) and 7% of one magnet is removed to model the magnet faults. Furthermore, the fault severity impact on the current and voltage signatures is studied using FEA. For this purpose, the fault intensity imposed to a motor is increased in four steps by removing 25% of one magnet at each step. Throughout each fault level, the simulations are carried out at different operating points to obtain a comprehensive severity assessment for magnet faults in PM motor.

CHAPTER 2

MAGNET DEFECT FAULT ANALYSIS USING MAGNETIC EQUIVALENT CIRCUIT METHOD[1,2]

2.1 Stator Flux Linkage Calculation

The fault related signatures raising in the motor variables spectrums are mainly due to air-gap flux density changes which are created by the magnet defects. These signatures can be obtained by calculating no load stator flux linkage at healthy and faulty conditions.

For this purpose, the stator flux linkages due to each individual magnet is calculated separately using presented MEC model and then the net flux linkage is obtained by iterative process for superposition. This approach helps to characterize any magnet defect in various PM motors topologies. This method can also be employed to investigate the electromagnetic reflections of multiple faulty magnets on stator flux linkage and back emf.

In order to analyze the effects of magnet faults, the permanent magnet synchronous motor (PMSM) depicted in Figure 2.1.a is employed in theoretical and experimental case studies. Electrical and mechanical motor parameters are given in Table 2.1.

---

[1] © 2016 IEEE. Reprinted, with permission, from M. Zafarani, T. Goktas and B. Akin, " A comprehensive analysis of magnet defect faults in permanent magnet synchronous motors," in IEEE Transactions on Industry Applications, vol. 52, no. 2, pp. 1331-1339, March-April 2016.

[2] © 2015 IEEE. Reprinted, with permission, from M. Zafarani, T. Goktas and B. Akin, " A comprehensive analysis of magnet defect faults in permanent magnet synchronous motors," 2015 IEEE Applied Power Electronics Conference and Exposition (APEC), Charlotte, NC, 2015, pp. 2779-2783.

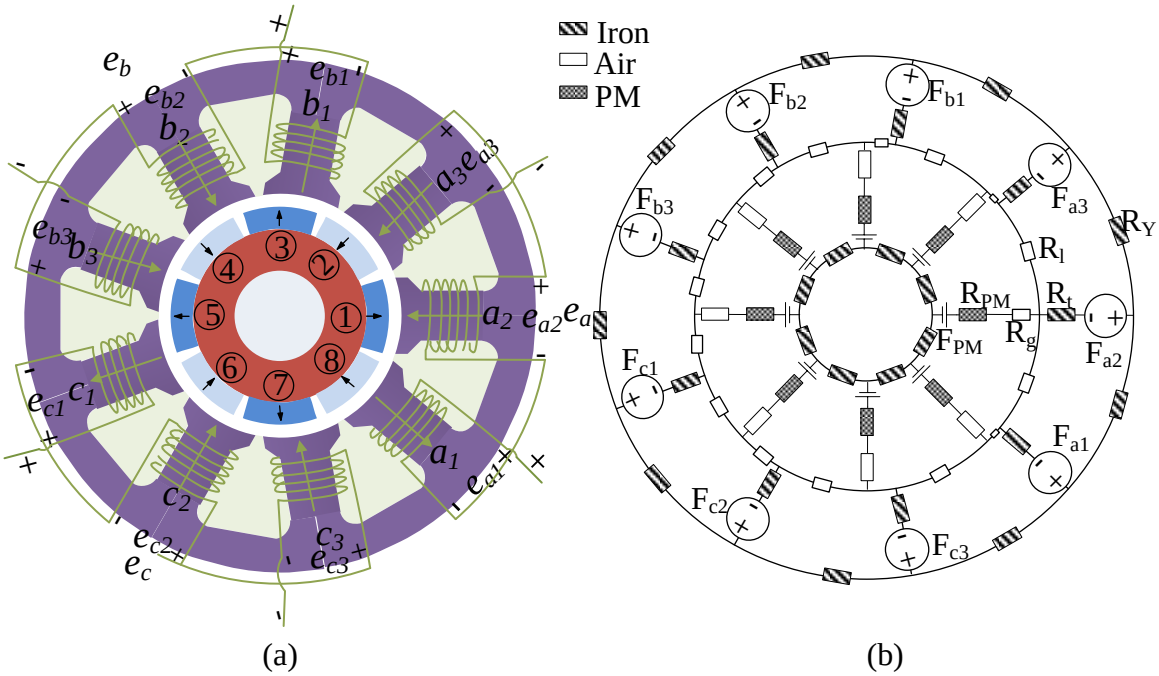

Figure 2.1. Side view of a) motor winding/magnet configuration b) corresponding magnetic equivalent circuit

Table 2.1. Electrical and mechanical parameters of PMSM

Parameter	Value	Dimension
Rated voltage	133	V
Rated current	2.8	A
Rated torque	1.27	Nm
Rated speed	3000	Rpm
Number of poles	8	-
Number of stator slots	9	-
Number of stator turn	71	-
Stator resistance	2.25	Ω
Stator outer diameter	56	mm
Rotor outer diameter	28	mm
Air-gap length	0.5	mm
Stack length	60	mm
Stator yoke length	3	mm
Rotor shaft diameter	6.5	mm

The motor is a three phase PMSM consisting of distributed double layer winding with 9 stator slots and 8 poles. Each magnet on the rotor is cut into two pieces along through the shaft axis to minimize the eddy current losses. Figure 2.1.b shows the magnetic equivalent circuit of the test motor with distributed winding on the stator which includes the air, core and PM reluctances. Initially, the motor is assumed to be slot less and the iron cores have infinite permeability.

Following the air-gap flux density calculations, the effect of stator slots is taken into account using slot correction factor. As the PMs are on the rotor surface, the equivalent air-gap is quite large, saturation level is negligible and superposition of variables is possible [24]. Even though the slot effects and corresponding reluctances are neglected at this stage, they will be taken into account later. Initially, the stator windings flux linkage due to each magnet is calculated separately to model magnet defect faults. The equivalent reluctances are calculated through (2.1)-(2.4).

$$F_{PM} = H_c l_{PM} \tag{2.1}$$

$$R_{PM} = \frac{l_{PM}}{\mu_0 \mu_{rPM} A_{PM}} = \frac{l_{PM}}{\mu_0 \mu_{rPM} r_g l_{st} \theta_{PM}} \tag{2.2}$$

$$R_{g1} = \frac{g}{\mu_0 A_{g1}} = \frac{g}{\mu_0 r_g l_{st} \theta_{PM}} \tag{2.3}$$

$$R_{g2} = \frac{l_{PM} + g}{\mu_0 A_{g2}} = \frac{l_{PM} + g}{\mu_0 r_g l_{st} \left(2\pi - \theta_{PM}\right)} \tag{2.4}$$

where R_{g1} is the reluctance of the air-gap over one PM and R_{g2} is the reluctance of the rest of the air-gap considering the PMs as air and A_{g1} and A_{g2} are the corresponding areas. For the sake of simplicity, the leakage reluctances are neglected. The length of the first gap is the same as the

air-gap and the length of the latter one is the combination of air-gap and the length of PMs. The flux densities in these two air-gaps are calculated through (2.5)-(2.8).

$$\varphi = \frac{l_{st} r_g \theta_{PM} \left(1 - \left(\theta_{PM} / 2\pi\right)\right)}{1 + \mu_{rPM} \left(g / l_{PM}\right) + \left(\mu_{rPM} - 1\right)\left(\theta_{PM} / 2\pi\right)} B_r \tag{2.5}$$

$$B_{g1} = \frac{\varphi}{A_{g1}} = \frac{\left(1 - \left(\theta_{PM} / 2\pi\right)\right) B_r}{1 + \mu_{rPM} \left(g / l_{PM}\right) + \left(\mu_{rPM} - 1\right)\left(\theta_{PM} / 2\pi\right)} \tag{2.6}$$

$$B_{g2} = \frac{\varphi}{A_{g2}} = \frac{\left(\theta_{PM} / 2\pi\right) B_r}{1 + \mu_{rPM} \left(g / l_{PM}\right) + \left(\mu_{rPM} - 1\right)\left(\theta_{PM} / 2\pi\right)} \tag{2.7}$$

$$B_g = \begin{cases} B_{g1} & \theta_r - \frac{\theta_{PM}}{2} \le \theta \le \theta_r + \frac{\theta_{PM}}{2} \\ B_{g2} & other \end{cases} \tag{2.8}$$

where B_g is the function of the air-gap flux density with respect to the stator space angle θ and electrical rotor position θ_r , and B_{g1} and B_{g2} are the flux densities in the two air-gap sections. The effect of the stator slots is taken into account by considering correction factor [25] which is given in (2.9).

$$B_{g-new}\left(\theta, \theta_r\right) = k_{sl}\left(\theta\right) B_g\left(\theta, \theta_r\right) \tag{2.9}$$

where $B_{g\text{-}new}$ is the air-gap flux density taking the effect of stator slots into account, k_{sl} is the slot correction factor (2.10) and k is the air- gap ratio defined in (2.11).

$$k_{sl} = \frac{\mu_{rPM}\, g + l_{PM}}{k\, \mu_{rPM}\, g + l_{PM}} \tag{2.10}$$

$$k = \begin{cases} 1 & |\theta| \le \theta_t / 2 \\ 1 + \frac{\pi}{2}\frac{r_g}{g}(\theta - \theta_t/2) & \theta_t/2 \le \theta \le \theta_s/2 \\ 1 - \frac{\pi}{2}\frac{r_g}{g}(\theta + \theta_t/2) & -\theta_s/2 \le \theta \le -\theta_t/2 \end{cases} \tag{2.11}$$

In this case, as each coil is turned around one slot, the flux linkage of a stator coil is the integral of flux on one tooth (2.12). This integral represents the flux which passes through the air-gap and links to a particular coil.

$$\lambda_{coil}(\theta_r) = N l_{st} r_g \int_{\theta=-\frac{\theta_t}{2}}^{\theta=\frac{\theta_t}{2}} B_g(\theta, \theta_r) d\theta \tag{2.12}$$

where λ_{coil} and N are the flux linkage and the number of turns of each coil. Now that the flux linkage of stator coils due to each magnet is calculated separately, the magnet fault can be introduced by changing the flux amplitude of the corresponding magnet. The net stator phase-a flux linkage is obtained as the cumulative flux linkage of each coil created by each magnet.

2.2 Mathematical Analysis of Magnet Defect Fault

Back-emf in PMSMs is the induced voltage across the stator phases due to relative change in rotor PM flux linking the stator coils. Mathematical definition of phase-a back-emf which is given in (2.13) as the rate of the flux linkage change in stator coils when the terminals are disconnected and the rotor is tested at constant speed.

$$e_a = \frac{d\lambda_{coil}}{dt} = \frac{d\theta_r}{dt}\frac{d\lambda_{coil}}{d\theta_r} = \omega_r \frac{d\lambda_{coil}}{d\theta_r} \tag{2.13}$$

As any fault on the rotor affects the flux density in the air-gap and is reflected to the back-emf, it is an ideal variable to analyze the rotor or stator faults. According to (2.13), when the motor operates at constant speed, any signature introduced into flux linkage will be reflected to the back-emf at the same frequency with 90^o phase shift. In order to define the fault related components, the back emf of each coil created by every single magnet are calculated individually. The fourier series of the induced voltage by all rotor magnets in the first coil of phase-*a* are written in (2.14) where the voltage in z^{th} coil induced by rotor magnets is the summation of all voltage components created by each magnet. In this equation $e_{azPM\text{-m}}$ represents the induced voltage in z^{th} coil of phase-a due to the magnet number m shown in Fig. 2.1.a, E_n is the amplitude of nth component of this voltage, θ_m is the mechanical rotor position, p is the number of rotor poles. The induced voltage changes in every rotational period because the fundamental frequency of the induced voltage in (2.14) is mechanical frequency. In order to mimic the effect of fault in the calculations, a fault coefficient, ki, is multiplied by each induced voltage before superposing as given in (2.15) where e_{az} and θ_{cz} are the induced voltage and the mechanical position of z^{th} coil of phase-a respectively and k_i is the normalized fault severity factor. Depending on the number of poles and slots, the coil angle changes and there is no unique way of calculating it [25].

$$\begin{aligned} e_{a1PM1} &= \sum_{n=-\infty}^{+\infty} E_n e^{jn\theta_m} \\ e_{a1PM2} &= \sum_{n=-\infty}^{+\infty} -E_n e^{jn\frac{360}{p}} e^{jn\theta_m} \\ &\vdots \\ e_{a1PMp} &= \sum_{n=-\infty}^{+\infty} -E_n e^{jn(p-1)\frac{360}{p}} e^{jn\theta_m} \end{aligned} \tag{2.14}$$

$$e_{az} = \sum_{n=-\infty}^{+\infty} \left(\sum_{i=1}^{p} (-1)^{i-1} k_i e^{jn(i-1)\frac{360}{p}} \right) e^{jn\theta_{cz}} E_n e^{jn\theta_m} \tag{2.15}$$

$$\theta_{cz} = (z-1)\frac{C_p}{N_s}360 \tag{2.16}$$

$$C_p = \left\lfloor \frac{N_s}{p} \right\rfloor \tag{2.17}$$

In this case, the coil angle is calculated through (2.16) where C_p is stator slot-pole ratio which is calculated through (2.17) and N_s is the number of stator slots. The induced cumulative voltage in one phase is the summation of all induced coil voltages considering the direction of the coils which is given in (2.18). As shown in Figure 2.1.a, the consecutive coils of each phase are in the reverse direction with respect to each other.

$$e_a = \sum_{n=-\infty}^{+\infty} E_n e^{jn\theta_m} \underbrace{\left(\sum_{z=1}^{N_{coil}} (-1)^{z-1} e^{jn\theta_{cz}} \right)}_{k_{san}} \underbrace{\left(\sum_{i=1}^{p} (-1)^{i-1} k_i e^{jn(i-1)\frac{360}{p}} \right)}_{k_{mn}} \tag{2.18}$$

The first part of (2.18), $E_n e^{jn\theta m}$ is related to the shape of induced voltage waveform in one coil and include all multiples of mechanical frequencies. This part can be calculated based on the procedures explained in the previous section and is related to the motor dimensions such as coil pitch, pole pitch and magnet dimension.

The second part, k_{san} –coil factor coefficient–, is related to the number and location of the coils in each phase (2.19). This coefficient for other phases has the same amplitude but a phase shift of 120^o mechanical degrees. This phase shift depends on the mechanical location of the stator

phases with respect to each other. In this case study, the three phases are located in a way that they have phase shift of 120^o mechanical and electrical degrees.

$$k_{san} = \sum_{z=1}^{N_{coil}} (-1)^{z-1} e^{jn\theta_{cz}} \tag{2.19}$$

The last part, k_{mn} corresponds to the number of the rotor magnets and the percentage of magnet defect. This coefficient is called magnet factor and is shown in (2.20).

$$k_{mn} = \sum_{i=1}^{p} (-1)^{i-1} k_i e^{jn(i-1)\frac{360}{p}} \tag{2.20}$$

It can be proved that in healthy condition when all k_i coefficients are one, for all values of n in (2.20), k_{mn} is zero except the odd multiple of $p/2$. But, in the faulty case, all components with the multiples of mechanical frequencies are involved in the back emf waveform. These harmonics follow a certain pattern and have a relation with mechanical and electrical frequencies as shown in (2.21) [5].

$$f_f = \left(1 \pm \frac{k}{p/2}\right) f_s = k f_m \qquad k = 1, 2, 3, \ldots \tag{2.21}$$

where f_f is the fault frequencies in the spectrum, f_s is the fundamental electrical frequency of the back-emf and f_m is the rotational frequency. In some cases, depending on the winding configuration or the type of fault, some harmonics are suppressed in either current or back emf which is discussed in the next sections. For other phases the back emf has the same equation with different coil factor which is shown in (2.22).

Table 2.2. Phase shift of harmonics in back-emf for 9-slot/8-pole motor

Harmonic order	Phase shifts between stator phases
0.25^{th}	120^o
0.5^{th}	240^o
0.75^{th}	0^o
1^{th}	120^o
1.25^{th}	240^o
1.5^{th}	0^o

$$e_b = \sum_{n=-\infty}^{+\infty} k_{mn} k_{sbn} E_n e^{jn\theta_m}$$
$$e_c = \sum_{n=-\infty}^{+\infty} k_{mn} k_{scn} E_n e^{jn\theta_m} \quad (2.22)$$

Briefly, in order to investigate magnet defect fault, the induced voltage in the stator coils due to each rotor magnets is calculated separately. For this purpose, first the induced voltage in an individual stator coil is calculated using MEC. Then the whole induced voltage in each phase is extracted using coil and magnet coefficients, where the effect of fault is involved in magnet coefficient terms.

According to the abovementioned equations, k_{mn} is the coefficient corresponds to the fault related harmonics and is common in all three phases. On the other hand, the coil factor corresponds to the phase difference between stator phase variables. Table 2.2 shows the phase shift between the same back emf harmonics in different stator phases. It can be seen that the fault signatures at 0.75^{th} harmonic and multiples of it (triplen multiples of the mechanical frequency) has the same phase shift in between phases. This finding is very useful for the separation of PMSM faults which is partially discussed in the following sections.

Table 2.3. Normalized product of coil factor and magnet coefficient for different number of poles and slots

		$\lvert k_{mn}\, k_{san}\rvert$							
N_s	p	$1/(p/2)$	$2/(p/2)$	$3/(p/2)$	$4/(p/2)$	$5/(p/2)$	$6/(p/2)$	$7/(p/2)$	$8/(p/2)$
9	6	0	0	1	0	0	0	0	0
9	8	0.02603	0.03193	0.09785	1	0.1409	0.09785	0.03193	0.02603
12	8	0	0	0	1	0	0	0	0.1429
12	10	0.02976	0	0.0813	0	1	0	0.1111	00
15	8	0.01609	0.02196	0.0951	1	0.02939	0.03633	0.01502	0.01502
24	8	0	0	0	1	0	0	0	0
48	8	0	0	0	1	0	0	0	0

2.3 Different Number of Poles and Slots

In order to investigate the magnet faults comprehensively and verify the proposed analytical approach, various topologies with different number of poles and slots are analyzed through the aforementioned process. Though the proposed method is applicable for all kinds of winding configurations, here, the test motor's double layer winding configuration is taken as reference. According to (2.18) and (2.22), the multiples of coil and magnet related coefficients define the amplitude of fault harmonics. Table 2.3 shows the results of this product for different number of poles/slots and associated fault harmonic when one rotor magnet is damaged. As seen here, if the slot-pole ratio is integer multiple of 3/2, the product of these two coefficients results in fault related harmonics' elimination. In other cases, the fault signatures following the pattern given in (2.21) appear in the back-emf. This fact explains the case discussed in [11] where the fault signatures in the back-emf of an 18 slot and 6 pole motor do not exist. Hence, zero sequence

voltage component (ZSVC) analysis is proposed to detect the demagnetization fault in that particular motor.

2.4 The Effect of Winding Connection

The additional harmonics created by magnet faults in the flux and back-emf are the source of fault signatures in the stator current. However, in some situations some of these harmonics do not show up in the current spectrum though they do exist in back-emf spectrum. If all three phases are perfectly balanced and the overall system is uniform throughout the air- gap, the in-phase harmonics will not flow in a star connected motor windings. As derived before, the coil factor represents the phase shift between stator phases for different harmonics. When there is magnet fault on the rotor, all the components at the multiples of mechanical frequency can be observed in back- emf spectrum. These harmonics in the stator phase back-emf are the source of the harmonics in the stator phase current and both variables' spectrums should be very similar to each other. However, in a star connected balanced three phase system with floating neutral point, the harmonics having the same phase angle with respect to each other cannot flow. In this case, according to the theoretical derivations, the 0.75^{th} component and it's multiples in the back-emf have the same phase angle in all three phases which significantly suppress them depending on the inherent unbalance in motor. Table 2.2 shows the phase difference between phase a and b back-emf in the case of 9 slots and 8 poles. As it is shown, the triplen multiples of the mechanical frequency have the same phase shift in both phases which means that this component

(a) (b) (c)

Figure 2.2. Different type of crack a) Horizontal b) Vertical c) Zigzag

will not appear in the current spectrum. On the other hand, in a delta connected three phase motor spectrum, this is not the case and harmonics with any phase shift with respect to each other can be observed in stator phase current spectrum.

2.5 Simulation Results

In this section, the effect of magnet defect faults on the stator currents are simulated by means of MEC and compared to FE results. The magnet defect is modeled in Ansys-Maxwell software by removing certain part of a magnet. This segregated part can be in different sizes and directions. In order to investigate the effect of crack direction, horizontal, vertical and zigzag type cracks are created to clarify whether the length or the width of the crack has more effect on the signatures. In the experimental setup, 7% of the rotor magnet is removed carefully through a fine cutter vertically. To be consistent with the experimental setup, in each simulation, 7% of the magnets have been removed which the same percentage of the removed part in the test motor rotor as shown in Figure 2.2 The motor variables are normalized with respect to rated current in all simulation and experimental results and given in per-unit.

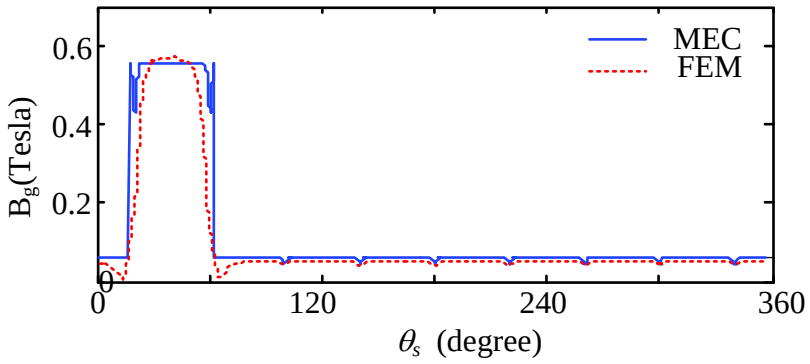

Figure 2.3. Air-gap flux density when the rotor is located at θ_r=42.5^o

2.5.1 Simulation Results for Back-emf

In order to verify the validity MEC and MEC based discussions, the test motor simulated using finite element software as well and the results are compared to each other. For instance, the air-gap flux density due to one magnet when the rotor is located at θ_r=42.5^o is shown in Figure 2.3 which is calculated through both analytical and numerical methods. As shown in this figure, the maximum error between two results is on the edges of stator teeth as expected due to rough slot approximations. It is possible to include further details for more accurate results; however, the approximations made in this study do not affect the fault analysis. Because the flux linkage is integration of flux density, the higher order harmonics representing fine details are naturally filtered.

Figure 2.4 and Figure 2.5 show the frequency spectrum of phase-a back emf in healthy and faulty conditions obtained with MEC and FE methods, respectively. In magnet defect simulation, 7% of the magnet is cut vertically along through the shaft. Both simulations show that when just one defective magnet, all side bands of fundamental and low order harmonics given in (2.21) increase.

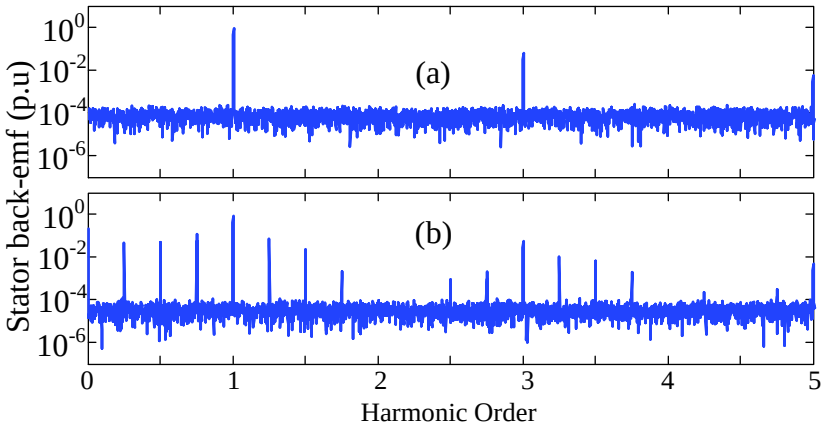

Figure 2.4. Stator back-emf spectrum at rated speed, MEC results a) Healthy b) Faulty

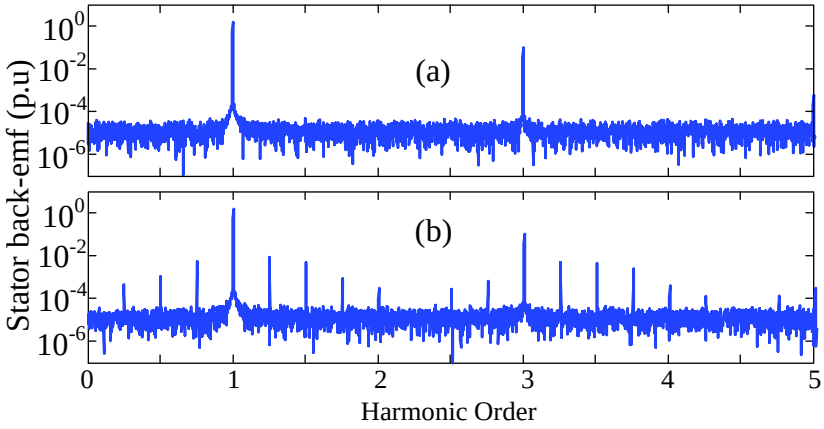

Figure 2.5. Stator back-emf spectrum at rated speed, FE results a) Healthy b) Faulty

2.5.2 Location and Number of Magnet Defects

The number and location of the magnet defects affecting the signature content in the motor variables can easily be analyzed through MEC. When there is only one magnet defect, pre-defined harmonics pattern in (2.21) appear in the back-emf spectrum. In the case of two or more defects, depending on the location of the magnets, the spectrum can be different. Here, it is assumed that the severities of faults in all magnets are exactly the same. If two magnets magnetized in opposite direction have defects, the spectrum does not change. However, if two consecutive magnets with the same magnetization direction have defects (e.g. magnet 1 and 3 in

Figure 2.1.b), the odd multiples of 0.5th harmonic disappear from the spectrum as shown in Figure 2.6. If the defects are on the opposite magnets on the rotor (e.g. magnet 1 and 5) then flux linkage spectrum does not include the odd multiples of 0.25^{th} harmonic as shown in Figure 2.7. Likewise, if the consecutive pole pairs have defects (e.g. magnets 1-2 and 5-6), then the back emf has the same spectrum as in Figure 2.7.

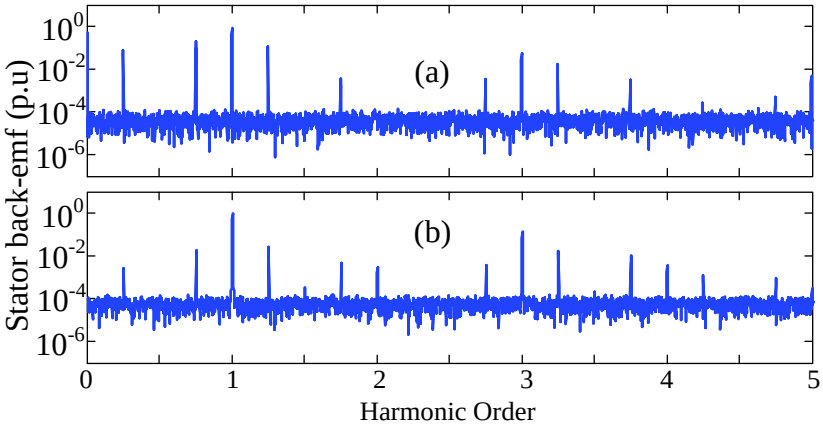

Figure 2.6. Phase "a" back emf spectrum when magnet number 1 and 3 are faulty a) MEC result b) FE result

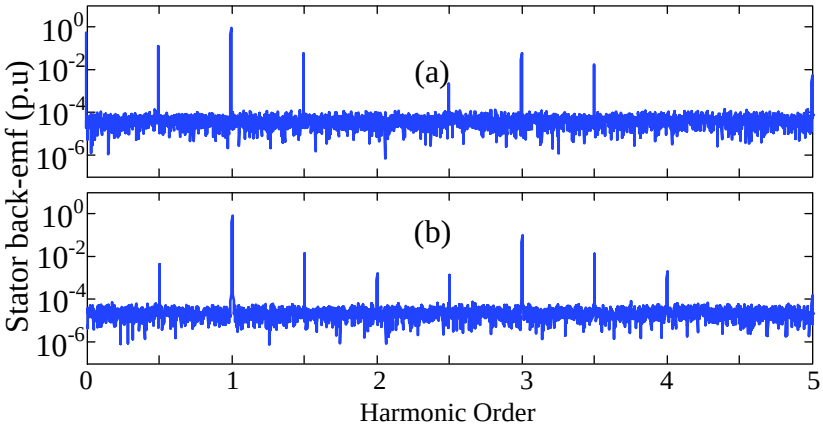

Figure 2.7. Phase "a" back emf spectrum when magnet number 1 and 5 are faulty a) MEC result b) FE result

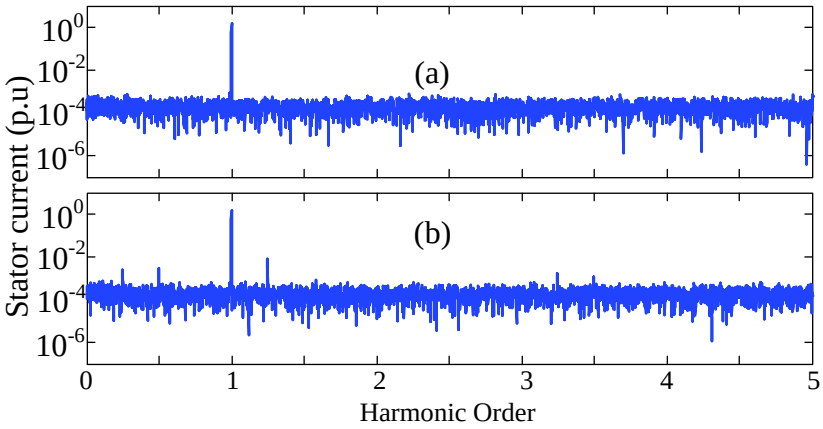

Figure 2.8. Stator current spectrum at rated speed and rated torque, FE results a) Healthy b) Faulty

These two cases follow the same defect pattern, and therefore they exhibit similar behaviors. If all the magnets with the same polarity have defects, the spectrum looks the same as the healthy case without any additional signature. If more than half of the magnets are damaged, the same fault patterns are observed for each complimentary version of aforementioned scenarios.

For instance, for six cracked magnets, the spectrum is the same as two defect case. If all magnets have the same defect, then none of the signatures can be observed in the spectrums.

In healthy motor, though the applied voltage or back-emf may include third harmonics as shown in .a and .a, these harmonics are not observed in the stator phase current since the winding is star connected with floating neutral point. Similarly, as shown in .b and .b, faulty motor back-emf spectrum includes all fault related side band components including triplen multiples of the mechanical frequency (i.e 0.75^{th} and its integer multiples). However, these sidebands do not appear in the current spectrum as depicted in Figure 2.8 since they have the same phase in all three phases as shown in Table 2.2 and cannot flow in a star connected system. According to the simulation results obtained under different load and speed conditions, the most affected and

responsive harmonics in magnet defect fault are 0.25^{th} and 0.5^{th}. Other components are also affected but not as much as these two components.

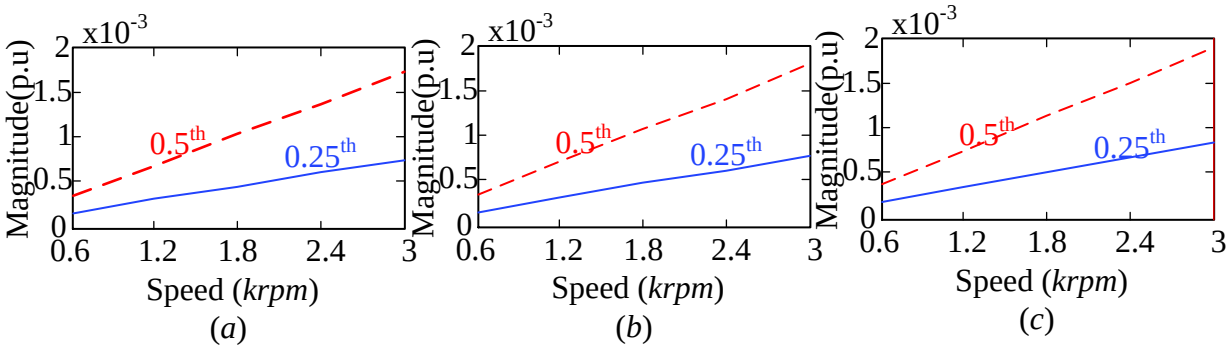

Figure 2.9. Simulation results, the behavior of fault related harmonics in back-EMF at different speeds, a) Vertical crack b) Horizontal crack c) Zigzag crack

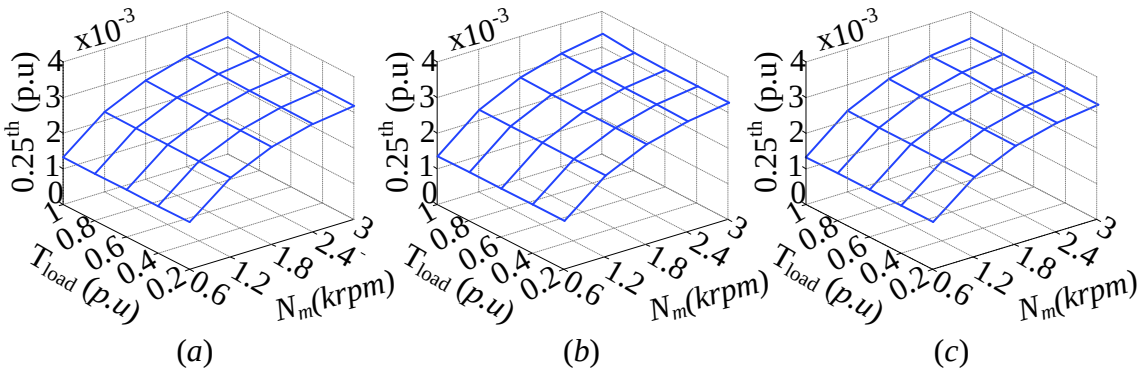

Figure 2.10. Simulation results, the behavior of 0.25^{th} harmonic in phase current, a) Vertical crack b) Horizontal crack c) Zigzag crack

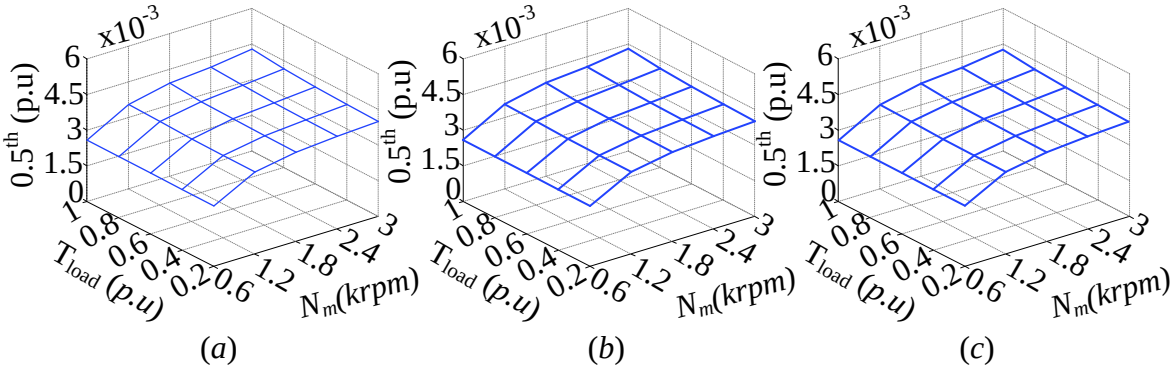

Figure 2.11. Simulation results, the behavior of 0.5^{th} harmonic in phase current, a) Vertical crack b) Horizontal crack c) Zigzag crack

The effect of load and speed on these two components in both stator phase current and back-emf are investigated, and the results are shown in Figure 2.9 to Figure 2.11. The signature amplitudes in back-emf with respect to the rotor speed is shown in Figure 2.9. The change in amplitude is almost linear and the differences in between two signatures are reasonable because of flux linkage derivative terms. Figure 2.10 and Figure 2.11 summarize several simulation results run under various load-speed conditions to analyze the effects of crack types on signature amplitudes. The behaviors of the most responsive harmonics show that magnet defect fault signatures are more speed dependent than torque. According to simulation results, the dynamic current signature behaviors are nearly the same for all crack types. This shows that the fault signatures do not remarkably depend on the direction, length or shape of crack. After making several experiments, it is concluded that the most significant parameter in magnet defect faults is the overall volume of the crack.

2.6 Experimental Results

In order to justify the simulation results, one of the rotor magnets is cut vertically using a fine cutter and is tested under different speed and torque conditions. Figure 2.12 shows the healthy and broken magnet fault rotor. An experimental setup is prepared which is shown in Figure 2.13. The test motor on the setup is the PMSM with the specification is given in Table 2.1. The motor is coupled with a high-end hysteresis dynamometer to apply adjustable load and measure shaft torque and speed. In order to measure and store the current data for post processing, NI USB-6351 data acquisition board is used providing 16 bit resolution and up to 1MS/s sampling rate. Both faulty and healthy motors are run at 5 different speed and torque levels. Figure 2.14 shows the measured back-emf spectrum of faulty and healthy motor at rated speed.

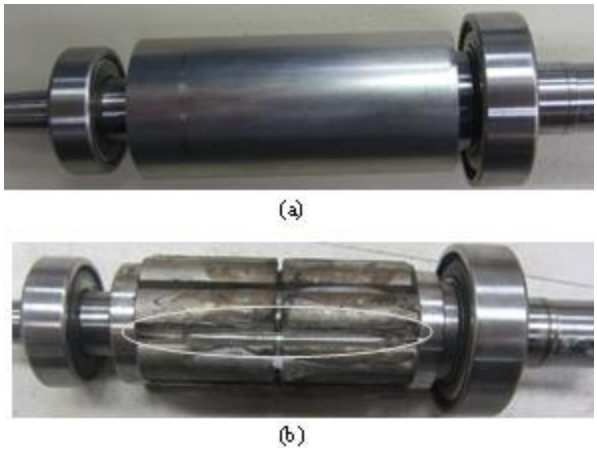

Figure 2.12. a) Healthy motor with rotor cover b) Vertically cut magnet

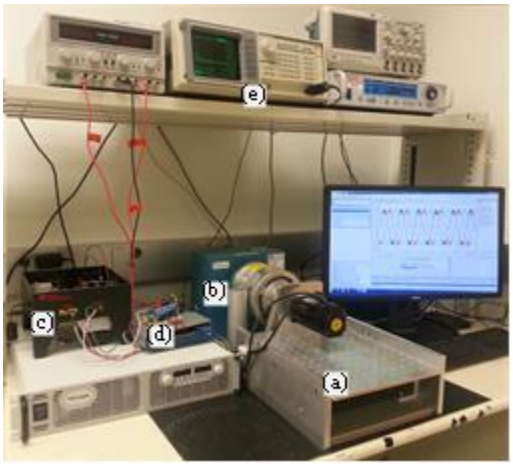

Figure 2.13. Experimental setup a) PMSM b) Dynamometer c) Motor drive d) Data acquisition e) Spectrum analyzer

In healthy motor spectrums, the signatures following the pattern (2.21) can be observed due to inherent manufacturing asymmetries. In a faulty motor spectrum, these harmonics increase significantly. The corresponding current spectrum for rated speed and torque are shown in Figure 2.15. In the current spectrum, the signatures at 0.75^{th} and 1.25^{th} harmonics do not change too much both for healthy and faulty cases (Figure 2.15). On the other hand, the introduced faults affect other harmonics, particularly 0.25^{th} and 0.5^{th} ones more than others as justified in the simulations as well.

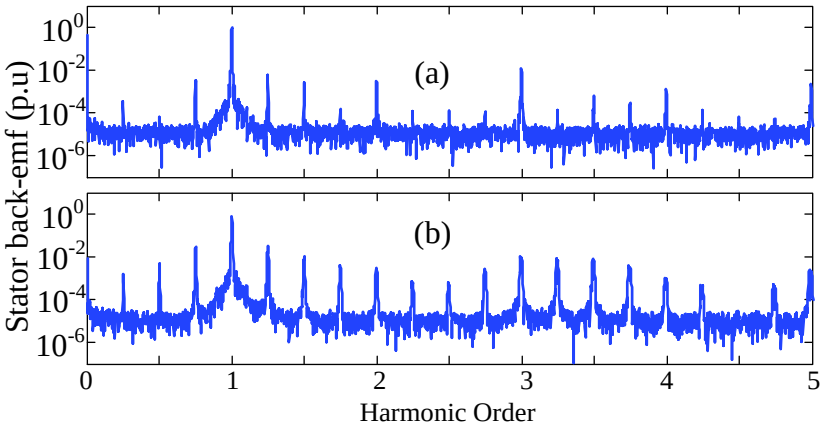

Figure 2.14. Stator back-emf spectrum at rated speed, experimental results a) Healthy b) Faulty

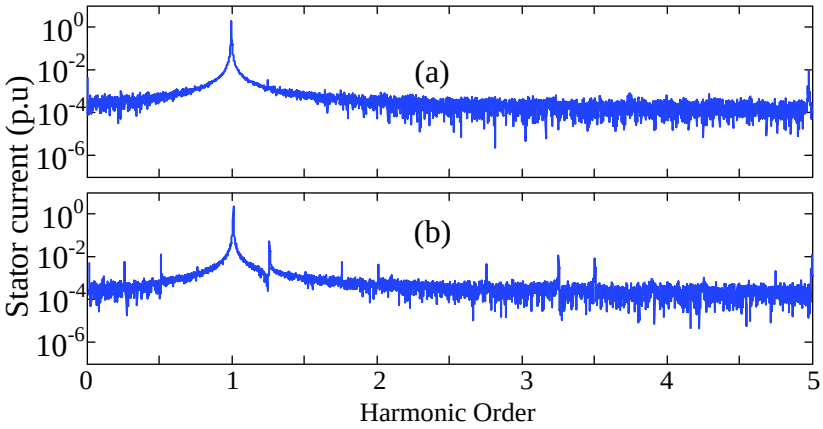

Figure 2.15. Stator current spectrum at rated speed and rated torque, experimental results a) Healthy b) Faulty

In addition, the magnet defect effect on the low order harmonics sidebands is also remarkable. For instance, the 3.25^{th} and 3.5^{th} harmonics can be considered as alternative indicators of magnet fault due to the significant change in their amplitudes. These components exhibit the same behavior in other magnet fault types as well. Figure 2.16 shows the variation of the most affected harmonics by magnet fault with respect to the speed and torque. Figure 2.16.a shows the variation of 0.25^{th} harmonic in the stator phase current. The amplitude of this signature increases linearly with respect to the speed like in simulations. In high speed region, the rate of signature change is less than the lower speed. Figure 2.16.b shows the behavior of 0.5^{th} harmonic in stator

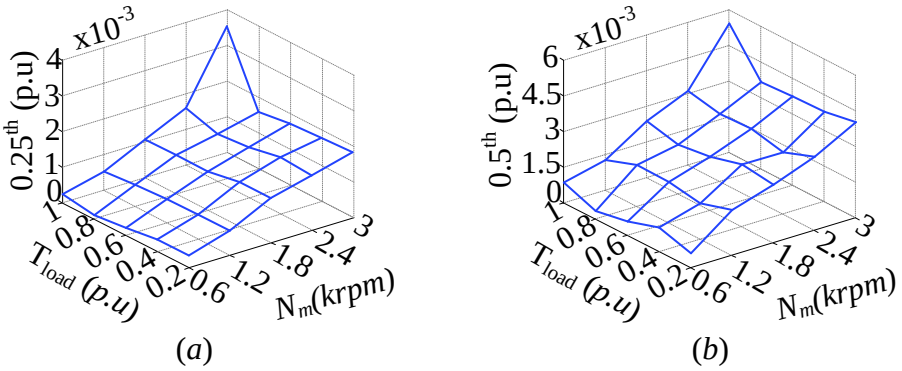

Figure 2.16. Experimental results, the behavior of fault harmonics in phase current under different speed and load conditions a) 0.25^{th} b) 0.5^{th}

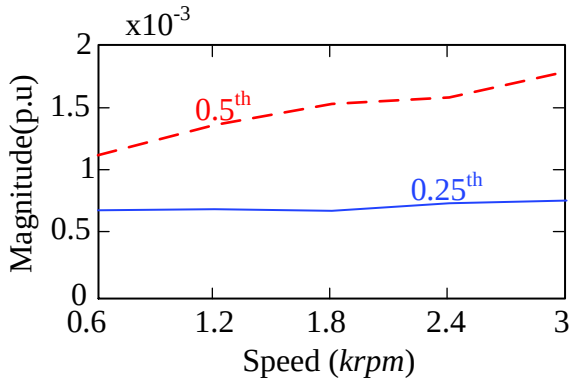

Figure 2.17. Experimental results, the behavior of fault harmonics in back-EMF at different speeds

phase current at different rotor speed and torque levels. Similar to the 0.25^{th} harmonic, this component is also speed dependent. The variation of these harmonics in the back-emf with respect to speed is shown in Figure 2.17 and is similar to the variation in stator current where at low speed range, the rate of magnitude change for both harmonics is more than the high speed range.

2.7 Conclusion

In this chapter, the effects of magnet defects on the stator phase back-emf and current is investigated through MEC. As an analytical tool, partitioned MEC is developed in a flexible

manner to investigate winding configurations and fault locations effect on the motor variable spectrums. Using the partitioned MEC, it is shown that the effect of each rotor magnet on each stator coil can be calculated to obtain the induced back-emf under various magnet defect combinations and observe the corresponding fault signatures in the frequency spectrum. In the case of multiple magnet defects, depending on the number and location of the defects, the back-emf and current spectrums vary. In addition, it is shown through the phase information of the fault signatures that, the signatures at triplen multiples of mechanical frequency disappear depending on the winding connection. If not taken into account, these missing or additional components may result in false alarms. After several tests including various shape and direction combinations, it is concluded that the direction or the shape of the crack has no additional effect on the current and back-emf waveforms where the only critical parameter found to be the overall volume of the magnets. The effects of load and speed on the amplitude of the faulty signatures are also studied to clarify the speed and torque dependency. The simulated fault scenarios are implemented on the experimental setup to show the consistency of simulations and experimental findings. It is shown that the key fault signatures are less torque more speed dependent which should carefully be taken into account for variable speed drive applications.

CHAPTER 3

AN INVESTIGATION OF MOTOR TOPOLOGY IMPACTS ON MAGNET DEFECT FAULT SIGNATURES[1,2]

3.1 PM MOTOR WINDING LAYOUT

In order to investigate the topology specific discrepancies of the fault reflections on the current or back-emf spectrums, it is necessary to analyze the machine design details and fault mechanisms together. Otherwise, as detailed in next sections, assuming that all three phase permanent magnet motors respond to the faults in the same manner leads to false or missing alarms. For this purpose, some of the design terms are revisited such as coil pitch which is the distance between two sides of an individual coil. Mathematically coil pitch is the round ratio of number of slots and poles defined in (3.1).

$$C_P = \left\lfloor \frac{N_s}{p} \right\rceil \tag{3.1}$$

If the ratio is an integer value then it is called full pitch, otherwise fractional pitch. Depending on the number of stator phase and winding layer, the number of coil per phase will be different which is defined in (3.2).

---

[1] © 2017 IEEE. Reprinted, with permission, from M. Zafarani, T. Goktas, B. Akin and S. E. Fedigan, " An Investigation of Motor Topology Impacts on Magnet Defect Fault Signatures," in IEEE Transactions on Industrial Electronics, vol. 64, no. 1, pp. 32-42, Jan. 2017.

[2] © 2016 IEEE. Reprinted, with permission, from M. Zafarani, T. Goktas and B. Akin, " A comprehensive assessment of PM motor topology impact on magnet defect fault signatures," 2016 IEEE Applied Power Electronics Conference and Exposition (APEC), Long Beach, CA, 2016, pp. 1096-1101.

$$N_{coil} = \begin{cases} \dfrac{N_s}{m} & Double\ layer \\ \dfrac{N_s}{2m} & Single\ layer \end{cases} \tag{3.2}$$

In order to clarify the winding design procedure in this paper [3.24], one of the test motors with 9 slots and 8 poles is depicted. Since it is a 9-slot, 3-phase motor and it is supposed to have a double layer winding, according to (3.2) totally there are 9 coils inside the motor which should be distributed between 3 phase which are connected in series. In order to connect 3 coils in series these three coils must have the same or similar electrical phase angle to get the maximum output voltage. The magnetic field vector is an index which shows the electrical phase shift of the coils with respect to each other. Figure 3.1 shows the magnetic field vector of a 9-slot/8-pole motor. As seen here, there are 18 vectors representing 9 coils. If this scenario is applied to other coils, the vectors are distributed in the space in a way that they divide the space into 18 regions shown in Figure 3.1. Here, 3 vectors which have space angle closer to zero are chosen for phase-a. Figure 3.2 shows the winding layout of the test motor with 9-slot/8-pole.

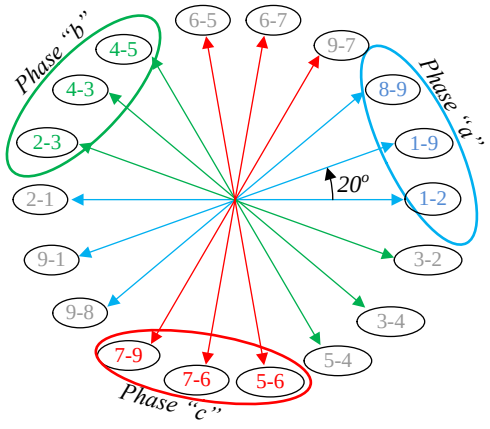

Figure 3.1. Coil magnetic field vectors of a double layer winding for a 9-slot and 8-pole PMSM, one of the test motors used in this study.

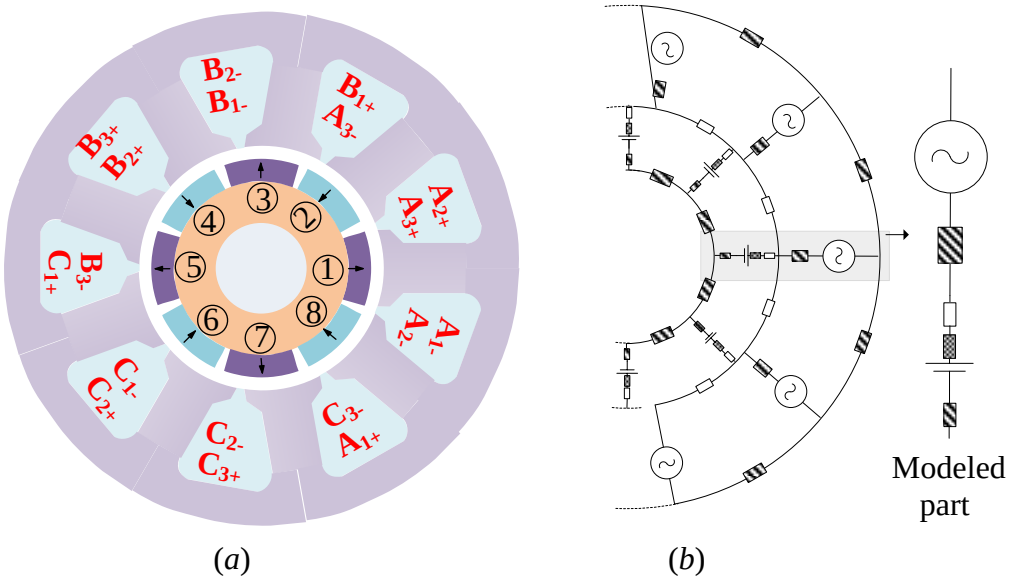

(*a*) (*b*)

Figure 3.2. Magnetic equivalent circuit of the test motor

As seen here, the three coils in each phase are in the same neighborhood and their magnetic vectors have 40° mechanical degree with respect to each other which cause elimination of some fault signatures as detailed in the next sections. Depending on the number of pole and slot, there are cases where some coils are located at the same electrical positions. For example, in the case of double layer, 36-slot and 6-pole, the number of coils in the motor is 36 and the number of coils located at the same electrical position (NSC) is 6 and there are 6 magnetic field vectors NSR. If the slot / pole ratio is multiple of 1.5 in a three phase double layer winding motor, the coils create only 6 vectors in the space which have 60 electrical degrees with respect to each other. The number of coils which are located at the same electrical position is calculated through

$$N_{SC} = \begin{cases} \gcd(N_s, p) & Double\ layer \\ \frac{1}{2}\gcd(N_s, p) & Single\ layer \end{cases} \tag{3.3}$$

$$N_{SR} = \frac{2mN_{coil}}{N_{SC}} = \frac{2N_s}{\gcd(N_s, p)} \tag{3.4}$$

(3.3) and the number of space division is calculated through (3.4).

3.2 Partitioned MEC Implementation

The magnetic equivalent circuit calculations are meant to obtain electromagnetic system variables theoretically. In order to understand the effects of magnet faults and dynamics of the corresponding signatures, basic MEC calculations are reorganized and resorted. This enables comprehensive understanding of each stator coils and rotor magnets interaction and its reflection on the induced back-emf voltage. This approach is very practical and useful to characterize any magnet defect in various PM motors topologies. In addition, it is used to investigate the electromagnetic reflections of multiple faulty magnets on the stator flux linkage and back emf, which is important to discern variable spectrums of motors with multiple magnet faults that are located at various rotor positions.

3.2.1 Stator flux linkage calculation

First, the stator flux linkages due to each individual magnet are calculated separately using MEC tools and then the overall flux linkage is obtained by superposing these components. In order to elaborate and justify the implementation, two PM motors including a permanent magnet surface mounted (PMSM) motor with 9-slot/8-pole, double layer winding and an interior permanent magnet (IPM) with 36-slot/6-pole, single layer winding are used. The specifications of these two motors are summarized in Table 3.1 and the magnetic equivalent circuit of the PMSM is shown in Figure 3.2.

Table 3.1. Specifications of the test motors

Parameter	PMSM	IPM
Rated voltage	133 V	360 V
Rated current	2.7 A	1.72 A
Rated torque	1.27 Nm	3.95 Nm
Rated speed	3000 rpm	3000 rpm
Number of poles	8	6
Number of stator slots	9	36
Number of stator turn	71	68
Stator resistance	2.25 Ω	4.28 Ω
Slot/Pole	9slots/8poles	36slots/6poles

In the following discussions, just one magnet and one coil are modeled before superposition. At this stage slot effects and associated reluctances are neglected which will be taken into account later. The equivalent reluctance and magnetic calculated through (3.5)-(3.8).

$$F_{PM} = H_c l_{PM} \tag{3.5}$$

$$R_{PM} = \frac{l_{PM}}{\mu_0 \mu_{rPM} A_{PM}} = \frac{l_{PM}}{\mu_0 \mu_{rPM} R_s L_{st} \theta_{PM}} \tag{3.6}$$

$$R_{g1} = \frac{Length}{\mu \times Area} = \frac{g}{\mu_0 A_{g1}} = \frac{g}{\mu_0 R_s L_{st} \theta_{PM}} \tag{3.7}$$

$$R_{g2} = \frac{l_{PM} + g}{\mu_0 A_{g2}} = \frac{l_{PM} + g}{\mu_0 R_s L_{st} \left(2\pi - \theta_{PM}\right)} \tag{3.8}$$

For the sake of simplicity, the leakage reluctances are neglected. The air gap reluctance is divided into two parts: the one over the stator teeth and the other one over the slot. The length of the former one is the same as the air-gap and the length of the latter one is the combination of

air-gap and the length of PMs. The flux densities in these two air-gaps are calculated through (3.9)-(3.12).

$$\varphi = Flux\ density \times Area = \frac{l_{st} r_g \theta_{PM} \left(1 - \left(\theta_{PM} / 2\pi\right)\right)}{1 + \mu_{rPM} \left(g / l_{PM}\right) + \left(\mu_{rPM} - 1\right)\left(\theta_{PM} / 2\pi\right)} B_r \tag{3.9}$$

$$B_{g1} = \frac{\varphi}{A_{g1}} = \frac{\left(1 - \left(\theta_{PM} / 2\pi\right)\right) B_r}{1 + \mu_{rPM} \left(g / l_{PM}\right) + \left(\mu_{rPM} - 1\right)\left(\theta_{PM} / 2\pi\right)} \tag{3.10}$$

$$B_{g2} = \frac{\varphi}{A_{g2}} = \frac{\left(\theta_{PM} / 2\pi\right) B_r}{1 + \mu_{rPM} \left(g / l_{PM}\right) + \left(\mu_{rPM} - 1\right)\left(\theta_{PM} / 2\pi\right)} \tag{3.11}$$

$$B_g = \begin{cases} B_{g1} & \theta_r - \dfrac{\theta_{PM}}{2} \le \theta \le \theta_r + \dfrac{\theta_{PM}}{2} \\ B_{g2} & other \end{cases} \tag{3.12}$$

where B_{g1} and B_{g2} are the flux densities in the two air-gap sections and B_g is the function of the air-gap flux density with respect to the stator space angle θ. The effect of the stator slots is taken into account by considering correction factor [3.24] which is given in (3.13).

$$B_{g-new}\left(\theta, \theta_r\right) = k_{sl}\left(\theta\right) B_g\left(\theta, \theta_r\right) \tag{3.13}$$

where $B_{g\text{-}new}$ is the air-gap flux linkage taking the effect of stator slots into account, k_{sl} is the slot correction factor (3.14) and k is the air- gap ratio defined in (3.15), θ_t and θ_s are the stator tooth and slot pitch.

$$k_{sl} = \frac{\mu_{rPM}\, g + l_{PM}}{k\, \mu_{rPM}\, g + l_{PM}} \tag{3.14}$$

$$k = \begin{cases} 1 & |\theta| \le \theta_t / 2 \\ 1 + \dfrac{\pi}{2}\dfrac{R_s}{g}\left(\theta - \theta_t / 2\right) & \theta_t / 2 \le \theta \le \theta_s / 2 \\ 1 - \dfrac{\pi}{2}\dfrac{R_s}{g}\left(\theta + \theta_t / 2\right) & -\theta_s / 2 \le \theta \le -\theta_t / 2 \end{cases} \tag{3.15}$$

The flux linkage of each coil given in (3.16) represents the flux which passes the air-gap and links that particular coil.

$$\lambda_{coil}(\theta_r) = N l_{st} r_g \int_{\theta=-\frac{\theta_t}{2}}^{\theta=\frac{\theta_t}{2}} B_g(\theta, \theta_r) d\theta \tag{3.16}$$

where λ_{coil} and N are the flux linkage and the number of turns of each coil.

3.2.2 Back-Emf Calculation

Back-emf in PMSMs is the induced voltage across the stator phases due to relative change in rotor PM flux linking the stator coils. Mathematical definition of back-emf which is given in (3.17) as the rate of the flux linkage change in stator coils when the terminals are disconnected and the rotor is run at constant speed.

$$e_a = \frac{d\lambda_a}{dt} = \frac{d\theta_r}{dt}\frac{d\lambda_a}{d\theta_r} = \omega_r \frac{d\lambda_a}{d\theta_r} \tag{3.17}$$

where e_a is the induced voltage across the stator coil or back-emf, λ_a is stator flux linkage, ω_r and θ_r are the electrical rotor speed and position respectively. As any fault on the rotor affects the flux density in the air-gap and is reflected to the back-emf, it is an ideal variable to analyze the rotor or stator faults. According to (3.17), when the motor operates at constant speed, any

signature introduced into flux linkage will be reflected to the back-emf at the same frequency with 90^o phase shift. The induced voltage in one stator coil due to one rotor magnet can be expressed in Fourier series as in (3.18).

$$e_{a1PM1} = \sum_{n=-\infty}^{+\infty} E_n e^{jn\theta_m} \tag{3.18}$$

In this equation e_{a1PM1} is the induced voltage in first coil of phase-a due to the first rotor magnet, E_n is the amplitude of nth component of this voltage component, θ_m is the mechanical angle of the rotor. The induced voltage changes in every rotational period because the fundamental frequency of the induced voltage in (3.18) is mechanical frequency. Since the system is assumed to be linear, the induced voltage in the same coil due to other magnets is obtained by introducing a phase shift in (3.18). This phase shift is equal to the angle between two neighboring PMs. In addition, the magnet direction is inserted as negative or positive sign which is shown in (3.19). For instance if the induced voltage across the first coil of phase "a" due to the first magnet is given in (3.18), the induced voltage across the same coil due to the next magnet is calculated by replacing i=2 in (3.19).

$$e_{a1PMi} = \sum_{n=-\infty}^{+\infty} (-1)^{i-1} e^{jn(i-1)\frac{360}{p}} E_n e^{jn\theta_m} \tag{3.19}$$

where e_{a1PMi} is the induced voltage in the first coil due to the ith rotor magnet. The induced voltage in one coil due to all magnets is given below in (3.20) which are the cumulative of all induced voltages due to each individual magnet.

$$e_{a1} = \sum_{i=1}^{p} \sum_{n=-\infty}^{+\infty} (-1)^{i-1} e^{jn(i-1)\frac{360}{p}} E_n e^{jn\theta_m} \tag{3.20}$$

The presented equation in (3.20) can be simplified and re-written as in (3.21).

$$e_{a1} = \sum_{n=-\infty}^{+\infty} k_{mn} E_n e^{jn\theta_m} \tag{3.21}$$

where k_{mn} is the magnet coefficient which is calculated using (3.22).

$$k_{mn} = \sum_{i=1}^{p} (-1)^{i-1} e^{jn(i-1)\frac{360}{p}} \tag{3.22}$$

This coefficient represents the effect of different magnets on the induced voltage. The induced voltage in other coils in the same phase is calculated by phase shifting (3.21) as shown in (3.23).

$$e_{az} = \sum_{n=-\infty}^{+\infty} D_z k_{mn} E_n e^{jn\theta_m} e^{jn(z-1)\theta_z} \tag{3.23}$$

where θ_z is the mechanical angle between the zth and first coil which is multiple of slot angle (the mechanical angle between each coil with respect to the first one) and D_z is the coil direction factor which is defined based on the magnetic field vectors. If the magnetic field vector of the z^{th} coil is in the same direction with the first coil, then it is 1, otherwise it is -1. In the PMSM test motor, the distance between each coil is one slot or 40° mechanical degrees. The total induced voltage in the phase-a is the cumulative of induced voltages in all coils of the same phase (3.24).

$$e_a = \sum_{z=1}^{N_{coil}} \sum_{n=-\infty}^{+\infty} D_z k_{mn} E_n e^{jn\theta_m} e^{jn(z-1)\theta_z} \tag{3.24}$$

which can be simplified as follows.

$$e_a = \sum_{n=-\infty}^{+\infty} k_{mn} k_{san} E_n e^{jn\theta_m} \tag{3.25}$$

where k_{san} is coil coefficient which is calculated through (3.26). This coefficient considers the location of all coils in one phase with respect to each other.

$$k_{san} = \sum_{z=1}^{N_{coil}} D_z e^{jn(z-1)\theta_z} \tag{3.26}$$

Regarding the stator winding coils there are two parameters which should be taken into account. The first one is the mechanical location of each coil from the first coil (choosing the first coil is optional but it has to be considered as the base coil during all calculations). This location is critical for the phase shift of coils with respect to each other. The second parameter is the direction of each coil with respect to the first coil. The induced voltage in other phases is also calculated through (3.25). The only difference between different phases is coil coefficient. In this case, all three coils in the phase-b is located at 120° beyond the corresponding coil in the phase-a. This difference is inserted by changing just coil coefficient in other phases which is shown in (3.27).

$$\begin{cases} k_{sbn} = \sum_{z=1}^{N_{coil}} D_z e^{jn(z-1)\theta_z} e^{jn\frac{2\pi}{3}} \\ k_{scn} = \sum_{z=1}^{N_{coil}} D_z e^{jn(z-1)\theta_z} e^{jn\frac{4\pi}{3}} \end{cases} \tag{3.27}$$

This coefficient represents the phase difference between two stator phases for different harmonics. In the following sections, this coefficient will be used to explain the difference between stator winding connections.

Another parameter taken into account is the skew angle. The skew effect is taken into account by introducing skew factor into (3.28).

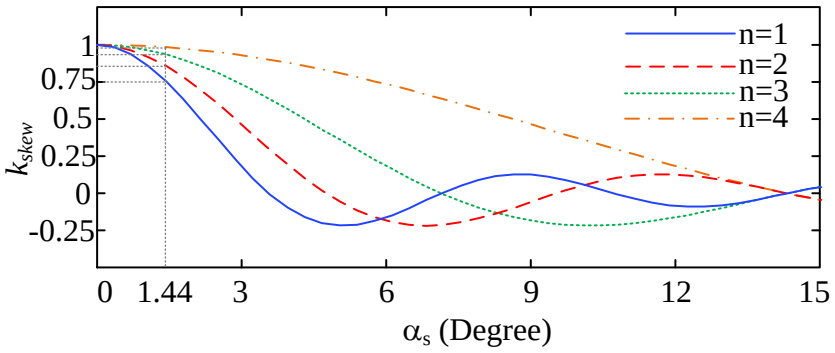

Figure 3.3. Skew factor for different skew angle and harmonics

$$e_a = \sum_{n=-\infty}^{+\infty} k_{skew} k_{mn} k_{san} E_n e^{jn\theta_m} \tag{3.28}$$

where k_{skew} is the skew factor which is calculated through (3.29).

$$k_{skew} = \sin c\left(n \frac{p}{2} \frac{\alpha_s}{2} \right) \tag{3.29}$$

where α_s is the skew angle in mechanical degree [3.24]. Figure 3.3 shows the skew factor for different harmonics and various skew angles. As shown here, unlike the mechanical fundamental component, the skew factor does not significantly affect the low order harmonics. For example, when the skew angle is 1.44° mechanical degree, the amplitude of skew factor for fundamental electrical frequency (n=4 in Figure 3.3) is 0.9831 while this factor for the fundamental mechanical frequency (n=1 in Figure 3.3) is 0.75 which means that this factor can be neglected for higher order harmonics.

3.2.3 Magnet Defect Fault Modelling

Magnet faults including demagnetization or broken magnet cause reduction in PM flux and consequently affect the stator phase back emf. Under such circumstances, in order to drive the

same amount of load, the controller increases the stator q-axis current. This increase in current raises the copper loss and motor temperature. Increase in copper loss leads to reduction in efficiency and high temperature affects the rotor magnets. In addition, magnet defects can cause torque ripples due to non-uniform distribution of magnet flux on the rotor. Since this phenomenon corresponds to the rotor magnets, it affects the magnet coefficient k_{mn} in (3.22). In this study, fault severity factor is inserted into the magnet coefficient to model magnet fault. This parameter shows the condition of each magnet which becomes zero when the magnet is totally defected, one for healthy ones and fractional number in between. The magnet coefficient given in (3.22) is re-written as (3.30) to point out the fault severity.

$$k_{mn} = \sum_{i=1}^{p} (-1)^{i-1} k_{fi} e^{jn(i-1)\frac{360}{p}} \tag{3.30}$$

where $k_{fi} \in [0,1]$ is the fault severity index of i^{th} rotor magnet. In the next sections, this coefficient is used to investigate the effect of location and number of faulty magnets on the motor variables.

3.3 Analysis of Magnet Faults Signatures and Topology Dependencies

Unless evenly distributed throughout the rotor, the magnet defects and demagnetization issues create fault signature pattern given in (3.31). These magnetic rotor faults introduce asymmetry on the rotor flux distribution cycling at every mechanical period. This asymmetry is reflected on the back-emf and current waveforms, and creates signatures in the associated frequency spectrums at mechanical frequency. However, the frequency spectrum of back-emf and current waveforms can be different depending on machine design schemes, number and location of the

faulty magnets. Even the identical faults may result in different spectrums with missing or additional components depending on the motor structure.

In this section, these cases are studied elaborately so that one can predict the machine specific spectrum content of the faulty motor and develop diagnosis algorithms based on that to minimize false alarms.

$$f_{f,k} = \left(1 \pm \frac{k}{p/2}\right) f_s = k f_m \qquad k = 1, 2, 3, \ldots \tag{3.31}$$

3.3.1 Winding Configuration, Number of Poles and Slots

In order to analyze the topology dependency of magnet faults, a number of 3-phase PM motors with different number of pole and slot are selected for various case studies. Different types of winding configurations are taken into account including full, short and fractional coil pitch, single and double layer to investigate the effect of all these on the fault signatures.

The motors analyzed with different pole, slot and winding configuration combinations are given in Table 3.2 . As it is mentioned earlier, the multiples of magnetic and coil coefficients determine the frequency content of the back-emf waveform and the phase shift between various harmonics on different stator phases. Based on these two characteristics, this multiplication is called construction filter and is shown with Ran for phase-a (3.32).

$$R_{an} = k_{mn} k_{san} \tag{3.32}$$

In the healthy condition, the amplitude of this filter is zero for all mechanical components except than those which are odd multiple of p/2.

Table 3.2. Phase shift of harmonics in back-emf for 9-slot/8-pole motor

N_s	*p*	*Layer*	N_s /p	C_p	*pitch*
9	6	Double	1.5	2	Fractional
9	8	Double	1.125	1	Fractional
12	8	Double	1.5	2	Fractional
12	8	Single	1.5	2	Fractional
12	10	Double	1.2	1	Fractional
12	10	Single	1.2	1	Fractional
18	6	Double	3	3	Full
18	6	Single	3	3	Full
18	12	Double	1.5	2	Fractional
36	6	Double	6	6	Full
36	6	Single	6	6	Full

These components are actually odd multiple of fundamental electrical frequency as the fundamental electrical frequency is product of p/2 and mechanical frequency. However, in the faulty condition, all mechanical harmonics are let to pass through the filter. Table 3.3 shows the construction filter magnitude for different fault harmonics in the case of double layer winding and different number of pole and slot combinations. As shown here, in the cases where the number of slot and pole ratio is multiple of 1.5, the fault related signatures are not observed. When a motor has a three phase double layer winding and the number of slot/pole ratio is multiple of 1.5, all coils in the same phase are mechanically located in the space such that the mechanical phase shift with respect to each other leads to cancellation of all fault harmonics which can be proven through the given equations in the previous section.

Table 3.3. Normalized construction filter magnitude for different number of poles and slots (Double layer winding)

		$\lvert R_{an} \rvert$											
N_s	*p*	*1/(p/2)*	*2/(p/2)*	*3/(p/2)*	*4/(p/2)*	*5/(p/2)*	*6/(p/2)*	*7/(p/2)*	*8/(p/2)*	*9/(p/2)*	*10/(p/2)*	*11/(p/2)*	*12/(p/2)*
9	6	0	0	1	0	0	0.2	0	0	1	0	0	0.2
9	8	0.026	0.032	0.099	1	0.142	0.099	0.032	0.026	0.049	0.026	0.032	0.69
12	8	0	0	0	1	0	0	0	0.142	0	0	0	1
12	10	0.029	0	0.081	0	1	0	0.111	0	0.081	0	0.03	0
18	6	0	0	1	0	0	0	0	0	1	0	0	0
18	12	0	0	0	0	0	1	0	0	0	0	0	0.091
24	8	0	0	0	1	0	0	0	1	0	0	0	1
36	6	0	0	1	0	0	0	0	0	0.732	0	0	0

For instance, Figure 3.4.a shows the coil magnetic field vectors and winding layout for a three phase, 9-slot/6-pole double layer winding motor. As shown here, electrically, all coils in the same phase do not have any phase difference. Physically, all coils in one phase are located in the space in a way that they have 120^{o} mechanical degree with respect to each other (Figure 3.4.b).

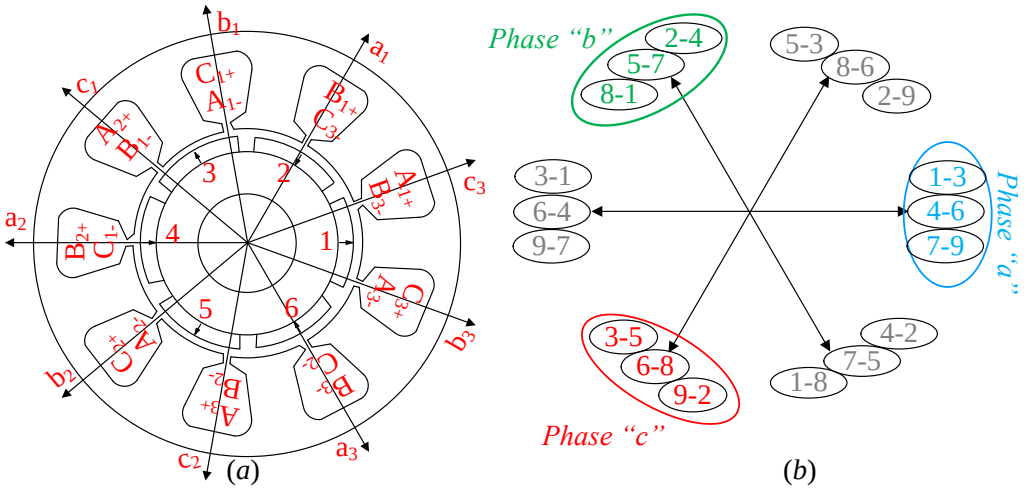

Figure 3.4. A three phase, 9-slot/6-pole double layer winding motor a) Magnetic field vector b) winding layout

The coil coefficient for this motor is expanded as given in (3.33).

$$k_{san} = e^{jn0} + e^{jn120} + e^{jn240} = \begin{cases} 3 & n = 3k \ , k = 1, 2, \cdots \\ 0 & other \end{cases} \tag{3.33}$$

Therefore, the coil coefficient for all mechanical components is zero except than those $p/2$ multiples of electrical frequency.

Table 3.4 shows the construction filter magnitude for different fault harmonics in the case of single layer winding and different number of poles and slots. As shown in this table, when the winding has single layer and slot and pole ratio is multiple of 3, none of the fault signatures are observed. When a motor has a three phase single layer winding configuration and the number of slot and pole ratio is multiple of 3, the mechanical phase shift between the coils eliminate all fault related harmonics. For instance, Figure 3.5 shows the coil magnetic field vectors and winding layout for a three phase, 36-slot/6-pole single layer winding motor. As shown in Figure 3.5.a, electrically, the coils in the same phase do not have any phase difference.

Table 3.4. Normalized construction filter magnitude for different number of poles and slots (Single layer winding)

		$\lvert R_{an} \rvert$											
N_s	p	*1/(p/2)*	*2/(p/2)*	*3/(p/2)*	*4/(p/2)*	*5/(p/2)*	*6/(p/2)*	*7/(p/2)*	*8/(p/2)*	*9/(p/2)*	*10/(p/2)*	*11/(p/2)*	*12/(p/2)*
12	8	0.101	0	0.101	1	0.101	0	0.101	0.142	0.101	0	0.101	1
12	10	0.111	0	0.111	0	1	0	0.111	0	0.111	0	0.111	0
18	6	0	0	1	0	0	0.2	0	0	1	0	0	0.2
18	12	0	0	0.091	0	0	1	0	0	0.091	0	0	0.091
24	8	0	0	0	1	0	0	0	0.142	0	0	0	1
36	6	0	0	1	0	0	0.179	0	0	0.732	0	0	0.103

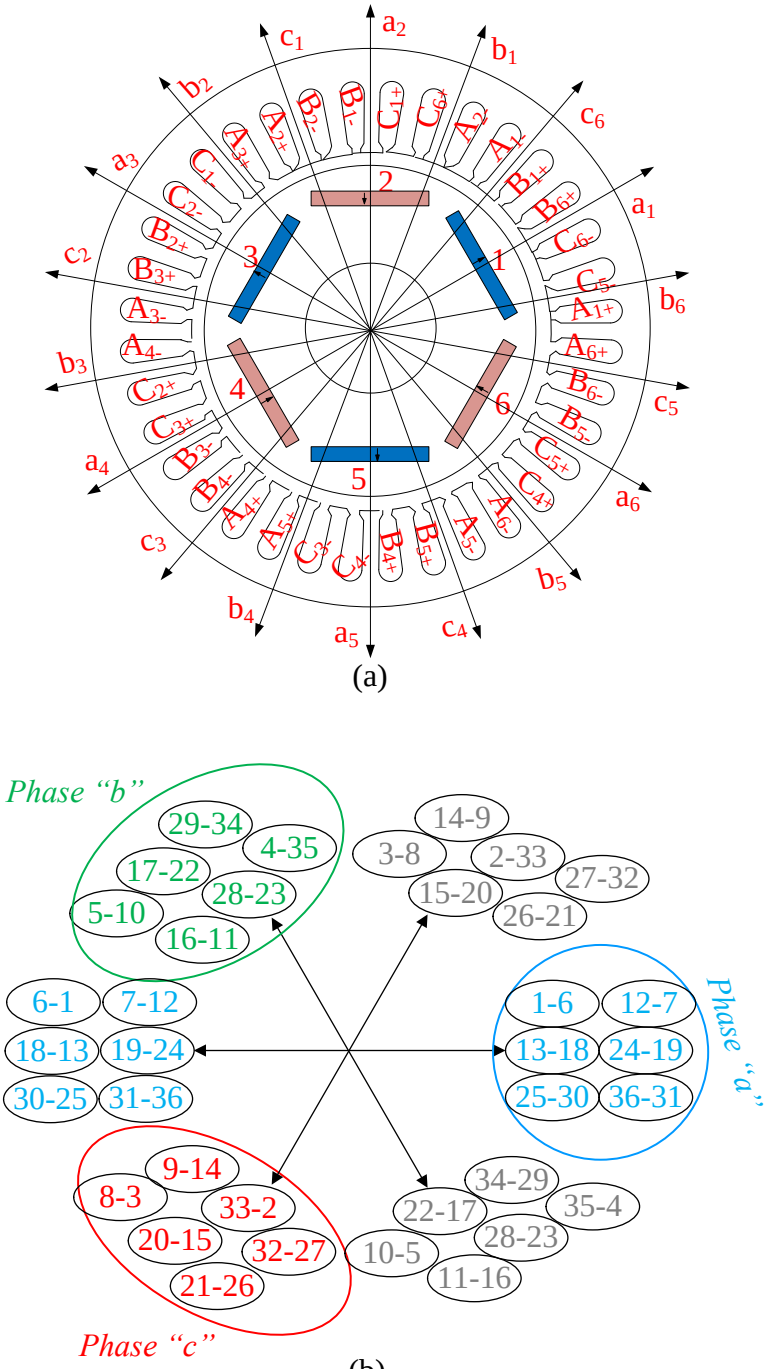

(a)

(b)

Figure 3.5. A three phase, 36-slot/6-pole double layer winding motor a) Magnetic field vector b) winding layout

Physically, all coils in one phase are located in the space in a way that they all have 60^o mechanical degree phase shift with respect to each other (Figure 3.5.b), which results in the same fact given in (3.33).

3.3.2 Number and Location of Magnet Defects

The number and location of the magnet defects affect the signature content in the motor variables which can easily be analyzed through partitioned MEC. During the analysis multiple defects, it is assumed that the defects are identical to each other. When there is only one defect or partially demagnetized magnet, all components defined in (3.31) appear in the back-emf spectrum. In the case of two or more defected magnets, depending on the location of the magnets, the spectrum can be different. This situation is observed when the severities of fault in all faulty magnets are exactly the same. This situation can be justified through magnet coefficient given in (3.30). As the number of magnet is an even value, the magnet coefficient can be simplified to (3.34).

$$k_{mn} = \sum_{i=1}^{\frac{p}{2}} (-1)^{i-1} e^{jn(i-1)\frac{360}{p}} \left(k_{fi} + k_{f(i+p/2)} e^{jn180} (-1)^{\frac{p}{2}} \right) \tag{3.34}$$

where k_{fi} and $k_{f(i+p/2)}$ are the i^{th} and $(i+p/2)^{\text{th}}$ magnet fault severity factor. In any number of poles, magnet coefficient expansion helps to estimate fault signatures in the stator phase back-emf.

For instance, in the case of 8 poles, the magnet coefficient expansion is given in (3.35).

$$\begin{aligned} k_{mn} = {} & \left(k_{f1} + (-1)^n k_{f5} \right) - e^{jn45} \left(k_{f2} + (-1)^n k_{f6} \right) \\ & + e^{jn90} \left(k_{f3} + (-1)^n k_{f7} \right) - e^{jn135} \left(k_{f4} + (-1)^n k_{f8} \right) \end{aligned} \tag{3.35}$$

In the healthy case when all fault severity factors are 1, all the components in k_{mn} is zero except

Table 3.5. Missing fault signatures due to magnet defect location

Missing Signatures	PM #							
	1	2	3	4	5	6	7	8
0.25(2k-1)	●				●			
0.25(2k-1)		●				●		
0.25(2k-1)			●				●	
0.25(2k-1)				●				●
0.25(2k-1)	●	●			●	●		
0.25(2k-1)	●		●		●		●	
0.25(2k-1)	●			●	●			●
0.25(2k-1)		●	●			●	●	
0.5(2k-1)	●		●					
0.5(2k-1)	●						●	
0.5(2k-1)			●		●			
0.5(2k-1)						●		●
0.5(2k-1)	●	●	●	●				
0.5(2k-1)	●	●		●			●	
0.5(2k-1)		●	●	●	●			
0.5(2k-1)		●		●	●		●	

than the odd multiple of $p/2$. If there is only one defected magnet, then the magnet coefficient will have non-zero value for all mechanical components which is not necessarily the case for some combinations where magnet coefficient filters some of the harmonics in the back emf. For instance, when two consecutive magnets with the same magnetization direction (e.g. magnet 1 and 3) are defected, the magnet coefficient is zero for odd multiple of 0.5^{th} harmonic (e.g. 0.5^{th},

1.5^{th},..). Similarly, if the position of two defected magnets are symmetrical with respect to center line (e.g. magnet 1 and 5) the magnet coefficient is zero for odd multiple of 0.25^{th} harmonic (e.g. 0.25^{th}, 0.75^{th},..). Table 3.5 summarizes some of the conditions in which the magnet coefficient is zero for some fault signatures. Here various scenarios are given when two or four magnets are defected. The table is created based on the corresponding magnet coefficients calculation through (3.34). It is shown that the magnet defects which are symmetrical with respect to rotor centerline suppress the odd multiple of 0.25^{th} harmonic. If the defects are not symmetrical with respect to rotor centerline, then the odd multiple of 0.5^{th} harmonic are found to be missing. If the number of magnet defects is odd, then all of the harmonics show up. Note that the findings here are limited to the test motor with 8-pole, and can be different for different motors. One can find out the missing components in the back emf frequency spectrum by re-deriving (3.34) for the given motor easily for various magnet fault combinations.

3.3.3 Winding Configuration

The fault related harmonics created by magnet faults in the back-emf is the source of fault signatures in the stator current. Therefore, the harmonic contents of both the stator phase back-emf and stator phase current spectrums should be very similar to each other. However, there are some components which show up in the back-emf but not in the stator current. This is mostly due to the winding connection type where it is essential to understand the phase shift between the fault signatures in any motor phases. Star, delta and separate excitations are the three types of possible connections in a three phase systems. In the star connection, which is the most common one, the neutral point is either floating or connected to the neutral point of the source. It is well known that, if all three phases are perfectly balanced and the overall system is uniform

Table 3.6. Phase different between two stator phase back-emf for different harmonics (double layer winding)

		Φ_{ab}(Degree)											
N_s	P	1/(p/2)	2/(p/2)	3/(p/2)	4/(p/2)	5/(p/2)	6/(p/2)	7/(p/2)	8/(p/2)	9/(p/2)	10/(p/2)	11/(p/2)	12/(p/2)
9	8	240	120	0	240	120	0	240	120	0	240	120	0
12	10	120	0	0	0	240	0	120	0	0	0	240	0

throughout the air-gap, the in-phase harmonics do not flow in star connected motor windings. As derived before, the coil factor represents the phase shift between stator phases for different harmonics which helps to identify in-phase harmonics. Table 3.6 shows the phase difference between back-emf fault signatures for two slot and pole combination. For instance, according to the theoretical derivations, in the case of 9-slot and 8-pole motor, the 0.75^{th} component and it's multiples in the back-emf have the same phase angle in all three phases. In a star connected motor the corresponding current harmonics eliminate each other and cannot flow. However in a delta connection or separate three phase connection, any harmonic with any phase shift can show up in stator phase current spectrum of a motor. This suggests that, in a balanced star connected system, some of the harmonics defined in (3.31) cannot be used as fault indicator which may lead to missing alarms.

3.4 Simulation and Experimental Results

In order to verify the theoretical findings, partitioned MEC and finite element tools are used to model the test motors given in Table 3.1. Figure 3.6 and Figure 3.7 depicted to compare the PMSM phase back emf for healthy and faulty conditions (when 7% of one magnet is removed) using the proposed MEC approach and non-linear FE tool, respectively. As shown in these figures, in the healthy case, back-emf spectrum contains only the fundamental component and

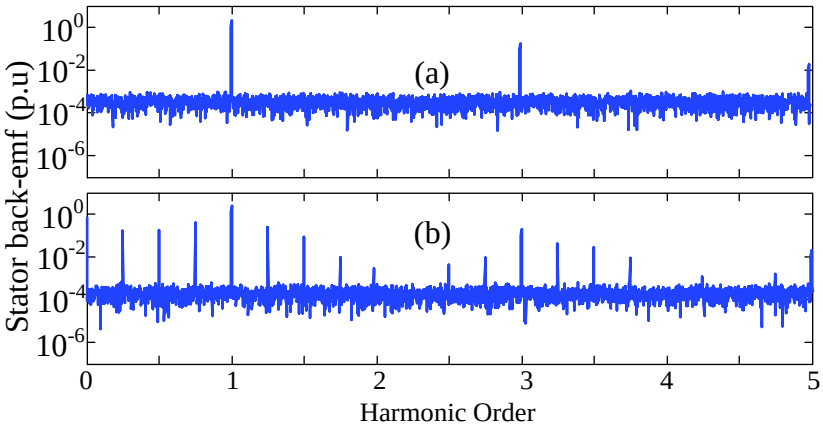

Figure 3.6. Stator back-emf spectrum at rated speed for the 9-slot/8-pole PMSM motor, MEC results a) Healthy b) One magnet defect

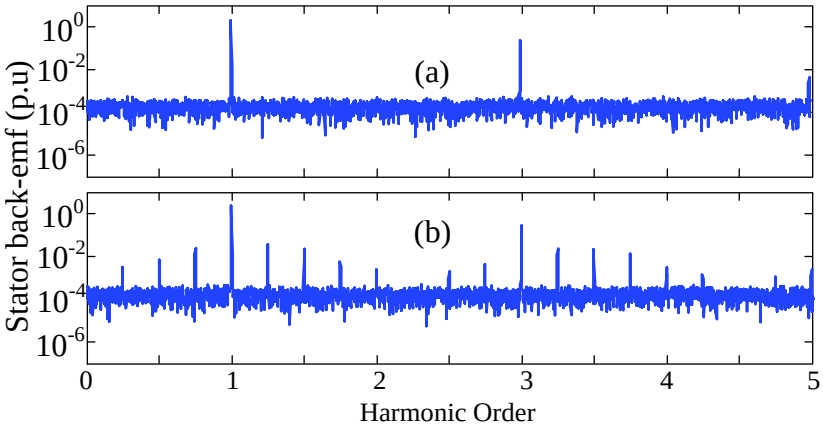

Figure 3.7. Stator back-emf spectrum at rated speed for the 9-slot/8-pole PMSM motor, FE results a) Healthy b) One magnet defect

odd multiples of fundamental electrical frequency generated by the flattened flux linkage waveform, whereas, in the faulty case, fault harmonics at the multiples of mechanical frequency show up in the spectrum as pointed out in Table 3.3. These figures show that the theoretical findings summarized in Table 3.3 match with the simulation results and the proposed method can estimate the behavior of a specific faulty motor accurately. Similarly, the phase back-emf voltage of the IPM obtained through MEC and FE tools for healthy and faulty conditions (when 25% of one magnet is removed) are shown in Figure 3.8 and Figure 3.9, respectively.

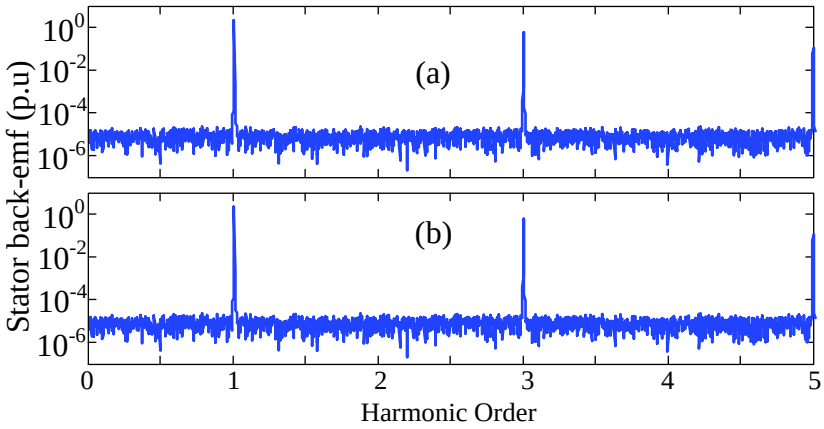

Figure 3.8. Stator back-emf spectrum at rated speed for the 36-slot/6-pole IPM motor MEC results a) Healthy b) One magnet defect

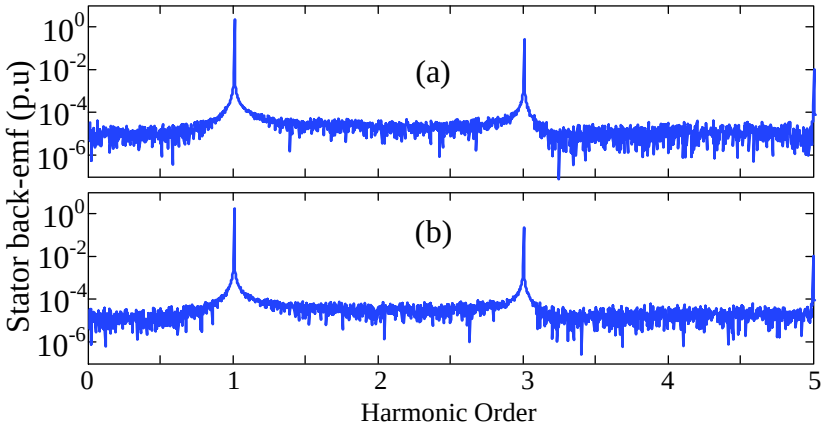

Figure 3.9. Stator back-emf spectrum at rated speed for the 36-slot/6-pole IPM motor, FE results a) Healthy b) One magnet defect

As the ratio of pole and slot is multiple of 3, it is expected not to observe any fault related signatures in the spectrum even if there is a broken magnet. These two figures also show that the theoretical findings summarized in Table 3.4 match with the simulation results. Regarding the number and locations of defected magnets, several simulations are run for the PMSM motor.

Figure 3.10 compares the back-emf results obtained through MEC and FE when the 1st and 3rd magnets are broken. As it is given in Table 3.5 and shown in Figure 3.10, in this scenario the odd multiples of 0.5^{th} harmonic do not show up in the spectrum.

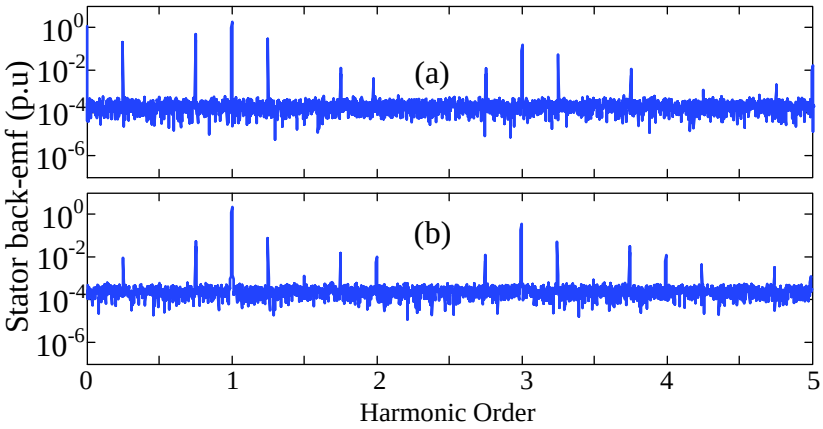

Figure 3.10. Phase "a" back emf spectrum when magnet number 1 and 3 are defected a) MEC result b) FE result

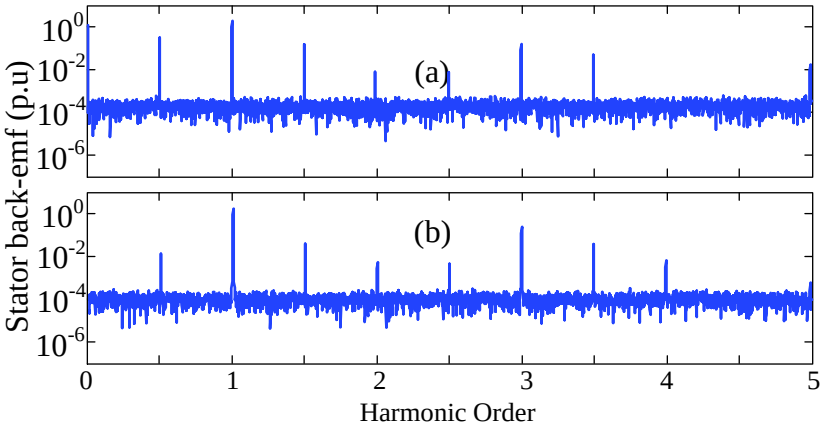

Figure 3.11. Phase "a" back emf spectrum when magnet number 1 and 5 are defected a) MEC result b) FE result

Similarly, Figure 3.11 shows the case where the 1st and 5th magnets are defected. In this situation, the odd multiple of 0.25th harmonics do not show up in the spectrum which exhibits a consistent result with the findings in Table 3.5. Figure 3.12 shows the back-emf of the PMSM at rated speed for healthy and faulty motors. As seen here, even in the healthy case, some fault related harmonics show up little bit due to inherent electromechanical imperfections and alignment issues. In the faulty condition, as it is clear in Figure 3.12.b, all mechanical harmonics raise which matches with the analytical discussions presented in the previous sections.

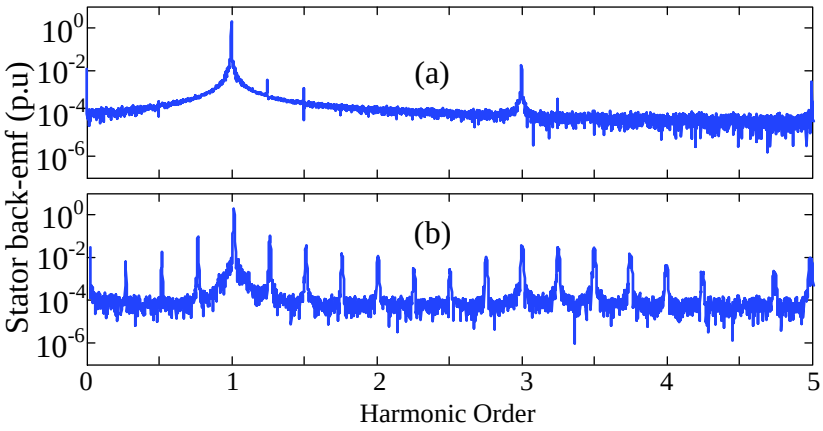

Figure 3.12. Stator back-emf spectrum at rated speed for the 9-slot/8-pole PMSM motor, experimental results a) Healthy b) One magnet cracked

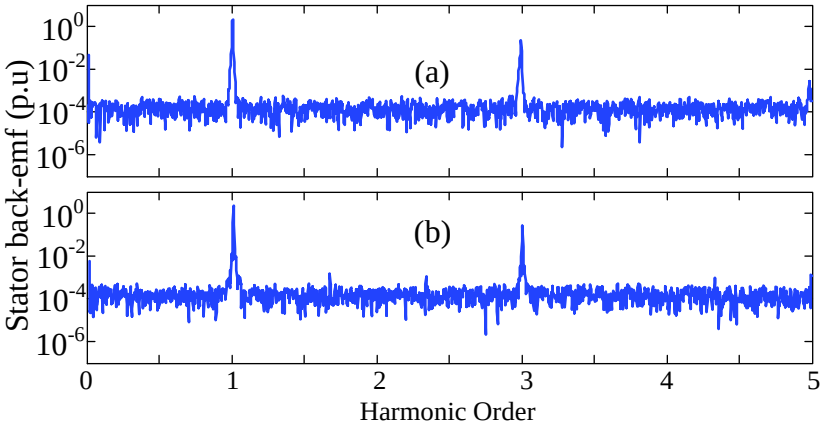

Figure 3.13. Stator back-emf spectrum at rated speed for the 36-slot/6-pole IPM, experimental results a) Healthy b) One magnet cracked

Figure 3.13 shows the experimentally obtained back emf frequency spectrums for the IPM motor. These experimental results support the simulation results shown in Figure 3.8 and Figure 3.9. Since the slot and pole ratio is multiple of 3 in the IPM motor, none of the fault related signatures appear in the back- emf spectrum, neither in the healthy nor faulty conditions which is consistent with analytical and simulation results.

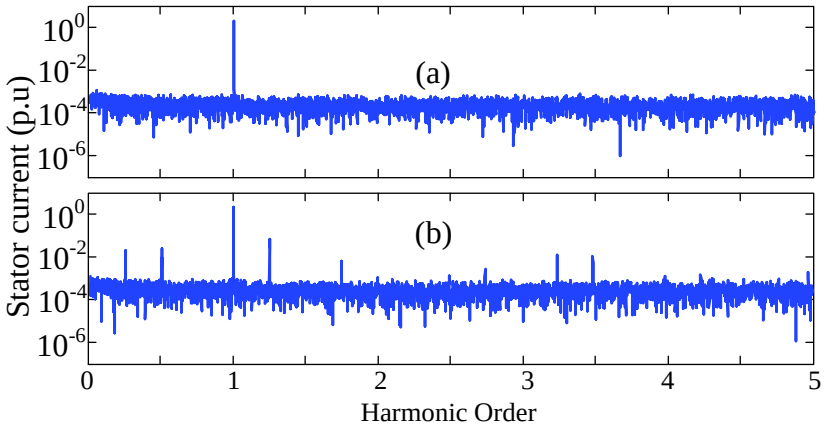

Figure 3.14. Stator current spectrum at rated speed and rated torque for 9-slot/8-pole PMSM motor, FE results a) Healthy b) One magnet defect

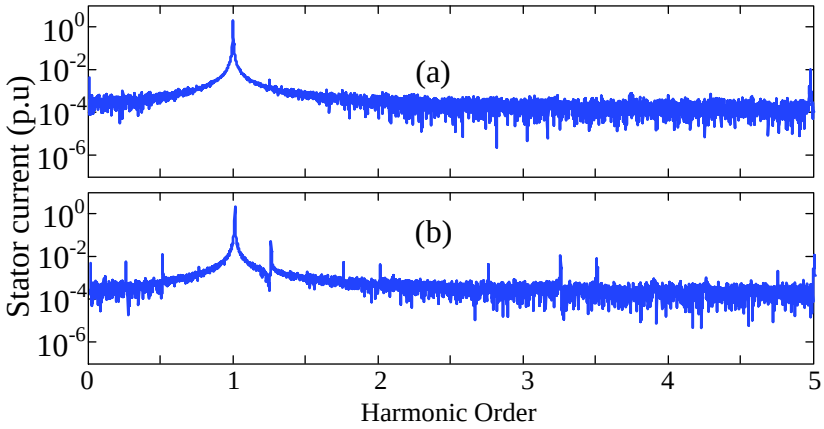

Figure 3.15. Stator current spectrum at rated speed and rated torque for a 9-slot/8-pole PMSM motor, experimental results a) Healthy b) One magnet defect

In Figure 3.14 and Figure 3.15, the corresponding FE and experimental stator current spectrum addressing the effect of winding configuration are given. The PMSM motor is tested at rated speed rated torque in both the healthy and faulty cases. As seen in these current spectrums, the signatures at the triplen multiple of mechanical frequency (i.e. 0.75^{th}, 1.5^{th} harmonics) do not show up due to star connection though they do exist in the back emf.

3.5 Experimental Setup

In order to verify the analytical and simulation results, both 9slot/8pole PMSM and 36slot/6pole IPM motors are tested experimentally. To mimic the magnet defect condition in PMSM motor, rotor magnets are cut vertically using a fine cutter and tested under different operating point conditions. For this purpose, an experimental setup is prepared shown in Figure 3.16. The motors are coupled with a high-end hysteresis dynamometer to apply adjustable load and measure shaft torque and speed. In order to measure and store the current data for post processing, NI USB-6351 data acquisition board is used which has up to 1MS/s sampling rate and 16 bit ADC.

To measure the back-emf three differential probes are connected to three phases and a high resolution oscilloscope is used to measure the voltage and transfer data to a PC through USB connection.

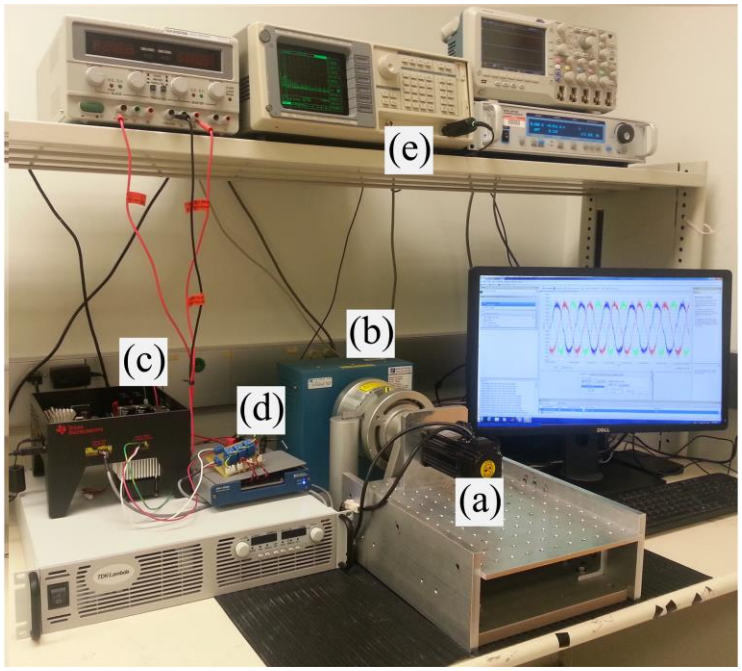

Figure 3.16. Experimental setup a) PMSM b) Dynamometer c) Motor drive d)Data acquisition card e) Spectrum analyzer

3.6 Conclusion

In this chapter, the effect of PM motor topology on the magnet defect fault signatures is investigated through proposed partitioned MEC. The proposed analytical tool has several advantages with respect to conventional tools such as shorter simulation time, analyzing the effect of individual stator coil and number and location of defected magnet separately. In this analytical method, the induced voltages across one stator coil due to individual magnets are carefully granulated to accurately introduce fault and then superposed. Several motors with different number of pole and slot are analyzed through this method in order to generalize the findings. In addition, various cases including full, fractional and short pitch winding, skew and stator winding connection types are also discussed. It is shown that in the case of single layer winding, when the number of slot and pole ratio is multiple of 3, magnet defect faults do not create any fault related signature in the stator back emf and current. Similarly, the PM motors with double layer winding and slot and pole ratio of 1.5 or multiples, the fault related signatures are not observed. The effect of the winding connection type is also investigated through phase information of fault signatures, and shown that the star connection suppresses current fault signatures at the triplen multiples of mechanical frequency. The location of the magnet defects are also studied and it is shown that if the magnet defect locations are symmetrical with respect to rotor centerline, some of the fault harmonics do not show up in the back emf and current spectrum. For instance, in the case of 8 pole motor, if there is even number of magnet defects and half of them are located in the first 4 poles and the second half is located symmetrically in the next 4 poles, the odd multiples of 0.25^{th} harmonic do not appear in motor back-emf. As an example, if 2 poles are defected such as magnet 1 and magnet 5, this phenomenon is observed. In

order to verify the analytical findings, two different PM motor with different number of slot and pole are used in the experiments and then simulated through FE, and the results are compared with the partitioned MEC results.

CHAPTER 4

MODELING AND DYNAMIC BEHAVIOR ANALYSIS OF MAGNET DEFECT SIGNATURES IN PERMANENT MAGNET SYNCHRONOUS MOTORS[1]

4.1 Modeling and Analysis of Magnet Defect Fault Signatures

4.1.1 Signatures in Back-emf

As well known, in synchronous motors, one of the components in the voltage equation is generated by the rate of rotor flux linkage changed on the stator windings. This back-emf component is measured by spinning the rotor at constant speed while stator phases are open. Mathematical definition of back-emf is given in (4.1)

$$e_a = \frac{d\lambda_a}{dt} = \omega_m \frac{d\lambda_a}{d\theta_m} \tag{4.1}$$

where e_a is the induced voltage across the stator coil or back-emf, λ_a is stator flux linkage, θ_m and ω_m are the mechanical rotor position and speed respectively. According to (4.1), any changes on the rotor magnets are reflected to the back-emf which makes it an ideal variable to analyze rotor and stator faults. As well known, most faults in PM motors trigger harmonics at multiples of mechanical frequency (4.2) in the stator back-emf and current spectrum [25]. In a faulty motor, the rotor is not symmetric anymore and the induced fault related components in the stator changes with mechanical frequency.

---

[1] © 2016 IEEE. Reprinted, with permission, from M. Zafarani, T. Goktas, B. Akin and S. E. Fedigan, " Modeling and Dynamic Behavior Analysis of Magnet Defect Signatures in Permanent Magnet Synchronous Motors," in IEEE Transactions on Industry Applications, vol. 52, no. 5, pp. 3753-3762, Sept.-Oct. 2016.

$$f_f = \left(1 \pm \frac{k}{p/2}\right) f_s = k f_m \qquad k = 1, 2, 3, \ldots \tag{4.2}$$

where f_f is the frequency of k^{th} component in the spectrum, f_s is the fundamental frequency of the back-emf or electrical frequency, f_m is the rotational frequency and p is the number of pole. The fourier series of stator flux linkage due to the rotor flux is given in (4.3) where n is mechanical harmonic order and λ_{an} is the amplitude of nth component.

$$\lambda_a = \sum_{n=-\infty}^{n=\infty} \lambda_{an} e^{jn\theta_m} \tag{4.3}$$

In healthy case, the stator flux linkage does not have any components except the multiples of $p/2$ or multiple of electrical frequency. However, in faulty conditions, all mechanical harmonics are expected to show up in the flux linkage spectrum. The fourier series of back-emf is calculated by deriving (4.3) as follows (4.4).

$$e_a = \frac{d\lambda_a}{dt} = \sum_{n=-\infty}^{n=\infty} jn\omega_m \lambda_{an} e^{jn\theta_m} \tag{4.4}$$

As seen in (4.4), the harmonics in the back-emf and flux linkage are located at the same frequency with a phase shift of 90 degrees. Theoretically, the back-emf harmonics are linearly correlated to the speed. However in practice, several factors such as eddy currents, mechanical oscillations and saturation affect the back-emf voltage and leads to a non-linear behavior when the speed increases.

4.1.2 Current Signatures - Open Loop Operation

In order to investigate the behavior of magnet fault signatures with respect to rotor speed and torque in open loop operation mode, a three phase balanced sinusoidal voltage source is used to excite the motor. Excitation voltage is related to rotor position through the equation (4.5)

$$v_a(\theta_m) = V_m \sin\left(\frac{p}{2}\theta_m + \delta\right) \tag{4.5}$$

where v_a is the phase-a input voltage and V_m and δ are the peak value and load angle of the input voltage. The amplitude and load angle are set manually in order to mimic the field oriented control (FOC) technique without using any controller. Figure 4.1 shows the linear model of PMSM and input voltage source. Stator voltage equation of one phase is given in (4.6).

$$v_a = r_s i_a + L_{aa}\frac{di_a}{dt} + M_{ab}\frac{di_b}{dt} + M_{ac}\frac{di_c}{dt} + e_a + v_{nN} \tag{4.6}$$

where r_s is the stator resistance, L_{jj} is the self-inductance of j^{th} phase, M_{ij} is the mutual inductance between phase "*i*" and "*j*" and v_{nN} is the voltage between the two neutral points of motor and source shown in Figure 4.1.

In order to analyze the stator current harmonics, it is assumed that the motor is at steady state condition. The variables in equation (4.6) are replaced by their fourier series and it is assumed that motor parameters such as resistances and inductances are frequency independent. Then the equation for each component is solved taking this assumption into account where the individual solutions are independent from other components. The voltage equation for all harmonics is given in (4.7).

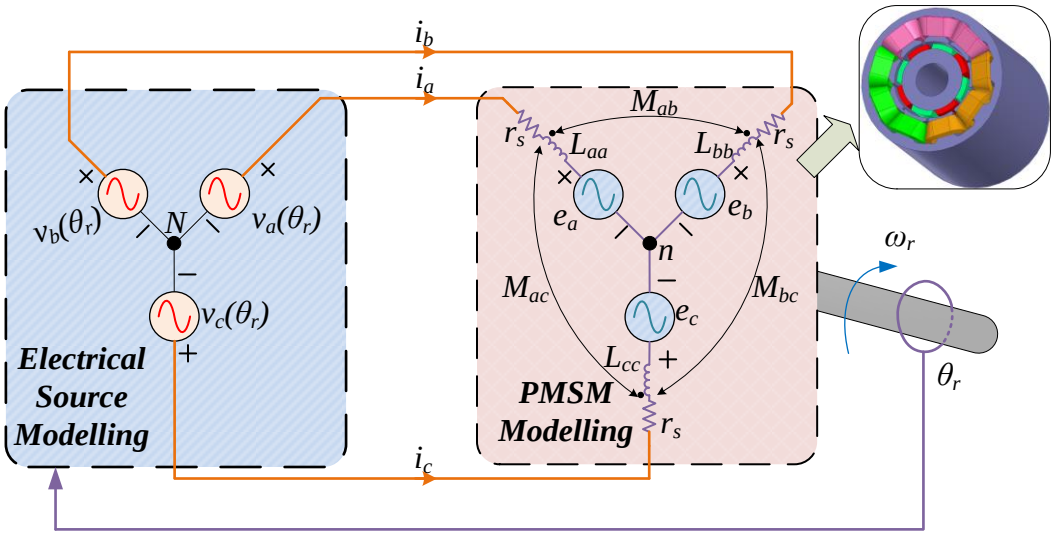

Figure 4.1. Linear model of PMSM

$$v_{an} = \left(r_s + jn\omega_m L_{aa}\right) i_{an} + jn\omega_m \left(M_{ab} i_{bn} + M_{ac} i_{cn}\right) + jn\omega_m \lambda_n + v_{nNn} \tag{4.7}$$

As the model is assumed to be linear, all mutual inductances and all self-inductances are equal and replaced by L_s and M_s, as self and mutual inductance respectively. Following several iterations under this assumption, the stator current harmonic equation is extracted as (4.8).

$$i_{an} = \frac{v_{an} - jn\omega_m \lambda_n - v_{nNn}}{r_s + jn\omega_m \left(L_s - M_s\right)} \tag{4.8}$$

In order to simplify the equation (4.8), the stator inductances in *abc* reference frame are replaced by their equivalences in rotor frame. The relation between inductances in the two reference frames is given by [4.21] and is shown in (4.9) and (4.10).

$$\begin{cases} L_s = L_{ls} + L_0 + L_2 \cos\left(2\left(\frac{p}{2}\right)\theta_m\right) \\ M_s = M_0 + M_2 \cos\left(2\left(\frac{p}{2}\right)\theta_m - 120^o\right) \end{cases} \tag{4.9}$$

$$L_d = L_{ls} + \left(L_0 - M_0\right) + \left(\frac{L_2}{2} + M_2\right)$$
$$L_q = L_{ls} + \left(L_0 - M_0\right) - \left(\frac{L_2}{2} + M_2\right) \tag{4.10}$$

where L_{ls} is stator leakage inductance, L_0, M_0, L_2 and M_2 are the dc and ac components of self and mutual inductances respectively, L_d and L_q are stator inductances along d and q axis in rotor frame, respectively. The air-gap in surface mounted PM motors is uniform and the inductance in both axes is equal and given in (4.11).

$$L_d = L_q = L_s - M_s \tag{4.11}$$

By substituting (4.11) into (4.8), the relation between the stator current harmonics, motor variables and parameters can be obtained as in (4.12).

$$i_{an} = \frac{v_{an} - jn\omega_m \lambda_n - v_{nNn}}{r_s + jn\omega_m L_d} \tag{4.12}$$

Equation (4.12) can be used to explain the behavior of fault signatures in the stator current for different motors and operating speeds. Note that in open loop operation the fault related harmonics do not exist in the voltage waveform. Also, the neutral voltage does not have any components except the 3rd mechanical harmonic and multiple of that (or 0.75^{th} harmonic of electrical frequency and multiple of that). Under these assumptions, (4.12) can be simplified as (4.13) for all fault harmonics.

$$i_{an} = \frac{-jn\omega_m \lambda_n}{r_s + jn\omega_m L_d} \tag{4.13}$$

This equation shows that for high order harmonics or at high speed operation, the effect of

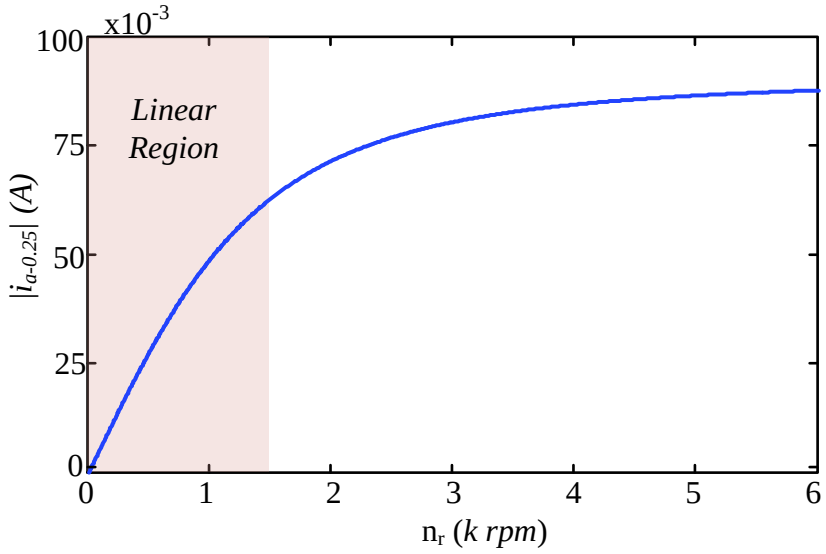

Figure 4.2. Characteristic of 0.25th component versus speed

resistance compared to the d-axis reactance is negligible. In these cases, the fault signatures are almost speed and torque independent. This phenomenon is shown in (4.14).

$$n\omega_m L_d >> r_s \Rightarrow i_{an} = \frac{-\lambda_n}{L_d} \tag{4.14}$$

Figure 4.2 shows the variation of signature at mechanical frequency for different rotor speeds. As shown here, at lower speeds the harmonic amplitude changes linearly with respect to rotor speeds whereas at higher speeds the variation rate decreases. According to (4.13), the load does not affect the fault harmonics, however in the simulation results the amplitude is affected by torque as well.

Since the stator core permeability highly depends on flux density, the stator flux linkages and inductances are affected by load variation. Therefore, the amplitude of fault signatures become slightly load dependent. However, when load and speed effects are compared, it is found that these components are remarkably speed dependent.

4.1.3 Current Signatures -Closed Loop Operation

Since the synchronous motors are driven through closed loop control, it is important to investigate the effect of controllers on the fault signatures. The most common control type for PM motors is FOC. This controller assures that the speed and stator d-axis component keep track of the corresponding references entered by the user. In order to fully understand the effect of controller on fault signatures, the model in rotor reference frame is used. The PM motor voltage equations in rotor reference frame [4.22] are given in (4.15)

$$\begin{aligned} v_{qs} &= r_s i_{qs} + \left(\frac{p}{2}\right)\omega_m \left(L_{ds} i_{ds} + \lambda_m\right) + p\left(L_{qs} i_{qs}\right) \\ v_{ds} &= r_s i_{ds} - \left(\frac{p}{2}\right)\omega_m \left(L_{qs} i_{qs}\right) + p\left(L_{ds} i_{ds} + \lambda_m\right) \end{aligned} \tag{4.15}$$

where v_{qs}, v_{ds}, i_{qs} and i_{ds} are the stator input voltage, current in d- and q-axis directions, respectively and λ_m is the stator flux linkage due to the rotor magnets.

Similar to the previous sections, all variables are replaced by their fourier series, and for each harmonics, equation (4.15) is used to analyze them at the given frequency. Here, it is assumed that the motor parameters are frequency and load independent, and harmonics at different frequencies do not affect each other. Considering these assumptions, the variables in (4.15) can be re-written for individual harmonics as in (4.16).

$$\begin{aligned} v_{qsk} &= r_s i_{qsk} + \left(\frac{p}{2}\right)\omega_m \left(L_{ds} i_{dsk} + \lambda_{mk}\right) + jk\omega_m \left(L_{qs} i_{qsk}\right) \\ v_{dsk} &= r_s i_{dsk} - \left(\frac{p}{2}\right)\omega_m \left(L_{qs} i_{qsk}\right) + jk\omega_m \left(L_{ds} i_{dsk} + \lambda_{mk}\right) \end{aligned} \quad , \quad k = [-\infty, +\infty] \tag{4.16}$$

where k, is number of mechanical component in the corresponding variable in rotor reference

frame. Here, i_{qsk} is the harmonic at k^{th} mechanical frequency in q-axis stator current. The symbol k is introduced for mechanical order components in rotor reference frame instead of n which is used in the previous section. Note that the components in this frame are not the same as the *abc* frame which is discussed later. According to FOC, the input voltage is determined by PI controller outputs which is given in (4.17) where k_{pq}, k_{iq}, k_{pd}, k_{id} and the controller parameters, i_{qs}^{*} and i_{ds}^{*} are the reference stator current.

$$\begin{aligned} v_{qs} &= \left(k_{pq} + \frac{k_{iq}}{s} \right) \left(i_{qs}^{*} - i_{qs} \right) \\ v_{ds} &= \left(k_{pd} + \frac{k_{id}}{s} \right) \left(i_{ds}^{*} - i_{ds} \right) \end{aligned} \tag{4.17}$$

By substituting (4.17) into (4.16), the stator d and q-axis currents are obtained through (4.18).

$$\begin{aligned} [I] &= [A]^{-1} [B] \\ [I] &= \begin{bmatrix} i_{qsk} \\ i_{dsk} \end{bmatrix} \end{aligned} \tag{4.18}$$

$$[A] = \begin{bmatrix} jk\omega_m r_s + jk\omega_m k_{pq} + k_{iq} - \left(k\omega_m \right)^2 L_{qs} & j\left(\frac{p}{2} \right) k\omega_m^2 L_{ds} \\ -j\left(\frac{p}{2} \right) k\omega_m^2 L_{qs} & jk\omega_m r_s + jk\omega_m k_{pd} + k_{id} - \left(k\omega_m \right)^2 L_{ds} \end{bmatrix}$$

$$[B] = \begin{bmatrix} \left(jk\omega_m k_{pq} + k_{iq} \right) i_{qsn}^{*} - j\left(\frac{p}{2} \right) k\omega_m^2 \lambda_{mk} \\ \left(jk\omega_m k_{pd} + k_{id} \right) i_{dsn}^{*} + \left(k\omega_m \right)^2 \lambda_{mk} \end{bmatrix}$$

where [I] is the stator current matrix, [A] is the equivalent impedance taking the PI controller parameters into account and [B] is the input voltage matrix. In all the equations given so far, it is

assumed that the rotor speed is constant and the mechanical disturbance is neglected since the mechanical time constants are much higher than electrical. The d-axis stator current reference is set to zero for the rotor speed lower than rated speed and negative value for field weakening region. In all conditions, both d and q-axis stator current are zero for all mechanical harmonics except the dc component and multiple of $(p/2)^{th}$ components which are multiple of electrical frequencies. The reference variables in input matrix are set to zero since they do not include any additional harmonic. The only unknown in input matrix is flux linkage harmonics which can be estimated. According to presented analytical method in [25], the fault signature amplitude is linearly related to fault severity. Knowing the fact that the amplitude of stator flux linkage signatures in a healthy motor are zero, and can be calculated at maximum fault level [25], the flux linkage amplitude of signatures at any fault level is predicted through (4.19).

$$\lambda_{mk,f_L} = \lambda_{mk,1} \times f_L \tag{4.19}$$

where $\lambda_{mk,1}$ and $\lambda_{mk,fL}$ are the amplitude of harmonic at k^{th} mechanical frequency in stator flux linkage when the fault level is 1 (for 100% fault) and f_L respectively, f_L is the fault level ($0 < f_L < 1.0$). Using this analytical method makes it easy to introduce a threshold value for fault signatures. In order to calculate the fault signature amplitudes in *abc* reference frame, motor variable harmonics are transferred to the *abc* frame. This transformation result is given in (4.20).

$$\begin{cases} f_a = \sum_{k=-\infty}^{+\infty} a_k e^{jk\theta_m} \\ f_b = \sum_{k=-\infty}^{+\infty} b_k e^{jk\theta_m} \\ f_c = \sum_{k=-\infty}^{+\infty} c_k e^{jk\theta_m} \end{cases} \tag{4.20}$$

where f_a, f_b and f_c are any three phase variable in *abc* frame, a_k, b_k and c_k are the coefficients at the k^{th} multiple of mechanical frequency which are complex numbers and linked to the harmonics in rotor reference frame through (4.21).

$$
\begin{aligned}
a_k &= \frac{1}{2}\left(d_{\left(k-\frac{p}{2}\right)} + jq_{\left(k-\frac{p}{2}\right)} \right) + \frac{1}{2}\left(d_{\left(k+\frac{p}{2}\right)} - jq_{\left(k+\frac{p}{2}\right)} \right) + o_k \\
b_k &= \frac{1}{2}\left(d_{\left(k-\frac{p}{2}\right)} + jq_{\left(k-\frac{p}{2}\right)} \right) e^{-j120} + \frac{1}{2}\left(d_{\left(k+\frac{p}{2}\right)} - jq_{\left(k+\frac{p}{2}\right)} \right) e^{j120} + o_k \\
c_k &= \frac{1}{2}\left(d_{\left(k-\frac{p}{2}\right)} + jq_{\left(k-\frac{p}{2}\right)} \right) e^{j120} + \frac{1}{2}\left(d_{\left(k+\frac{p}{2}\right)} - jq_{\left(k+\frac{p}{2}\right)} \right) e^{-j120} + o_k
\end{aligned}
\tag{4.21}
$$

These two equations show that k^{th} component in *abc* reference frame is the reflection of $(k\pm p/2)^{th}$ components in rotor reference frame. In order to estimate the k^{th} mechanical component in stator current for any speed and controller parameter values, the $(k\pm p/2)^{th}$ components are calculated through (4.18) and substituted in (4.21).

4.2 Simulation Results

4.2.1 Fault Signatures in Back-emf

In order to verify the introduced analysis, an 8-pole 9-slot PMSM motor is simulated using 2-D FEA. The schematic is depicted in Figure 4.3.a and the parameters given in Table 4.1. The motor has a double layer winding and three coils per phase. Magnets are glued as two pieces along through the shaft axis to reduce eddy current effect. To simulate the fault in FEA, 7% of one rotor magnet is removed and the motor is run at different operating points. Figure 4.3.b shows the faulty motor with one crack on a magnet on the rotor.

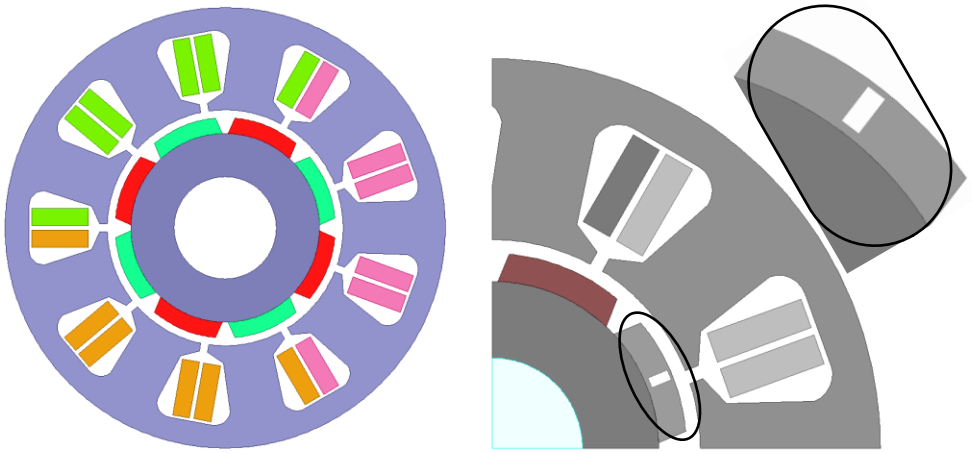

(a) (b)

Figure 4.3. Finite element model of test motor a) Healthy b) Faulty motor

Figure 4.4 shows the back emf spectrums for healthy and faulty motors at rated speed. As shown here, all mechanical harmonics rise up in the fault condition on both side of fundamental harmonic and gradually decrease.

This phenomenon is because of the inherent property of electric motors and can be explained by the derivations introduced in [25]. The change in speed affects the amplitude of harmonics which have higher amplitude.

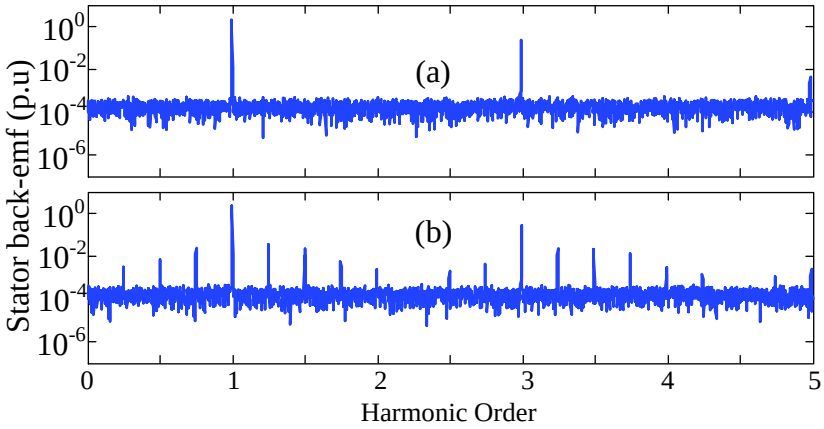

Figure 4.4. Stator back-emf spectrum at rated speed for the 9slot/8pole PMSM, FE results a) Healthy b) Faulty

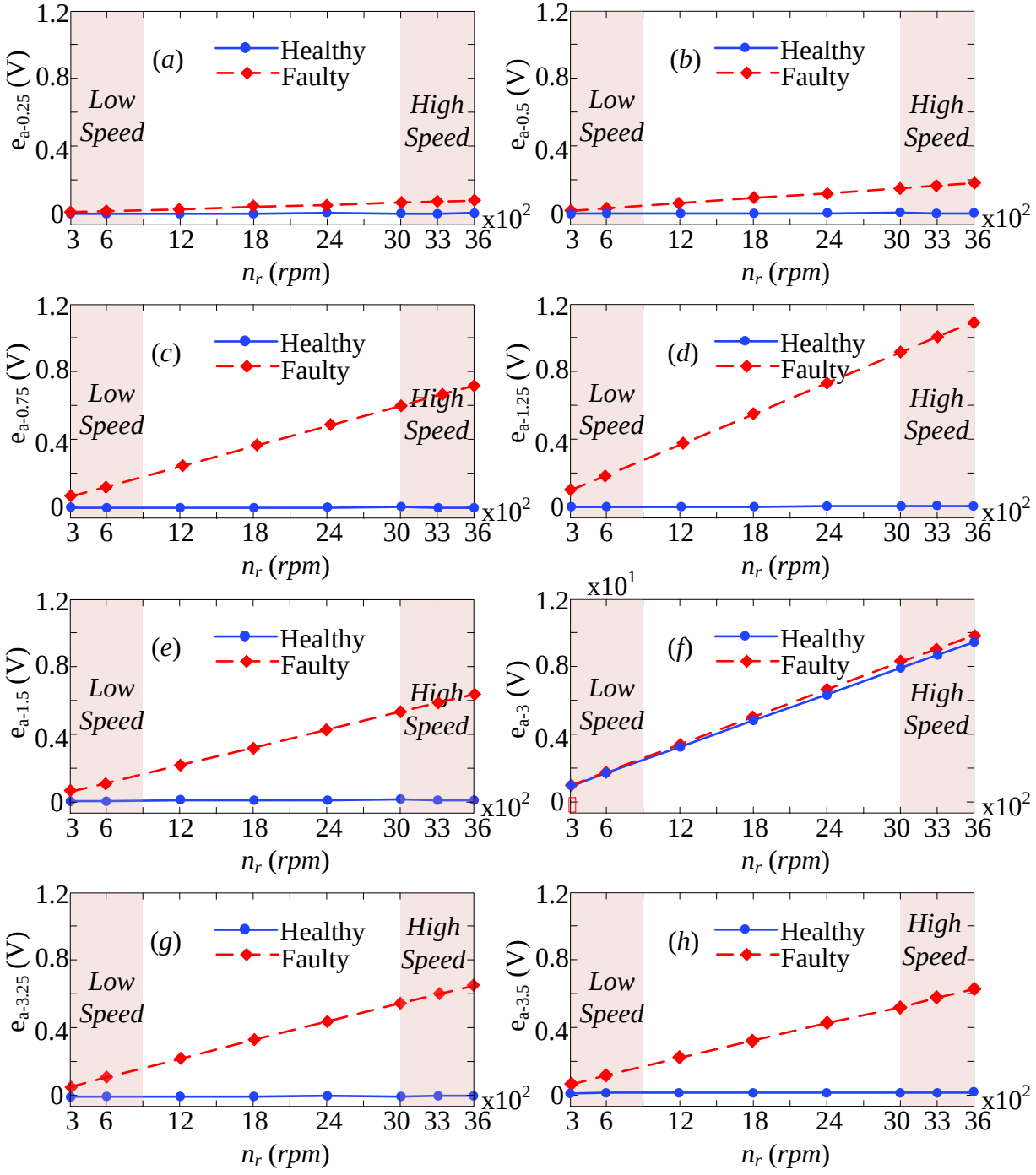

Figure 4.5. FE simulation results for back-emf harmonics behavior vs speed a) 0.25th b) 0.5th c) 0.75th d) 1.25th e) 1.5th f) 3rd g) 3.25th h) 3.5th

Figure 4.5 shows the behavior of different fault signatures in the stator back-emf at various rotor

speeds for healthy and faulty conditions. The simulation results are obtained in the interval of 300 rpm to 3600 rpm including over rated speed region where the rated speed is 3000 rpm. As shown in Figure 4.5, in the healthy condition, none of the fault signatures given in (4.2) appear in the back-emf spectrum. On the other hand, in the faulty motor, all harmonics show up in the spectrum and increase linearly with respect to rotor speed. It is observed that the higher harmonics have higher amplitude at the left hand side of the fundamental component. For instance, 0.75^{th} harmonic has the highest amplitude at all speeds with respect to the others. On the right hand side of the fundamental frequency, the 1.25^{th} component has the highest amplitude. Some of the higher order harmonics in the vicinity of third order harmonic are shown in Figure 4.5.f to Figure 4.5.h. The results show that the magnet defect fault does not affect the third harmonic which remains the same and exist due to the inherent asymmetries and manufacturing imperfections. The behavior of 3.25^{th} and 3.5^{th} harmonics are also similar to low order ones. These results are consistent with the equation (4.4) in which the back-emf fault harmonics vary linearly with respect to the rotor speed.

Table 4.1. Electrical and mechanical parameters of PMSM

Rated voltage	133	V
Rated current	2.8	A
Rated torque	1.27	Nm
Rated speed	3000	rpm
Number of poles	8	
Number of stator slots	9	
Number of stator turn	71	
Stator resistance	2.25	Ω
L_s	7	mH
M_s	1	mH
L_d	5.5	mH
L_q	5.5	mH

4.2.2 Current Fault Signatures-Open Loop Operation

In order to verify the stator current analysis, the PMSM motor described in Table 4.1 is simulated at different load and speed combinations in open loop mode. Figure 4.6 shows the behavior of stator current signatures due to the magnet fault at different speed and torque for faulty and healthy conditions. Before analyzing the current harmonic behaviors, it is worth to mention that some harmonics do not appear in the stator current while they show up in the back-emf. These are 0.75^{th} component (triplen multiple of mechanical frequency) and multiples of it. This is due to the winding connection type and the phase angle difference of each harmonics between the all three phases [25]. As shown in Figure 4.6, lower harmonics like 0.25^{th} and 0.5^{th} are more speed dependent than higher harmonics. The curved amplitude plane and speed dependency of the low order harmonics at lower speeds is because the stator resistance dominates the impedance given in (4.13) at lower frequencies. Higher order components are almost speed and torque independent. Besides the nominal operating points, field weakening and high torque regions are investigated as well. These two regions are examined in order to investigate the effect of negative ids and over current operation mode on the results.

According to the simulation results shown in Figure 4.6, in these regions, most signatures show similar response as in nominal operation points. These harmonics do not have any noticeable role in torque production and they are not affected by load unless the motor become saturated. Since saturation affects the amplitude of fault signatures in stator flux linkage and changes the effective stator inductances, according to (4.12), the amplitude of signatures in the current is affected.

As the saturation level in PM surface mounted motors is relatively low due to large uniform air-gap, it does not have significant effect when the air gap is uniform.

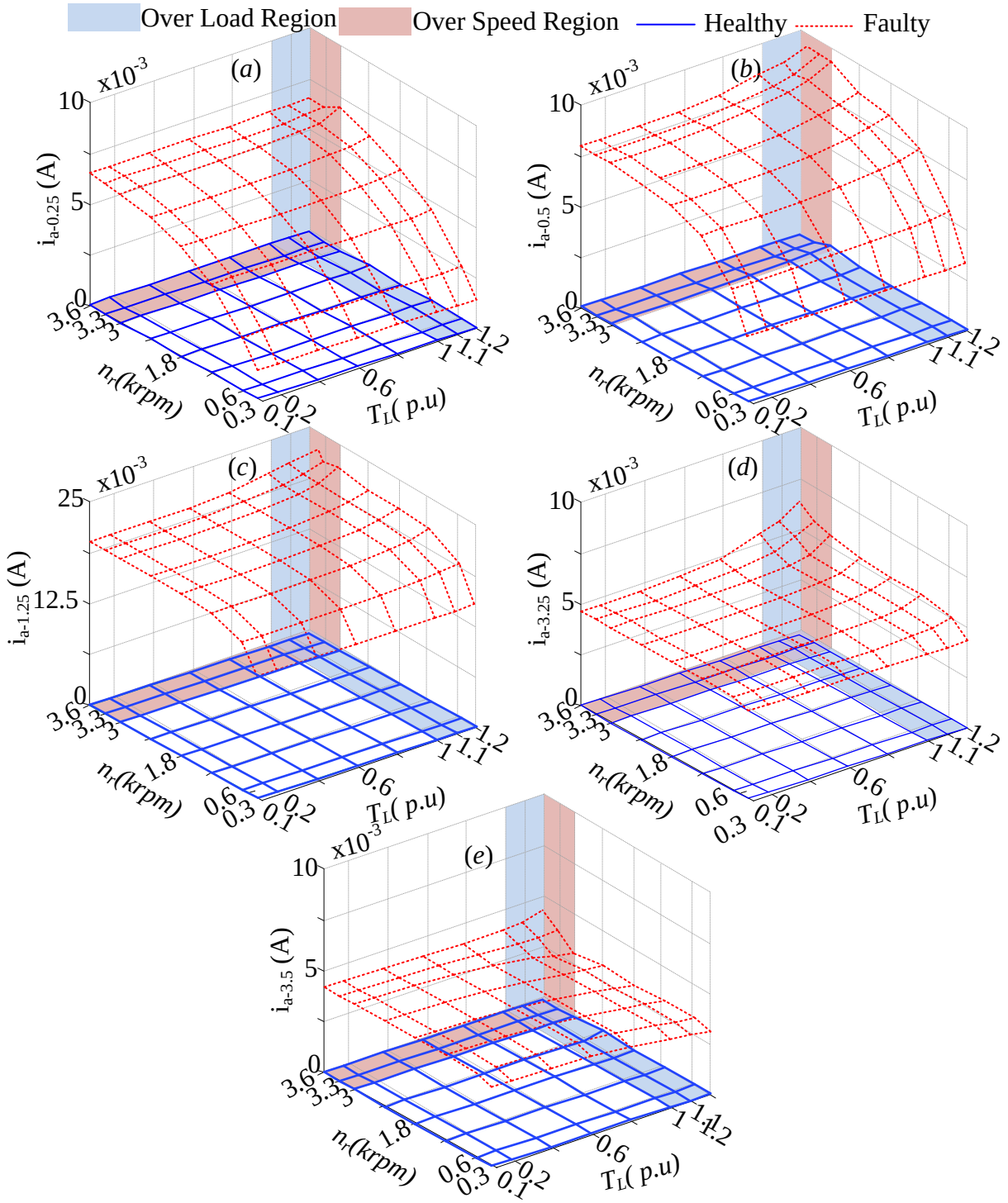

Figure 4.6. Stator current fault signature behavior versus speed and load of healthy and faulty conditions, FEA results a) 0.25th b) 0.5th c) 1.25th d) 2.75th e) 3.25th f) 3.5th

Table 4.2. The amplitude of 0.25^{th} component versus speed for different k_p and k_i coefficients

$\lvert i_{0.25} \rvert$ *(mA)*	k_i=1				k_p=1			
n_r *(k rpm)*	k_p=1	k_p=4	k_p=8	k_p=10	k_i=1	k_i=4	k_i=8	k_i=10
1	48.9	28.7	18.09	15.23	48.85	48.63	48.36	43.50
2	71.18	50.16	34.08	29.15	71.14	70.97	70.76	67.14
3	80	63.84	47.05	41.08	79.98	79.87	79.74	77.41
4	84	72.21	57.01	50.86	83.98	83.91	83.82	82.30
5	86.04	77.35	64.36	58.52	86.03	85.98	85.92	84.86
6	87.22	70.67	69.81	64.51	87.21	87.18	87.14	86.37

4.2.3 Current Fault Signatures-Closed Loop Operation

In order to investigate controller effect on the fault signatures in stator current, the mathematical derivation given in the previous section is used. There are two PI controllers in FOC current loop with two gains (P and I), and the amplitude of stator current fault signatures highly depend on these gains. Though not necessary, it is a common practice to set both P as well as both I coefficients in d and q-axis controllers the same. Taking this into account, the effect of PI parameters on the amplitude of the signature at the first mechanical frequency or 0.25^{th} component in stator current waveform is calculated and given in Table 4.2. The PM motor specification used as test motor in the calculations, simulations and experiments is given in Table 4.1. As seen here, proportional gains have significant effect on the amplitude of the signature. P coefficients suppress the amplitude and extend the linear region shown in Figure 4.2. According to the mathematical derivations and the results shown in Table 4.2, the integral gain does not exhibit a remarkable effect on the current signature amplitude.

As shown in Table 4.2, increasing the integral gain slightly affects the amplitude of 0.25^{th} harmonic in current spectrum.

4.2.4 Fault Severity

In order to investigate the effect of fault intensity on the motor variables in the open loop mode, the PMSM motor is simulated at various fault levels. To adjust the magnet fault severity, one magnet is gradually removed in four steps and during each simulation at different operating points. In this part of study, only two different speed (rated speed - 3000 rpm and low speed -600 rpm) and torque (rated torque -1.27 Nm and 20% of rated torque) are investigated. Figure 4.7 shows the fault signatures in the back-emf under various magnet defect percentages at 600 rpm. The same results are obtained at 3000 rpm and shown in Figure 4.8 to observe the speed effects on the fault signatures. According to (4.1) and (4.4), the back-emf harmonics are linearly dependent on the rotor speed. When Figure 4.7 and Figure 4.8 are compared, it is observed that all signature amplitudes at 3000 rpm are 5 times higher than the corresponding one at 600 rpm. As shown in Figure 4.8, lower harmonics have lower amplitudes and are linearly dependent on the rotor speed. Higher order components have speed dependency but not as much as left side-band components of the fundamental frequency. The 3^{rd} harmonic is not affected by the fault intensity which shows that this component is not a proper index to determine the magnet fault and fault intensity.

Instead, it can be used as separation signature for magnet defects and other electro-mechanical asymmetries. Based on the observations, lower harmonics located at the left hand side of the fundamental frequency are proposed as more reliable signatures to detect the fault as they are

linearly dependent on the rotor speed. Among these, 0.25th and 0.5th harmonics in the stator current are selected to investigate the effect of fault severity. Figure 4.9 shows the behavior of these signatures for various speed, load and fault severity levels.

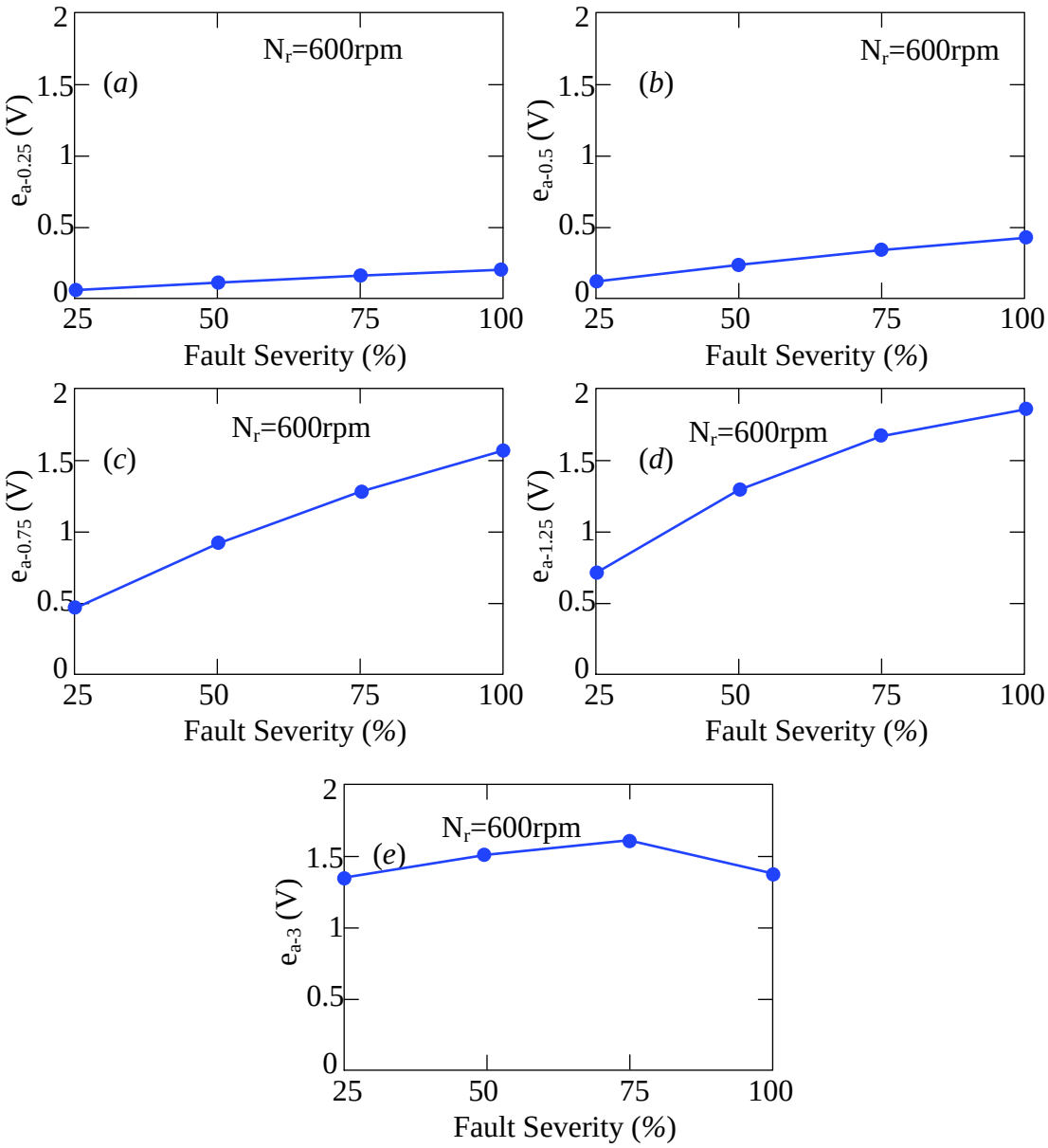

Figure 4.7. Stator back-emf fault signature behavior versus fault severity at 600 rpm a) 0.25th b) 0.5th c) 0.75th d) 1.25th e) 3rd

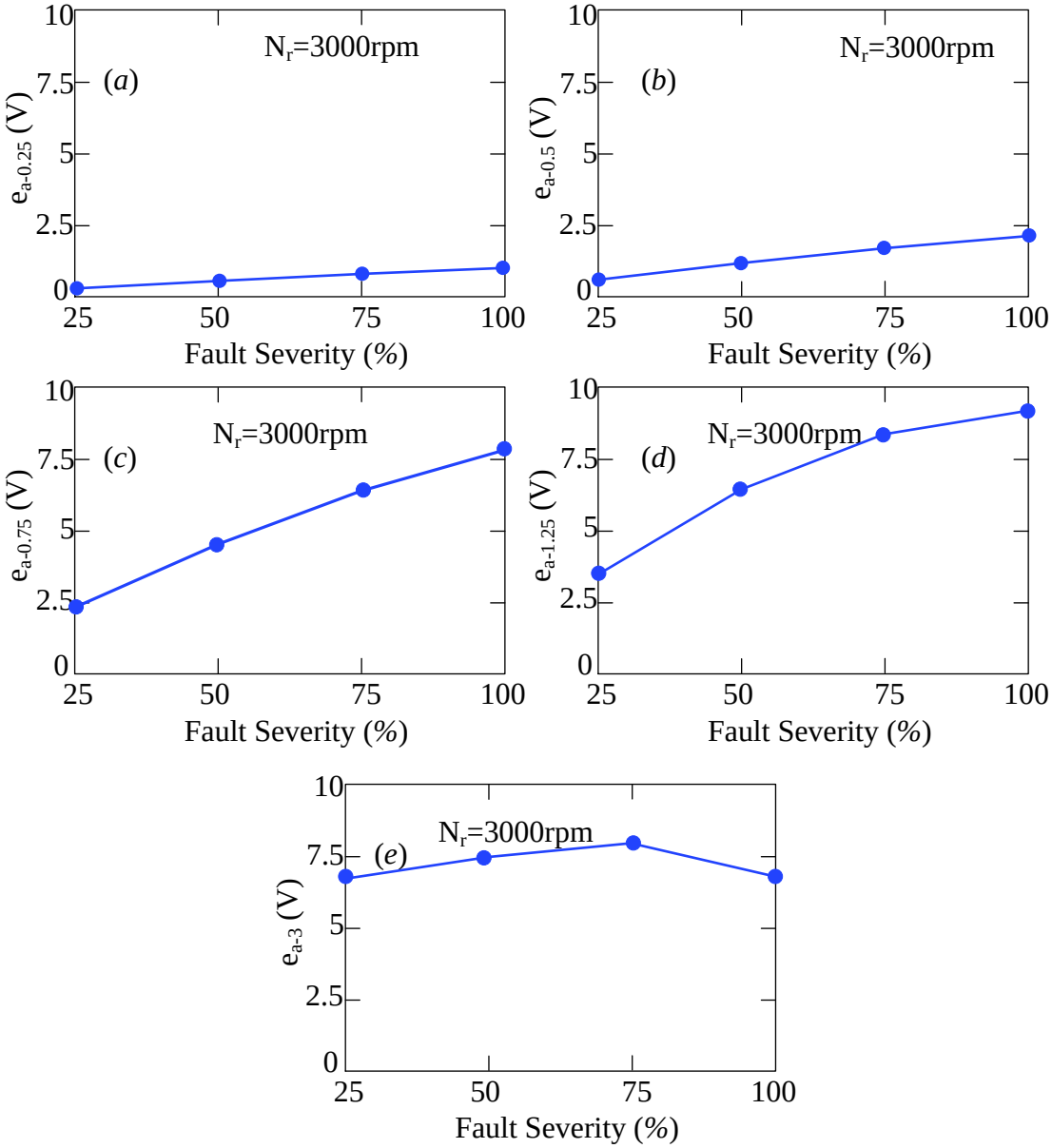

Figure 4.8. Stator back-emf fault signature behavior versus fault severity at 3000 rpm a) 0.25^{th} b) 0.5^{th} c) 0.75^{th} d) 1.25^{th} e) 3^{rd}

According to the presented results, these two harmonics in stator current are torque independent and increase linearly with respect to the fault severity. The amplitude of fault signatures in the stator current is calculated through (4.18).

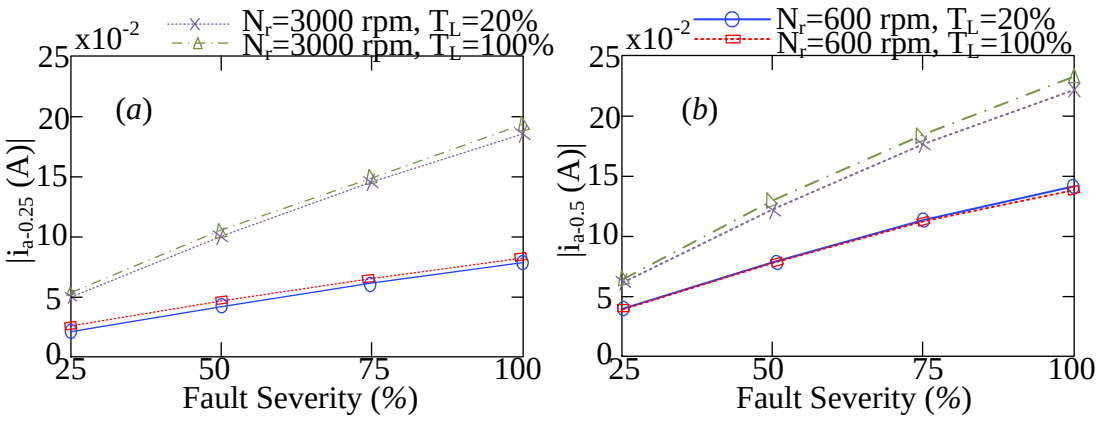

Figure 4.9. Stator current fault signature behavior versus fault severity for different rotor speed and torque a) 0.25^{th} harmonic b) 0.5^{th} harmonic

4.3 Experimental Result

4.3.1 Experimental Setup

In order to verify the findings experimentally, the PMSM motor dyno setup shown in Figure 4.10 is built and supported with necessary sensors and data acquisition systems.

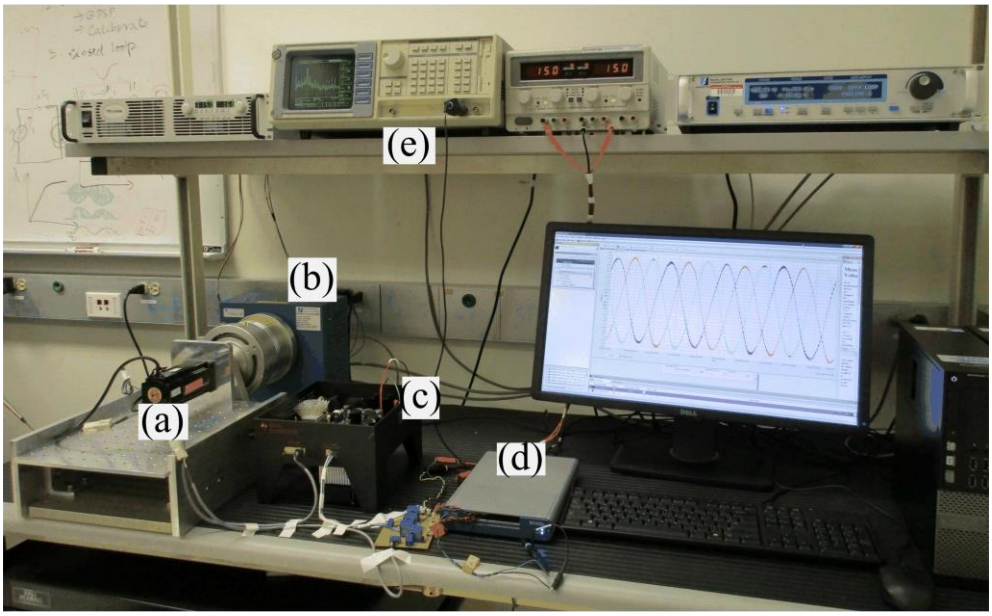

Figure 4.10. Experimental setup a) PMSM b) Dynamometer c) Motor drive d) Data acquisition card e) Spectrum analyzer f) Oscilloscope

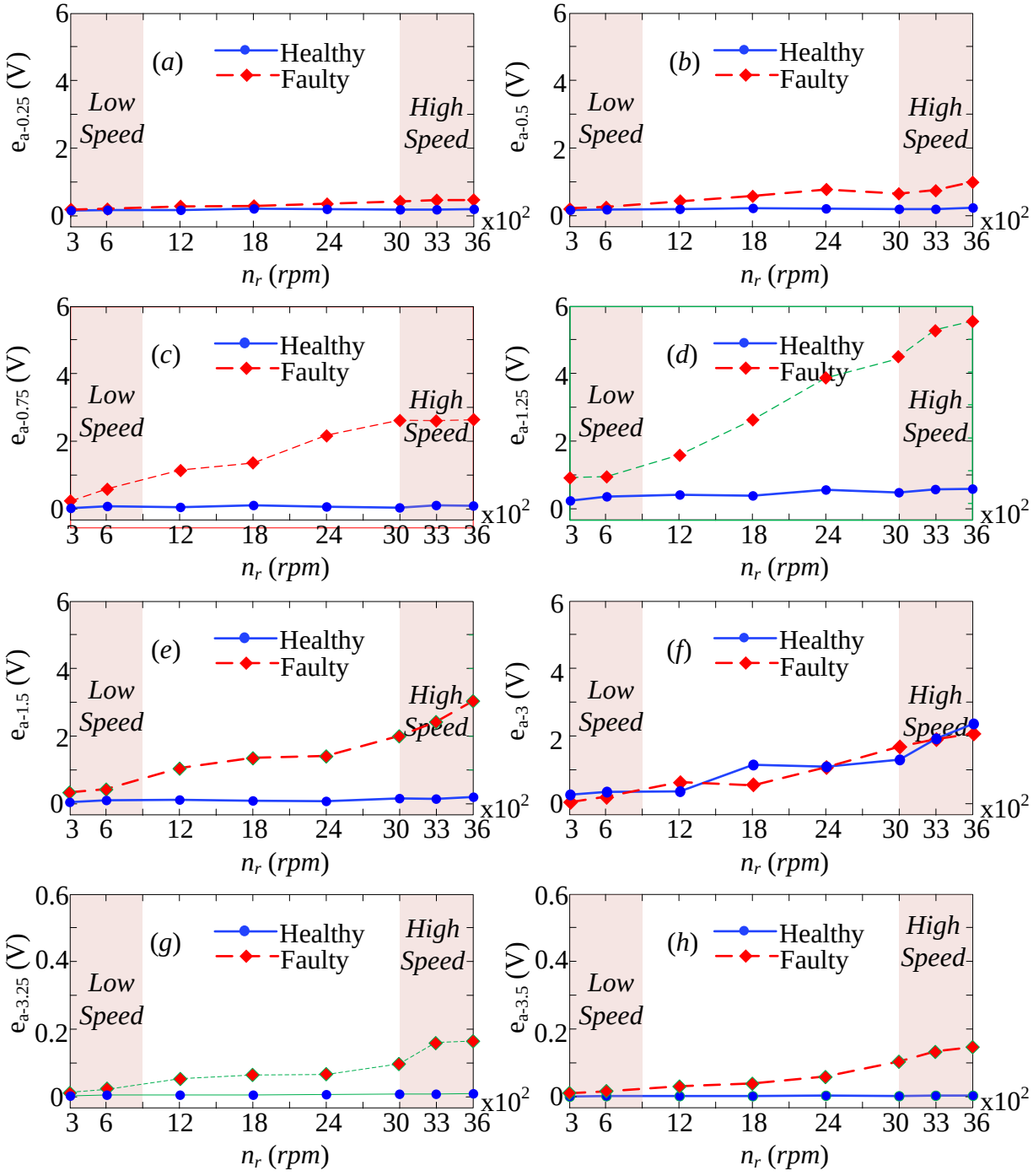

Figure 4.11. Experimental results for back-emf harmonic behavior vs speed a) 0.25th b) 0.5th c) 0.75th d) 1.25th e) 1.5th e) 3rd g) 3.25th h) 3.5th

The setup is controlled through C2000 MCU and Magtrol dynamometer controller to adjust the speed and torque precisely. The back-emf monitoring setup includes a prime mover to spin the test motor, three differential probes to measure the induced phase voltages and spectrum analyzer to observe the saved data in real-time. The setup includes an NI USB-6351 data acquisition board with 16 bit resolution and up to 1MS/s sampling rate to measure and store back-emf and stator current data for post processing.

4.3.2 Fault Signatures in Back-emf

In order to justify the back-emf results, 50% of one magnet is removed using a fine cutter and the faulty motor is run at different speeds to measure the induced voltages across three phases. Figure.4.11 shows the amplitude change of the fault related harmonics with respect to speed including over speed region. As shown in these figures, the amplitude of all signatures change almost linearly with respect to the rotor speed and exhibit consistent behaviors with simulation results. The difference between the experimental and simulation results is due to fault severity differences yet consistent according to the interpolations given in Figure 4.5. In addition, as discussed in the previous section, the fault signature amplitude is almost linearly related to the fault severity. Similar to the simulation results shown in Figure 4.5.f, the motor inherently has remarkable third harmonic in the back emf and the variation of this harmonic is not visible.

4.3.3 Stator Current Fault Signatures- Open Loop Operation

In this step, both healthy and faulty motor with 50% magnet defect are run at different speeds and torques levels in open loop mode [4.23-4.24]. During the open loop operation, the reference values for rotor speed and dq-axis stator voltages are set according to back-emf constant and V/f

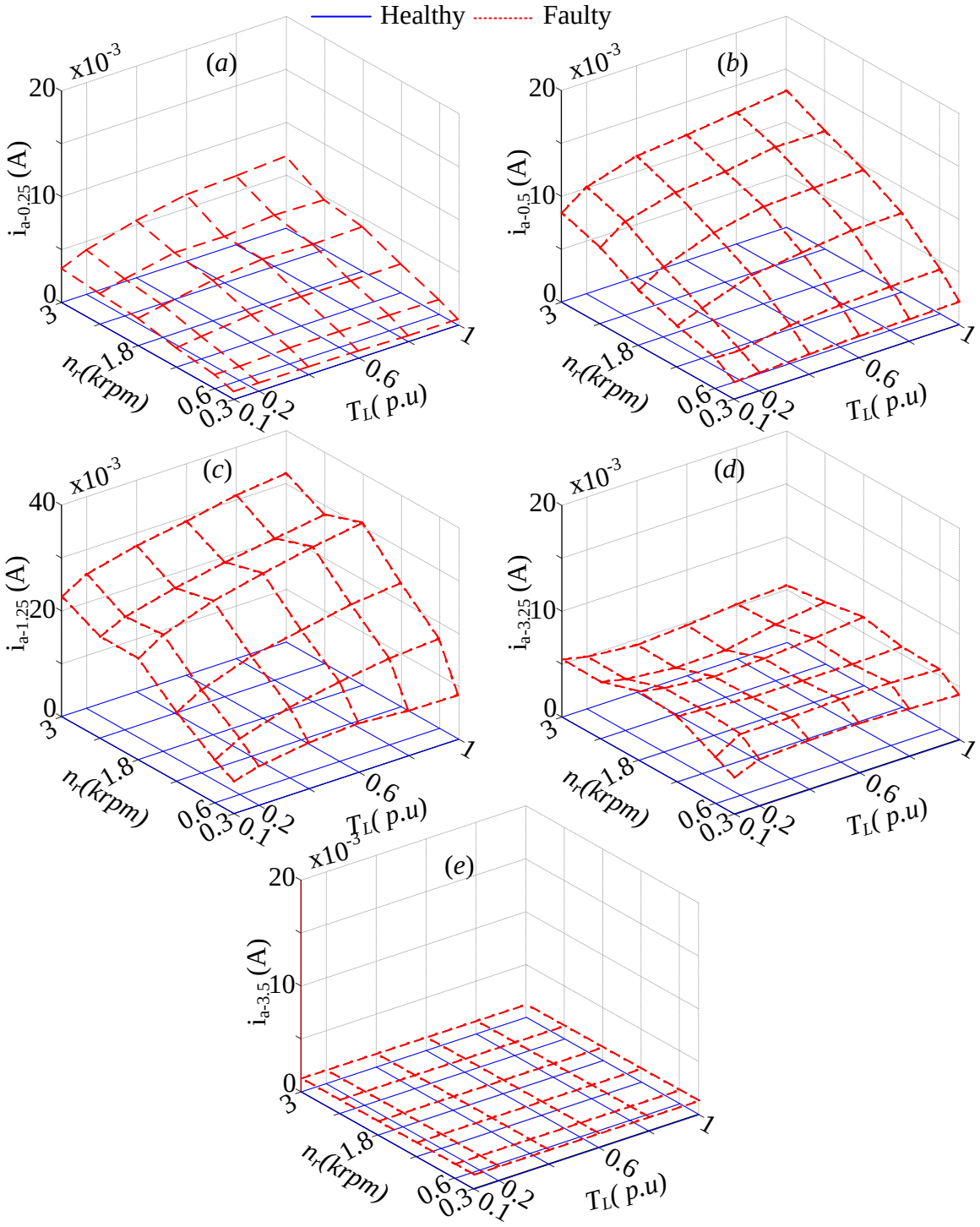

Figure 4.12. Stator current fault signature behavior versus speed and load for healthy and faulty conditions, open loop experimental results a) 0.25th b) 0.5th c) 1.25th d) 3.25th e) 3.5th

ratio. The q-axis voltage reference is carefully adjusted to handle the targeted load and compensate the losses. The experimentally obtained results corresponding to different stator current harmonics are shown in Figure 4.12. As expected, the low order fault signatures (like 0.25^{th} and 0.5^{th}) change linearly with respect to rotor speed in open loop operation mode. On the other hand, the behaviors of high order fault components do not show are makeable variation with respect to the rotor speed. Both high and low order fault signatures are torque independent as observed in the simulations. The experimental results show a good agreement with theoretical findings discussed in the previous section.

4.3.4 Stator Current Fault Signature –Closed Loop Operation

In order to investigate the controller effects on stator current fault signature behaviors, both healthy and faulty motors are tested at different operating points taking the current feedback into account. As discussed in the previous section, the proportional and integral gains in both current controllers are set equally. Figure 4.13 shows closed loop response of the stator current harmonic behaviors for various speed/load conditions. As seen here, lower harmonics change linearly with respect to the speed which is similar to the open loop results. However, the slope of each signature change is lower than open loop mode which is due to the controller effect and is consistent with the findings presented in the previous section. In high order harmonics, R_s in the effective impedance is not a dominant element anymore and the overall amplitude remains constant as discuss earlier. Due to the dominating effect of controllers, even high order harmonics change linearly with respect to the speed.

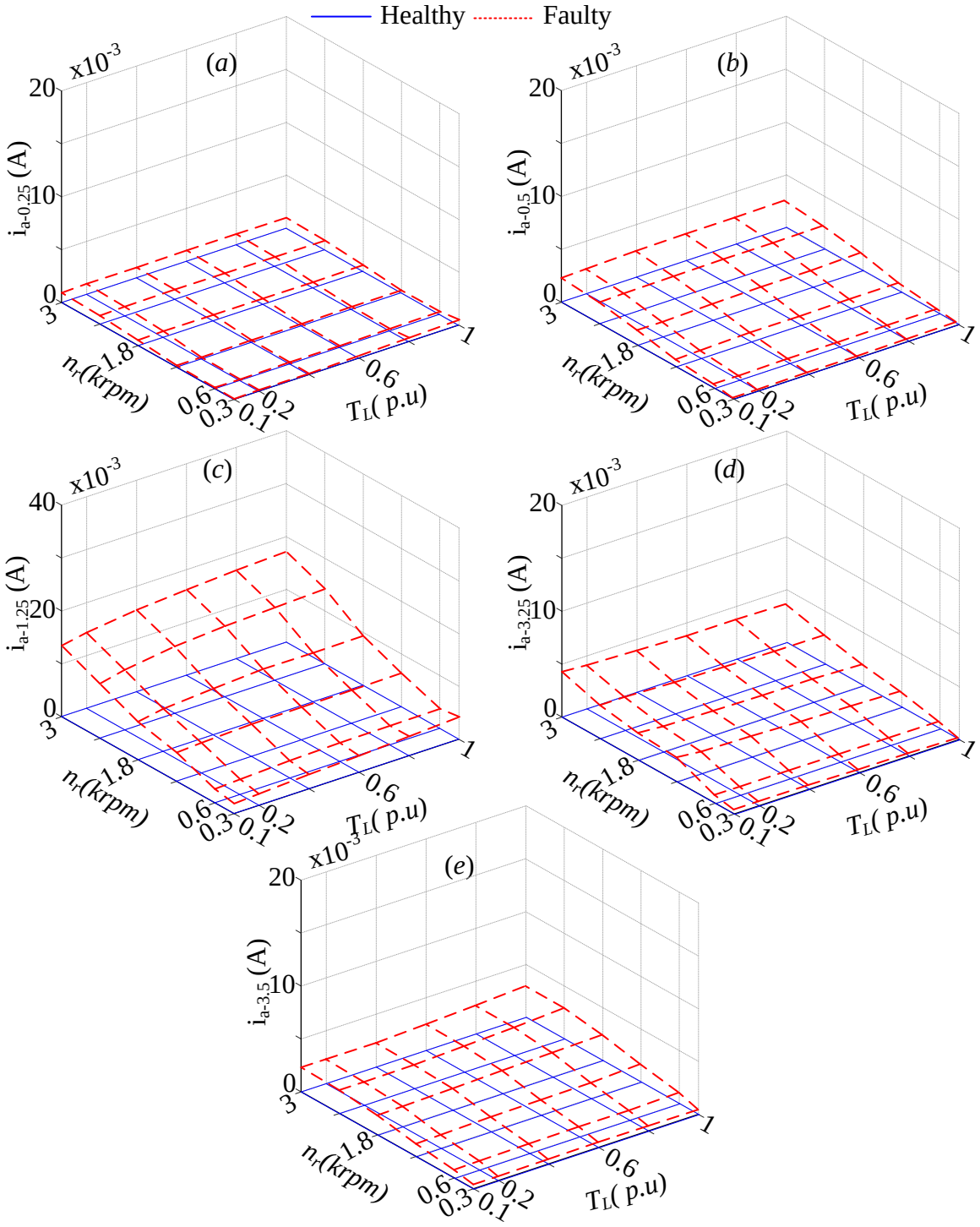

Figure 4.13. Stator current fault signature behavior versus speed and load for healthy and faulty conditions, closed loop experimental results a) 0.25th b) 0.5th c) 1.25th d) 3.25th e) 3.5th

4.4 Conclusion

In this chapter, a novel fault severity assessment is introduced to model the dynamic behavior of magnet defect fault signatures in the stator current using linear PM motor model and the corresponding derivations are validated throughout all possible operating points. Since the effect of current loop controller on the current fault signatures is not included in the model, it is investigated separately to observe the secondary changes on the signatures. Initially, the effect of fault on the back-emf at different speed is investigated and it is shown that the amplitudes of the fault signatures in back-emf are linearly dependent on the rotor speed. Similarly, another derivation is presented to calculate the current signature amplitude using motor parameters. According to these derivations, it is shown that amplitude of signatures in stator current depends on both the harmonic order and speed. For instance, the amplitude of a low order fault harmonic changes at low speed linearly due to dominating stator resistance term whereas at high speed it becomes almost constant due to dominating inductor reactance. In addition, the presented results clearly show that the proportional gains in current loop control have superior effects on the current fault harmonics than integral gains. The controllers change the open loop response and suppress the fault signatures which results in almost linear relationship between rotor speed and amplitude. Simulations and experimental results show consistency with the proposed theoretical analysis.

In addition to the proposed techniques in the literature, this paper provides a motor specific fault severity assessment based on PMSM drive parameters. Compared to counterparts, this approach is unique since it helps user to customize the fault analysis for a given motor and fine tune the fault threshold level to minimize the missing or false alarms.

CHAPTER 5

SUMMARY AND CONCLUSION

In this study, the effects of magnet defects on the stator phase back-emf and current is investigated through MEC. As an analytical tool, partitioned MEC is developed in a flexible manner to investigate winding configurations and fault locations effect on the motor variable spectrums.

Using the partitioned MEC, it is shown that the effect of each rotor magnet on each stator coil can be calculated to obtain the induced back-emf under various magnet defect combinations and observe the corresponding fault signatures in the frequency spectrum. The proposed analytical tool has several advantages with respect to conventional tools such as shorter simulation time, analyzing the effect of individual stator coil and number and location of defected magnet separately. In the case of multiple magnet defects, depending on the number and location of the defects, the back-emf and current spectrums vary. In addition, it is shown through the phase information of the fault signatures that, the signatures at triplen multiples of mechanical frequency disappear depending on the winding connection. If not taken into account, these missing or additional components may result in false alarms. After several tests including various shape and direction combinations, it is concluded that the direction or the shape of the crack has no additional effect on the current and back-emf waveforms where the only critical parameter found to be the overall volume of the magnets. The effects of load and speed on the amplitude of the faulty signatures are also studied to clarify the speed and torque dependency. The simulated fault scenarios are implemented on the experimental setup to show the consistency of simulations and experimental findings. It is shown that the key fault signatures are less torque

more speed dependent which should carefully be taken into account for variable speed drive applications.

In addition to the crack shape, the effect of PM motor topology on the magnet defect fault signatures is investigated through the proposed partitioned MEC. Several motors with different number of pole and slot are analyzed through this method in order to generalize the findings. In addition, various cases including full, fractional and short pitch winding, skew and stator winding connection types are also discussed. It is shown that in the case of single layer winding, when the number of slot and pole ratio is multiple of 3, magnet defect faults do not create any fault related signature in the stator back emf and current. Similarly, the PM motors with double layer winding and slot and pole ratio of 1.5 or multiples, the fault related signatures are not observed. The effect of the winding connection type is also investigated through phase information of fault signatures, and shown that the star connection suppresses current fault signatures at the triplen multiples of mechanical frequency. The location of the magnet defects are also studied and it is shown that if the magnet defect locations are symmetrical with respect to rotor centerline, some of the fault harmonics do not show up in the back emf and current spectrum. For instance, in the case of 8 pole motor, if there is even number of magnet defects and half of them are located in the first 4 poles and the second half is located symmetrically in the next 4 poles, the odd multiples of 0.25^{th} harmonic do not appear in motor back-emf. As an example, if 2 poles are defected such as magnet 1 and magnet 5, this phenomenon is observed. In order to verify the analytical findings, two different PM motor with different number of slot and pole are used in the experiments and then simulated through FE, and the results are compared with the partitioned MEC results.

In last part of study, a novel fault severity assessment is introduced to model the dynamic behavior of magnet defect fault signatures in the stator current using linear PM motor model and the corresponding derivations are validated throughout all possible operating points. Since the effect of current loop controller on the current fault signatures is not included in the model, it is investigated separately to observe the secondary changes on the signatures. Initially, the effect of fault on the back-emf at different speed is investigated and it is shown that the amplitudes of the fault signatures in back-emf are linearly dependent on the rotor speed. Similarly, another derivation is presented to calculate the current signature amplitude using motor parameters. According to these derivations, it is shown that amplitude of signatures in stator current depends on both the harmonic order and speed. For instance, the amplitude of a low order fault harmonic changes at low speed linearly due to dominating stator resistance term whereas at high speed it becomes almost constant due to dominating inductor reactance. In addition, the presented results clearly show that the proportional gains in current loop control have superior effects on the current fault harmonics than integral gains. The controllers change the open loop response and suppress the fault signatures which results in almost linear relationship between rotor speed and amplitude. Simulations and experimental results show consistency with the proposed theoretical analysis.

In addition to the proposed techniques in the literature, this paper provides a motor specific fault severity assessment based on PMSM drive parameters. Compared to counterparts, this approach is unique since it helps user to customize the fault analysis for a given motor and fine tune the fault threshold level to minimize the missing or false alarms.

REFERENCES

[1] Sung-Yoon Jung; Mi, C.C.; Kwanghee Nam, "Torque Control of IPMSM in the Field-Weakening Region With Improved DC-Link Voltage Utilization," *Industrial Electronics, IEEE Transactions on*, vol.62, no.6, pp.3380,3387, June 2015

[2] G.-A. Capolino, J.A. Antonino-Daviu, M. Riera-Guasp, "Modern Diagnostics Techniques for Electrical Machines, Power Electronics, and Drives," IEEE Trans. Ind. Electron, vol.62, no.3, pp.1738,1745, March 2015

[3] S. Moon, J. Lee; H. Jeong, S. W. Kim, "Demagnetization fault diagnosis of a PMSM based on structure analysis of motor inductance," IEEE Trans. Ind. Electron, vol. 63, no. 6, pp. 3795-3803, June 2016.

[4] Ostojic, P.; Banerjee, A.; Patel, D.C.; Basu, W.; Ali, S., "Advanced Motor Monitoring and Diagnostics," Industry Applications, IEEE Transactions on , vol.50, no.5, pp.3120,3127, Sept.-Oct. 2014

[5] Drif, M.; Cardoso, A.J.M., "Stator Fault Diagnostics in Squirrel Cage Three-Phase Induction Motor Drives Using the Instantaneous Active and Reactive Power Signature Analyses," Industrial Informatics, IEEE Transactions on , vol.10, no.2, pp.1348,1360, May 2014

[6] Ojeda, X.; Li, G.J.; Gabsi, M., "Fault diagnosis using vibration measurements of a Flux-Switching permanent magnet motor," Industrial Electronics (ISIE), 2010 IEEE International Symposium on, vol., no., pp.2091,2096, 4-7 July 2010

[7] Penman, J.; Sedding, H.G.; Lloyd, B.A.; Fink, W. T., "Detection and location of interturn short circuits in the stator windings of operating motors," Energy Conversion, IEEE Transactions on , vol.9, no.4, pp.652,658, Dec 1994

[8] Urresty, J.; Riba, J.; Romeral, L., "A back-emf based method to detect magnet failures in PMSMs," Magnetics, IEEE Transactions on, vol.49, no.1, pp.591,598, Jan. 2013

[9] Khan, M.; Azizur Rahman, M., "Development and implementation of a novel fault diagnostic and protection technique for ipm motor drives," Industrial Electronics, IEEE Transactions on, vol.56, no.1, pp.85,92, Jan. 2009

[10] Gandhi, A.; Corrigan, T.; Parsa, L., "Recent Advances in Modeling and Online Detection of Stator Interturn Faults in Electrical Motors,"Industrial Electronics, IEEE Transactions on, vol.58, no.5, pp.1564,1575, May 2011

[11] Sen, B.; Wang, J., "A fast detection technique for stator inter-turn fault in multi-phase permanent magnet machines using model based approach," Power Electronics, Machines and Drives (PEMD 2014), 7th IET International Conference on, vol., no., pp.1,6, 8-10 April 2014

[12] Drif, M'hamed; Cardoso, A.J.Marques, "Air-gap eccentricity fault diagnosis, in three-phase induction motors, by the instantaneous power signature analysis," Power Electronics, Machines and Drives, 2006. The 3rd IET International Conference on, vol., no., pp.349,353, 4-6 April 2006

[13] Kyung-Tae Kim; Jun-Kyu Park; Jin Hur; Byeong-Woo Kim, "Comparison of the fault characteristics of ipm-type and spm-type bldc motors under inter-turn fault conditions using winding function theory," Industry Applications, IEEE Transactions on , vol.50, no.2, pp.986,994, March-April 2014.

[14] Shin-Myung Jung; Jin-Sik Park; et. al. "An MRAS-Based diagnosis of open-circuit fault in PWM voltage-source inverters for PM synchronous motor drive systems," Power Electronics, IEEE Transactions on, vol.28, no.5, pp.2514,2526, May 2013.

[15] J. Faiz, B.M. Ebrahimi, B. Akin, H. Toliyat, "Finite-Element Transient Analysis of Induction Motors Under Mixed Eccentricity Fault," IEEE Trans. on Magn, vol.44, no.1, pp.66,74, Jan. 2008.

[16] S.M. Jung, J.S. Park, H.W. Kim, K.Y. Cho, M.J. Youn, "An MRAS-Based diagnosis of open-circuit fault in PWM voltage-source inverters for PM synchronous motor drive systems," IEEE Trans. on Power Electronics, vol.28, no.5, pp.2514,2526, May 2013.

[17] J.C. Urresty, J. R. Riba, L. Romeral, "Influence of the Stator Windings Configuration in the Currents and Zero-Sequence Voltage Harmonics in Permanent Magnet Synchronous Motors With Demagnetization Faults," IEEE Trans. on Magn, vol. 49, no. 8, pp. 4885-4893, Aug. 2013.

[18] M.A. Jabbar, A.B. Azeman, "Fast optimization of electromagnetic-problems: the reduced-basis finite element approach," IEEE Trans. on Magn, vol.40, no.4, pp.2161,2163, July 2004

[19] le Roux, W.; Harley, R.G.; Habetler, T.G., "Detecting Rotor Faults in Low Power Permanent Magnet Synchronous Machines," in Power Electronics, IEEE Transactions on , vol.22, no.1, pp.322-328, Jan. 2007

[20] Gritli, Y.; Rossi, C.; Casadei, D.; Zarri, L.; Filippetti, F., "Demagnetizations diagnosis for Permanent Magnet Synchronous Motors based on advanced Wavelet Analysis," in Electrical Machines (ICEM), 2012 XXth International Conference on , vol., no., pp.2397-2403, 2-5 Sept. 2012.

[21] J. Rosero, L. Romeral, J. Cusido, J. A. Ortega, "Fault detection by means of wavelet transform in a PMSM under demagnetization," IEEE The 33rd Annual Conf of IEEE Indust. Electr. Soc.(IECON) Transactions on Industry Applications, Taipei,Taiwan, pp. 1149-1154, Now. 2007.

[22] Urresty, J.-C.; Riba, J.-R.; Romeral, L., "Influence of the Stator Windings Configuration in the Currents and Zero-Sequence Voltage Harmonics in Permanent Magnet Synchronous Motors With Demagnetization Faults," in Magnetics, IEEE Transactions on , vol.49, no.8, pp.4885-4893, Aug. 2013

[23] J. De Bisschop, A.Abdallh,P. Sergeant,andL.Dupre, "Identification of Demagnetization Faults in Axial Flux Permanent Magnet Synchronous Machines Using an Inverse Problem Coupled With an Analytical Model," IEEE Trans. Magn., vol.50, no.11, pp. 1–4, Nov. 2014.

[24] B. M. Ebrahimi and J. Faiz, "Demagnetization fault diagnosis in surface mounted permanent magnet synchronous motors," IEEE Trans. Magn., vol. 49, no. 3, pp. 1185-1192, March 2013.

[25] Zafarani, M.; Goktas, T.; Akin, B., "A Comprehensive Analysis of Magnet Defect Faults in Permanent Magnet Synchronous Motors," in Industry Applications, IEEE Transactions on, vol.PP, no.99, pp.1-1, October 2015.

[26] Urresty, J.-C.; Riba, J.-R.; Saavedra, H.; Romeral, L., "Detection of inter-turns short circuits in permanent magnet synchronous motors operating under transient conditions by means of the zero sequence voltage," in Power Electronics and Applications (EPE 2011), Proceedings of the 2011-14th European Conference on , vol., no., pp.1-9, Aug. 30 2011-Sept. 1 2011

[27] Ruschetti, C.; Bossio, G.; De Angelo, C.; Verucchi, C., "Effects of partial rotor demagnetization on permanent magnet synchronous machines," in Industrial Technology

(ICIT), 2010 IEEE International Conference on , vol., no., pp.1233-1238, 14-17 March 2010.

[28] A. Gandhi, T. Corrigan, and L. Parsa, “Recent advances in modeling and online detection of stator inter-turn faults in electrical motors,” IEEE Trans. Ind. Electron., vol. 58, no. 5, pp. 1564–1575, May 2011.

[29] Jung-Seob Shin; Watanabe, R.; Koseki, T.; Houng-Joong Kim, "Transverse-Flux-Type Cylindrical Linear Synchronous Motor Using Generic Armature Cores for Rotary Machinery," Industrial Electronics, IEEE Transactions on , vol.61, no.8, pp.4346,4355, Aug. 2014

[30] Dong-Hee Lee; Trung Hieu Pham; Jin-Woo Ahn, "Design and Operation Characteristics of Four-Two Pole High-Speed SRM for Torque Ripple Reduction," Industrial Electronics, IEEE Transactions on, vol.60, no.9, pp.3637,3643, Sept. 2013

[31] Dong-Kuk Lim; Kyung-Pyo Yi; et. al. "Analysis and Design of a Multi-Layered and Multi-Segmented Interior Permanent Magnet Motor by Using an Analytic Method,"Magnetics, IEEE Transactions on, vol.50, no.6, pp.1,8, June 2014

[32] Li Yu; Zhuoran Zhang; Zhihui Chen; Yangguang Yan, "Analysis and Verification of the Doubly Salient Brushless DC Generator for Automobile Auxiliary Power Unit Application," Industrial Electronics, IEEE Transactions on, vol.61, no.12, pp.6655,6663, Dec. 2014

[33] Y.D. Chun, J. E. Oh, Y. Fujishima, S. Wakao, J. Lee, Y.H, Cho, "Comparison between three-dimensional (3D) equivalent magnetic circuit network method and 3D finite element method for magnetic-field computation," Journal of Applied Physics, vol.97, no.10, pp.10E105,10E105-3, May 2005

BIOGRAPHICAL SKETCH

Mohsen Zafarani received his M.Sc in Electrical Engineering from Isfahan University of Technology, Isfahan, Iran, in 2011. From 2014, he joined Power Electronic and Drives Lab at The University of Texas at Dallas as a PhD student. He has authored/coauthored over 20 journal and conference papers. His research interests include design and analysis of electric machines, modelling of electromagnetic devices and fault diagnoses in PM motors.

Mr. Zafarani was the recipient of the Louis Beecherl Jr. Graduate Fellowship for the 2017-2018 academic year from The University of Texas at Dallas.

CURRICULUM VITAE

Mohsen Zafarani

Education

- **University of Texas at Dallas**, **TX (GPA: 3.8/4)** (01/2014- 08/2018)
  Ph.D. in Electrical Engineering
- **Isfahan University of Technology, Iran (GPA: 17.76/20)** (09/2008-02/2011)
  M.Sc. in Electrical Engineering

Professional Experience

Research Assistant at Power Electronics Lab, University of Texas at Dallas (01/2014- 08/2018)

- **PMSMS Inductance characterizations (Sponsored by Texas Instruments)**
  - FEA model development to for motor parameter variation with current level and rotor position;
  - Develop an analytical function describes the *d-q* axes self and cross coupling inductances as a function of current and frequency;
  - Experimental verification of the developed model using a TI-based set up with Piccolo MCU;

- **Torsional and lateral vibrations analysis of in induction motor (Sponsored by Schlumberger Company)**
  - Numerical and analytical modeling of multi-rotor single-stator IM applicable in electric submersible pump (ESP);
  - A sophisticated mathematical approach to calculate air-gap flux density;
  - Eccentricity, torsional and lateral vibrations analysis using mathematical techniques;
  - Mathematical characterization of stator current spectrum based on different types and levels of fault;

- **Current Based Fault Diagnosis of PMSMs (Sponsored by Texas Instruments)**
  - Theoretical and mathematical analysis of faults in PMSMs
  - Analysis of controller parameter effects on fault diagnosis system

- **PMSM Fault Detection Using Flux Gate Sensor(Sponsored by Texas Instruments)**
  - The effect of various faults on leakage flux around several PM motors is investigated analytically and experimentally;
  - A sophisticated comparison between stator current and leakage flux spectrums is done;
  - A unique index is introduced for each failure to diagnose the type and severity of fault;

Electrical Engineer at P. Niro Inc. (04/2011- 07/2013)

- **Design and Analysis of Permanent Magnet Synchronous Machines**
  - Design and manufacture a 1kw PMSM motor with low torque ripple and high speed;
  - Implement an inverter for the designed motor using ARM microcontroller;
  - Design the PCB for the whole control part;
- **Design and Manufacture a DC motor drive**
  - Design all elements base on the rated voltage and current such as DC link capacitor and switches for both stator and rotor excitations;
  - Design the PCB for the whole control part;

Teaching Assistant at Isfahan University of Technology (09/2008- 01/2011)

- **Design and Manufacturing of Transverse Flux Permanent Magnet Machine (MSc thesis)**
  - An analytical magneto-static model for a transverse flux PM machines based on magnetic equivalent circuit is developed;
  - This method is useful for design and analysis of any salient motor;
  - A prototype of a transverse flux PM machine is manufactured and tested;

Computer Skills

- **Engineering Software**: MATLAB/Simulink, MAXWELL3D&2D and RMxprt; Simplorer, PSIM, Altium Designer
- **Programming languages**: MATLAB program language, Atmel studio, Code composer studio;
- **General Software**: Word, Excel, PowerPoint, Visio;

Graduate Courses

Adjustable Speed Motor Control	Comprehensive Theory of Electric Machines
Vector Control of AC Electric Machines	Power Electronic
Power System Dynamics	Power System Analysis
Reactive Power Control	Linear System Control

Publications

Journal Publications

- **M. Zafarani**, T. Goktas and B. Akin, "A Comprehensive Magnet Defect Fault Analysis of Permanent-Magnet Synchronous Motors," in IEEE Transactions on Industry Applications, vol. 52, no. 2, pp. 1331-1339, March-April 2016.

- **M. Zafarani**, T. Goktas, B. Akin and S. E. Fedigan, "An Investigation of Motor Topology Impacts on Magnet Defect Fault Signatures," in IEEE Transactions on Industrial Electronics, vol. 64, no. 1, pp. 32-42, Jan. 2017.
- **M. Zafarani**, T. Goktas, B. Akin and S. E. Fedigan, "Modeling and Dynamic Behavior Analysis of Magnet Defect Signatures in Permanent Magnet Synchronous Motors," in IEEE Transactions on Industry Applications, vol. 52, no. 5, pp. 3753-3762, Sept.-Oct. 2016.
- T. Goktas, **M. Zafarani** and B. Akin, "Discernment of Broken Magnet and Static Eccentricity Faults in Permanent Magnet Synchronous Motors," in IEEE Transactions on Energy Conversion, vol. 31, no. 2, pp. 578-587, June 2016.
- Y. Qi, **M. Zafarani**, B. Akin and S. E. Fedigan, "Analysis and Detection of Inter-Turn Short-Circuit Fault Through Extended Self-Commissioning," in IEEE Transactions on Industry Applications, vol. 53, no. 3, pp. 2730-2739, May-June 2017.
- T. Goktas, **M. Zafarani**, K. W. Lee, B. Akin and T. Sculley, "Comprehensive Analysis of Magnet Defect Fault Monitoring Through Leakage Flux," in IEEE Transactions on Magnetics, vol. 53, no. 4, pp. 1-10, April 2017.
- M. Peyvandi, **M. Zafarani**, E. Nasr, "Comparison of Particle Swarm Optimization and Genetic Algorithm in the Improvement of Power System Stability by a SSSC-based Controller", Journal of Electrical Engineering & Technology Vol. 6, No. 2, pp. 182-191, 2011.

Conference Publications

- **M. Zafarani** and B. Akin, "Comparison of real time motor fault signature analysis algorithms for drive embedded systems," 2017 IEEE International Electric Machines and Drives Conference (IEMDC), Miami, FL, 2017, pp. 1-7.
- M. Heydarzadeh, **M. Zafarani**, B. Akin and M. Nourani, "Automatic fault diagnosis in PMSM using adaptive filtering and wavelet transform," 2017 IEEE International Electric Machines and Drives Conference (IEMDC), Miami, FL, 2017, pp. 1-7.
- Y. Qi, **M. Zafarani** and B. Akin, "A diagnosis procedure in standstill mode for inter turn short circuit faults of PMSMs through modified self-commissioning," 2016 IEEE Energy Conversion Congress and Exposition (ECCE), Milwaukee, WI, 2016, pp. 1-7.
- M. Heydarzadeh, **M. Zafarani**, B. Akin and M. Nourani, "RUL estimation in rotary machines using linear dimension reduction and Bayesian inference," 2017 IEEE International Electric Machines and Drives Conference (IEMDC), Miami, FL, 2017, pp. 1-6
- T. Goktas, K. W. Lee, **M. Zafarani** and B. Akin, "Analysis of magnet defect faults in permanent magnet synchronous motors through fluxgate sensors," 2016 IEEE Applied Power Electronics Conference and Exposition (APEC), Long Beach, CA, 2016, pp. 2875-2880.
- **M. Zafarani**, T. Goktas and B. Akin, "A comprehensive assessment of PM motor topology impact on magnet defect fault signatures," 2016 IEEE Applied Power Electronics Conference and Exposition (APEC), Long Beach, CA, 2016, pp. 1096-1101 **(Student Travel Support Award)**.
- **M. Zafarani**, T. Goktas and B. Akin, "A comprehensive analysis of magnet defect faults in permanent magnet synchronous motors," 2015 IEEE Applied Power Electronics Conference and Exposition (APEC), Charlotte, NC, 2015, pp. 2779-2783 **(Best Paper Presentation Awarded)**.

- T. Goktas, M. Arkan, **M. Zafarani** and B. Akin, "Separation harmonics for detecting broken bar fault in case of load torque oscillation," 2015 IEEE International Electric Machines & Drives Conference (IEMDC), Coeur d'Alene, ID, 2015, pp. 1452-1458.
- **M. Zafarani**, T. Goktas and B. Akin, "A simplified numerical approach to analyze magnet defects in permanent magnet synchronous motors," 2015 IEEE Energy Conversion Congress and Exposition (ECCE), Montreal, QC, 2015, pp. 6117-6121.
- T. Goktas, **M. Zafarani** and B. Akin, "Separation of broken magnet and static eccentricity failures in PMSM," 2015 IEEE International Electric Machines & Drives Conference (IEMDC), Coeur d'Alene, ID, 2015, pp. 1459-1465.
- **M. Zafarani**, T. Goktas and B. Akin, "A simplified mathematical approach to model and analyze magnet defects fault signatures in permanent magnet synchronous motors," 2015 IEEE Industry Applications Society Annual Meeting, Addison, TX, 2015, pp. 1-6.
- **M. Zafarani**, M. Moallem and A. Tabesh, "Analytical Model for a Transverse Flux Permanent Magnet Machine Using Improved Magnetic Equivalent Circuit Approach," 2011 21st International Conference on Systems Engineering, Las Vegas, NV, 2011, pp. 96-99.